KATABATIC WINDS IN ADELIE LAND, ANTARCTICA

Yuji Kodama

Geophysical Institute
University of Alaska-Fairbanks
Fairbanks, AK 99775-0800

KATABATIC WINDS IN ADELIE LAND, ANTARCTICA

A

THESIS

— Revised version —

Presented to the Faculty of the University of Alaska

in Partial Fulfillment of the Requirements

for the Degree of

DOCTOR OF PHILOSOPHY

by

Yuji Kodama, B.S., M.S.

Fairbanks, Alaska

August, 1985

ABSTRACT

Data from Automatic Weather Stations (AWS) on Adelie Land, Antarctica, were analysed. These data were collected on a year-round basis, simultaneously at different stations on the ice-covered slope, where no such data have been previously obtained. The findings are:

1) The high directional constancy (ratio of resultant wind speed to mean wind speed) of the surface winds has been reported and explained by the inversion strength and steepness of the terrain. In summer, however, when the inversion is weak or destroyed, a high directional constancy of approximately 0.9, comparable to the mean annual value of 0.92, is found at the slope stations. An analysis of data and model simulations of diurnal variations of katabatic winds in summer show that synoptic geostrophic winds and eddy viscosity also effect the constancy of the wind direction in summer.

2) Wind directional constancies at the slope stations in winter, when the inversion is expected to

be stronger than that in summer, are sometimes lower than the mean annual constancies. These low constancies are associated with warm air advection from maritime air brought into Adelie Land when the continental anticyclonic ridge, connecting at times with New Zealand and Australia anticyclone, lies to the east of Adelie Land.

3) There is a superadiabatic surface temperature change between the high plateau and intermediate plateau stations. Station D80, a high plateau station showed a distinct flow pattern in winter, which suggested the importance of the influence of three factors on the total pressure gradient force: the inversion strength, the slope angle, and the surface potential temperature gradient along the slope. Total pressure gradient force is divided into three components, (buoyancy, surface temperature gradient, and boundary depth change) and their relative importances are evaluated. The results showed that the superadiabatic surface temperature change along the slope could be of importance when the buoyancy component is balanced or nearly balanced by an increase in depth of the katabatic wind layer.

4) The entrainment of blowing snow particles increases the density of the katabatic flow layer by two mechanisms: first, by the addition of snow particles to the air column; and second, by the sublimation of the snow particles, with the corresponding loss of latent heat from the air, which decreases air temperature and thereby increases air density. This increase in density in the katabatic flow layer leads to increased wind speed as a result of the change in air density in the boundary layer relative to the air density in the free atmosphere at the same height further down the slope. This accelerative effect occurs primarily at wind speeds exceeding 12 m/s, since at those high wind speeds there is usually a large amount of blowing snow.

Table of Contents

List of Figures

List of Tables

List of Symbols

		Page
ABL	Atmospheric Boundary Layer	125
AWS	Automatic Weather Stations	4
CF	Coriolis force	38
c	Constant	106
dH	Scale for depth change of an inversion layer	95
dT	Scale for equivalent potential temperature deficit	95
dθ	Scale for potential temperature change along the fall line	95
F	Total pressure gradient force	90
F_x, F_y	for down-slope component and cross-slope component	122
F_{sx}, F_{dx}	for stationary and diurnal parts of down-slope component	123
F_{sy}, F_{dy}	for stationary and diurnal parts of cross-slope component	123
f	Coriolis parameter	11
$\vec{G}=(u_g, v_g)$	Geostrophic wind vector at a height	11
$\vec{G}_d$, $\vec{G}_n$	for day and night	41
$\vec{G}_t$	Geostrophic wind vector at the top	

	of the boundary layer	11
g	Gravitational acceleration	105
H	Scale for depth of boundary layer	95
h	Depth of stable boundary layer	90
K	Eddy viscosity	125
K_n, K_o, K_{max}	for neutral, surface, and maximum	125
KF	Katabatic force	105
KF_a, KF_{bs}	for without and with blowing snow	105
k	Friction coefficient	95
k_s, k_d	for stationary and diurnal parts	123
$\vec{k}$	Vertical unit vector	11
L	Monin-Obukhov length	126
PF	Pressure gradient force	38
p	Atmospheric pressure	11
Q=uh	Net down-slope transport of medium	90
q	Directional constancy of winds	30
SF	Stress force	38
$S^*=(T_s-_{sp})/T_{sp}$		107
T_s	Virtual temperature at surface	107
T_{sp}	Temperature in the standard atmosphere corresponding to the surface pressure	107
t	Time	122
t_g	Time scale for gravity flow	111

$\vec{U}=(u,v)$	Wind vector at a height	39
u	Down-dlope component of wind speed	38
u_s, u_d	for stationary and diurnal parts	122
u_g, u_{go}	Down-slope components of geostrophic winds at a height and at the surface	38
u_*	Friction velocity	126
V	Wind speed	90
v	Cross-slope component of wind speed	38
v_s, v_d	for stationary and diurnal parts	123
v_g, v_{go}	Cross-slope components of gestrophic winds at a heght and at the surface	38
v_T	Thermal wind	11
v_{Td}, v_{Tn}	for day and night	40
x	Down-slope coordinate	38
$Z=z/h$ or z/z_i	Normalized height	126
z	Coordinate normal to slope plain	39
z_i	Height of convective boundary layer	126
α	Deviation angle from the fall line	90
β	Buoyancy parameter	39
γ	Angle between thermal wind and geostrophic wind at the top of the boundary layer	40
$\eta=h/L$	Stability parameter	126
ι	Down-slope length scale	95

ψ	Slope angle	39
θ'	Difference in potential temperature between the boundary layer and free atmosphere	39
$\bar{\bar{\theta}}$	Vertical average of potential temperature deficit in an inversion layer	92
κ	von Karman constant	126
ρ	Density	11
ρ_{bs}	Blowing snow density	105
σ_T	Standard deviation in temperature	73
$\vec{\tau}=(-\overline{u'w'},-\overline{v'w'})$	Shear stress vector	38
$\nabla_h p$	Horizontal pressure gradient	11
ΔT	Inversion strength	10
$\Delta x, \Delta z$	Small increments in x- and z-direction	10
ΔZ	Scale for surface elevation drop	10

ψ	Slope angle	39
θ'	Difference in potential temperature between the boundary layer and free atmosphere	39
$\bar{\bar{\theta}}$	Vertical average of potential temperature deficit in an inversion layer	92
κ	von Karman constant	126
ρ	Density	11
ρ_{bs}	Blowing snow density	105
σ_T	Standard deviation in temperature	73
$\vec{\tau}=(-\overline{u'w'},-\overline{v'w'})$	Shear stress vector	38
$\nabla_h p$	Horizontal pressure gradient	11
ΔT	Inversion strrength	10
$\Delta x, \Delta z$	Small increments in x- and z-direction	10
ΔZ	Scale for surface elevation drop	10

Acknowledgement

This thesis could not have been completed without the help and support of the following individuals and organizations. I would like to express special thanks to:

Dr. Gerd Wendler, chairman of my advisory committee, for his advise and encouragement throughout this study.

Drs. Joan Gosink, John Kelley, Takeshi Ohtake, Glenn Shaw, and Gunter Weller, who are the members of my advisory committee, for their assistance in their detailed comments on the manuscript.

Dr. Zbigniew Sorbjan, who allowed me to use and modify his non-steady model for planetary boundary layer, and also offered many suggestions over the topics related to the boundary layer meteorology.

Mr. William Fuller, who helped the editorial improvement of the manuscript, and Mr. Mark Erickson for his assistance in proofreading the entire thesis.

My wife, Tomoyo, and my daughters, Laura and Tina, who put up with cold and dark winters of the Arctic and encouraged me throughout my graduate study.

Many individuals of Expeditions Polaires Francaise,

the United States Antarctic Research Program, and Dr. Stearn's group in University of Wisconsin, Madison, who did a great job in maintaining our automatic weather stations.

Finally, the National Science Foundation, which granted the katabatic wind project (DPP 84-13367).

1. Introduction

The role of Antarctica as one of the principal heat sinks is very important in the complex global climate system. It is essential to investigate the heat budget of the polar regions in order to understand the mechanisms of global climate and its change. Since surface winds affect the heat fluxes at the ground and vice versa, the study of katabatic winds in Antarctica assumes great importance.

Mawson and his 1912 expedition were awed by the strength of the katabatic winds along the coast of Antarctica. They experienced the most violent surface winds ever recorded; episodes of wind storms exceeding 44 m/s (100 mph) lasting for days and even weeks were common. Gusts up to 112 m/s (250 mph) were observed (Mawson, 1915). This led Mawson to entitle his book "The Home of the Blizzard," which describes the area around Cape Denison.

Like Mawson and his party, many explorers and scientists who have traveled on the antarctic mainland have left numerous records, descriptions, and comments regarding the unique character of the surface wind. They observed that the surface wind has a strong

preference for certain directions, dependent upon the topography of the terrain. Ball (1960), in a study of the high winds along the coast of Adelie Land, found that topography determines the wind direction.

The main reason for the topographic dependency of the surface wind lies in the frequent occurrence of an inversion layer, a layer where the temperature increases with height. The formation of a very stable temperature stratification, a characteristic of an inversion layer, acts to inhibit convection. The mixing process in the surface layer is thus substantially reduced. In this fashion, the lowest layer of the atmosphere becomes decoupled from the effects of large scale pressure gradients. Since the Antarctic is characterized by a negative radiation budget most of the time, inversion conditions are strong, persistent, and exist over nearly the entire continent for much of the year. This phenomenon explains why explorers early in this century observed such high consistency in the behavior of surface winds.

Mather and Miller (1967) inferred the pattern of surface wind flow over Antarctica from prevailing wind direction and sastrugi formation (Fig. 1.1a). Parish (1980) estimated the mean surface winds over gentle

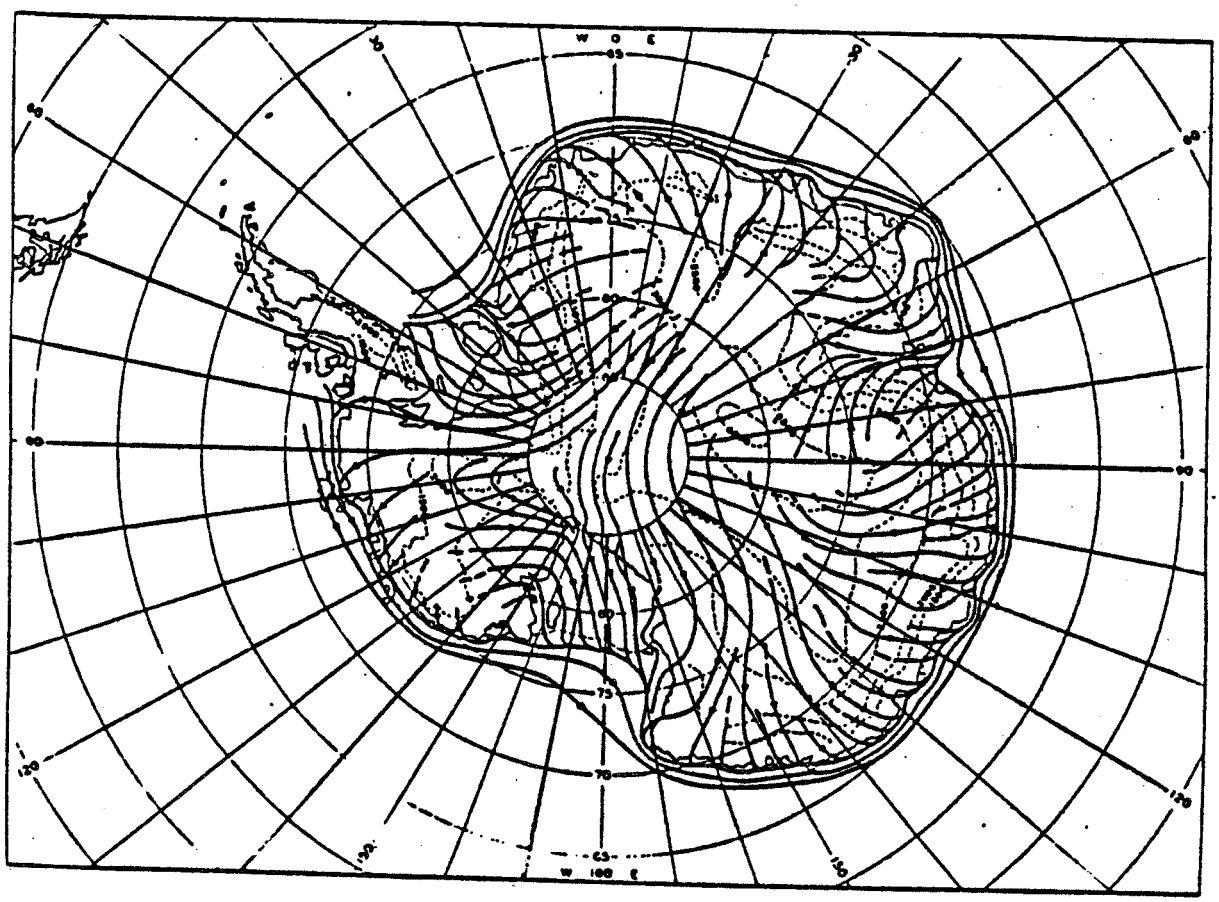

Fig. 1.1a Time-averaged surface airflow pattern over Antarctica, inferred from predominant wind directions and sastrugi orientation. (After Mather and Miller 1967.)

slopes in the interior of Antarctica, using simple diagnostic equations of motion, the terrain slope, and the strength of the temperature inversion (Fig. 1.1b). Generally, good agreement was found. The differences in the two figures are, as Parish (1980) argues, due to the fact that data in Fig. 1.1a were obtained from a sparse station network, which precluded any detailed analysis, and from the sastrugi reports, which have a seasonal bias since most observations were made during the summer months. The increased accuracies in the topographic maps of the Antarctic ice sheets used by Parish, relative to the one Mather and Miller used, would also help explain the differences in wind directions. However, do the differences depend only on these accuracies? Are there important factors other than the slope and the inversion strength factors, which would control surface winds in Antarctica? Is the topographic dependency of the surface winds true for summer, when the inversion is weak (Phillpot and Zillman 1970) or sometimes destroyed (Allison 1982, Sorbjan et al. 1985)? This study attempts to answer these questions.

Automatic Weather Stations (AWS) provide simultaneous data on a year-round basis at different locations on the continental slope, where no such data

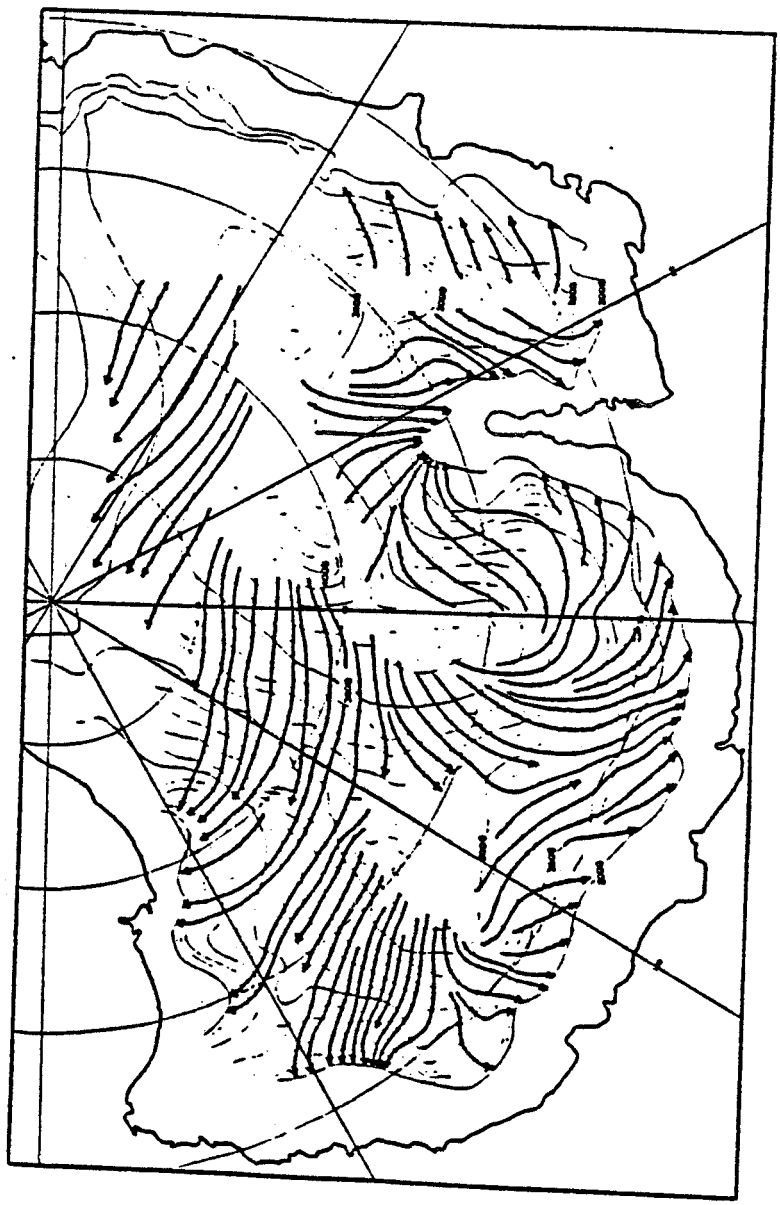

Fig. 1.1b Time-averaged winter flow pattern over Antarctica based on results from the two layer model by Parish (1980). The pressure gradient force in the free atmosphere is neglected.

have been previously obtained. Manned stations are sparsely distributed and there is rarely more than one station on the continental slope. Data from field trips are not obtained simultaneously at different positions on the slope, or on a year round basis. The AWS, however, only provide surface data and do not supply information on the vertical profiles of temperatures or winds. This shortcoming is a big disadvantage in katabatic wind studies, because the katabatic wind is known to be mainly dependent on the inversion strength. Much effort was made to overcome this disadvantage in this study.

Chapter 1 reviews the theories of katabatic winds and the definitions of katabatic force and its relation to thermal wind, and describes the topography of Adelie Land and the AWS. Chapter 2 outlines the general climate of Adelie Land, with emphasis on the annual variations of the meteorological components. Questions concerning katabatic winds in Adelie Land are brought up in chapter 2, and answers to the questions are offered in chapters 3 to 6. The diurnal variations of katabatic wind are treated in chapter 3, and in chapter 4 warm spells during winter months and their relationship to katabatic winds are discussed. Chapter

5 describes the large surface temperature gradient in Adelie Land, which influences katabatic flow, and in chapter 6, the effect of blowing snow on the katabatic wind is discussed. A summary and guidelines for future studies of katabatic winds are given in chapter 7.

1.1 Theories of Katabatic Winds

The word "katabatic" consists of two Greek words: "kata", which means "downwards", and "batos", which means "moving beyond" (Fairbridge 1967). Katabatic winds are winds which are due to the effect of gravity, and thus have the alternative name, "gravity wind." The term is in contrast to anabatic, meaning "moving upward."

Theoretical development of the subject of katabatic winds began relatively early. The analytic approach taken by Prandtl (1942; see Sutton(1953)) regards the katabatic winds as being in a steady state and having identical profiles anywhere on the slope. By taking exchange coefficients to be constant and the slope to be small the equations of motion can be solved to obtain the velocity and temperature fields as functions

of distance normal to the slope. The predicted functional forms for the velocity profile agree well with experiments (Defant 1951, Lettau 1966). Gutman (1953) extended Prandtl's approach to include diurnal variations, height dependent exchange coefficients, or nonstationary conditions. Later, the Coriolis force was also included (Lykosov and Gutman 1972).

Another approach to understanding katabatic flow was first taken by A. Defant (1933, quoted by F. Defant (1949)) and later by Fleagle (1950). They considered only the "average" flow within an identified cooled layer. All internal structure of the flow was eliminated and only variation with time was considered. Petkovsek and Hocevar (1971) extended Fleagle's idea to include a stable temperature stratification but obtained the anomalous result that predicted katabatic velocity to become infinite as the ambient stratification approaches adiabatic lapse rate. Streten et al. (1974) have compared their wind observations with the model of Petkovsek and Hocevar, and concluded that more detailed observations were required. For a model of drainage flow down a slope from a cold source, Ball (1956) drew on the similarity of Fleagle's approach to the theory of open-channel

hydraulics, and modeled a steady flow that depended on the thickness of the layer. Weller (1969) used Ball's theory successfully to explain the surface wind vector profile along the 62° East meridian in MacRobertson Land, Antarctica.

Lettau and Schwerdtfeger (1967) placed an important limitation on the possible extent and occurrence of pure downslope or drainage flow. When the trajectory length approaches 10 - 100 km, continuity of flow cannot be maintained since it does not occur under equilibrium conditions. This means that steady downslope winds in Antarctica may generally be expected on the steep coastal slopes up to 100 km inland. On the less steeply inclined interior slopes, they suggested the use of the term "thermal inversion wind" to replace the term " katabatic wind."

When an inversion layer is present over sloping terrain, a horizontal pressure gradient force becomes established (Fig. 1.2). This is an additional pressure gradient force which is induced by the thermal structure of the boundary layer over the slope. The magnitude of such a pressure gradient force is dependent upon two factors: the inversion strength and the slope of the terrain. A term combining these two

$$p_1 = p_3 + \rho_2 g \Delta z$$

$$p_2 = p_4 + \rho_1 g \Delta z$$

$$p_2 - p_1 = (p_4 - p_3) + (\rho_1 - \rho_2) g \Delta z$$

$$-\frac{1}{\rho_1}\frac{\Delta p}{\Delta x} = -\frac{1}{\rho_1}\left(\frac{p_4 - p_3}{\Delta x}\right) - g\left(\frac{\rho_1 - \rho_2}{\rho_1}\right)\frac{\Delta z}{\Delta x}$$

$$\left(-\frac{1}{\rho_1}\frac{\partial p}{\partial x}\right) \cong -\left(\frac{1}{\rho_1}\frac{\partial p}{\partial x}\right) - g\frac{\Delta T}{T}\left(\frac{\partial z}{\partial x}\right)$$

inversion layer — above inversion — sloped inversion force

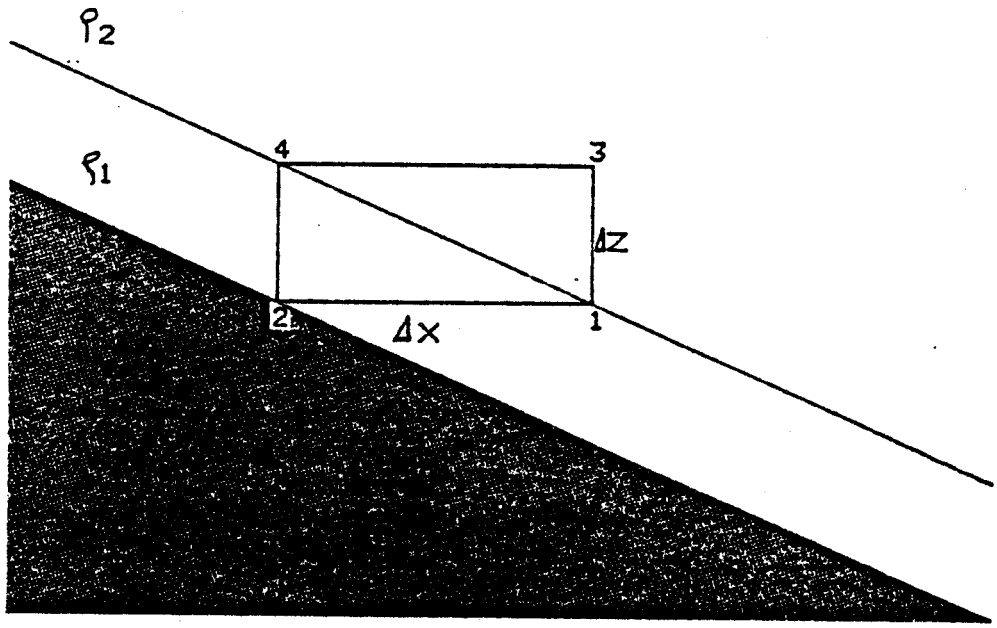

Fig. 1.2 The sloped-inversion pressure gradient force. The inversion strength and the terrain slope determins the magnitude of the horizontal pressure gradient force.

factors is called by different names depending on the researcher. Ball (1956) called it "katabatic force", Parish (1980) "sloped-inversion force", and Gosink (1981), and Turner (1973) "buoyancy". The names express, respectively, its result, its cause, and its character.

Since the pressure gradient force can be expressed as a geostrophic wind, the katabatic force is frequently related to the slope-induced thermal wind (Sorbjan 1982). The geostrophic relationship is expressed as follows:

$$\vec{G} = \vec{k} \times \frac{1}{\rho f} \nabla_h p = \vec{G}_t - [0, v_T] \qquad (1.1)$$

where $\vec{G}$ and $\vec{G}_t$ are the geostrophic winds at a height and in the free atmosphere, $\vec{k}$ is the vertical unit vector, ρ is the air density, f is the Coriolis parameter, $\nabla_h p$ is the horizontal pressure gradient. v_T is the thermal wind induced by a slope. It should not be confused with the thermal wind produced by the synoptic baroclinicity. The last equation in Fig. 1.2 expresses the same relationship as Eq. 1.1, but the former is described by forces and the latter by velocities. Thus the magnitude of a thermal wind is the katabatic force divided by the Coriolis parameter.

1.2 Topography of Adelie Land

Antarctica is almost entirely covered by a permanent ice sheet. Less than 3 % of its 14×10^6 km^2 is free of snow or ice for at least part of the year. The average elevation of Antarctica's surface is a little more than 2300 m. About 3.5×10^6 km^2 of the high plateau of East Antarctica lies above 3000 m. The slope of the major part of the plateau is very small, less than 1/500 (Schwerdtfeger 1984). The slope increases towards the edge of the ice continent, so that the antarctic continent can be represented approximately by a parabolic ice dome. A simple mathematical equation for the parabola gives surprisingly realistic values (Miller 1974).

Adelie Land is a sector located between George V Land to the east and Wilkes Land to the west (Fig. 1.3). An elevation profile from Dome C to D10 is shown in Fig. 1.4. The slope varies from less than 10^{-3} in the vicinity of Dome C to approximately 10^{-2} at D10 (Table 1.1). The determination of the slope is subject to the distance taken for the calculation. Therefore

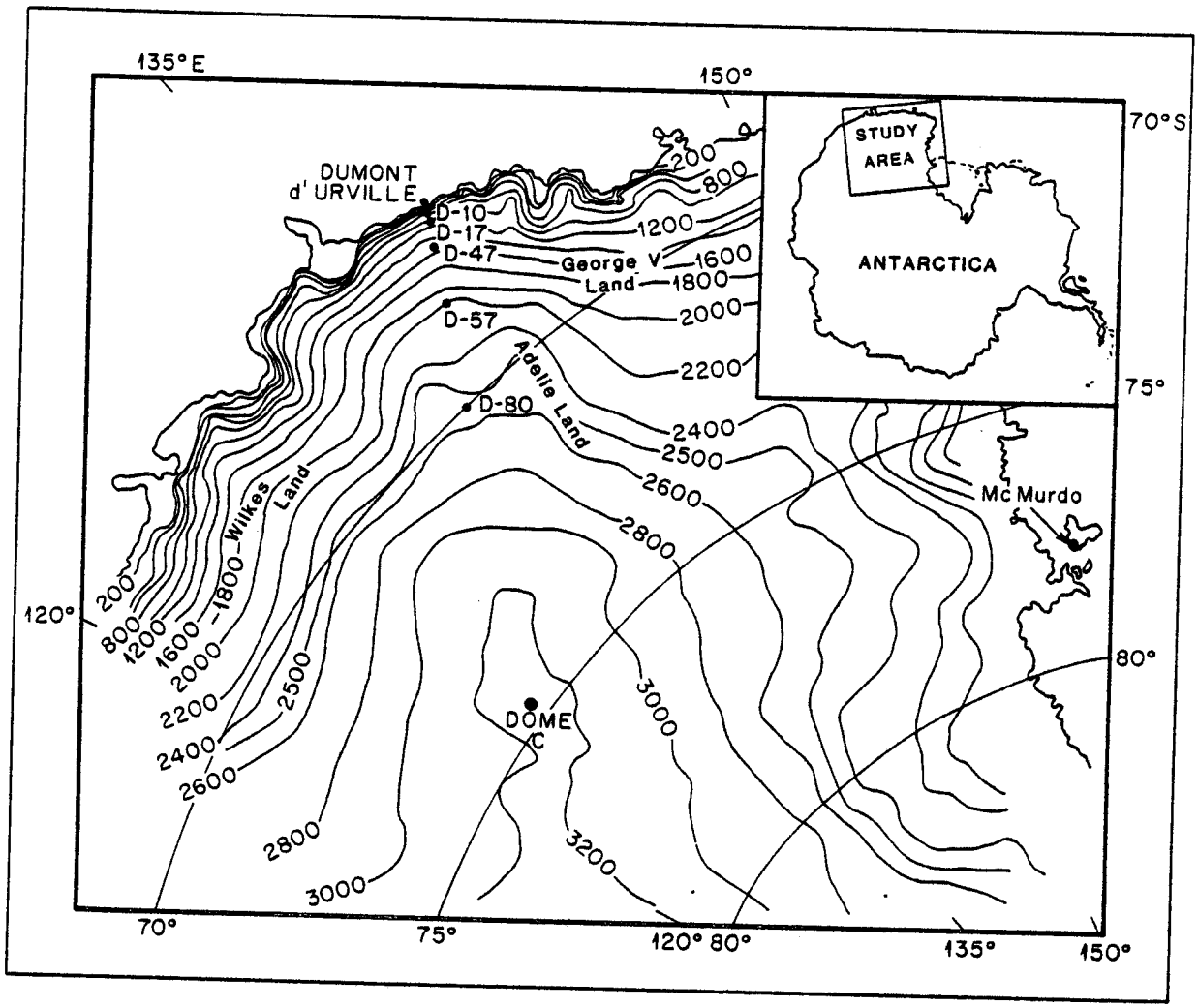

Fig. 1.3 The locations of Automatic Weather Stations and topographical features in Adelie Land, Antarctica.

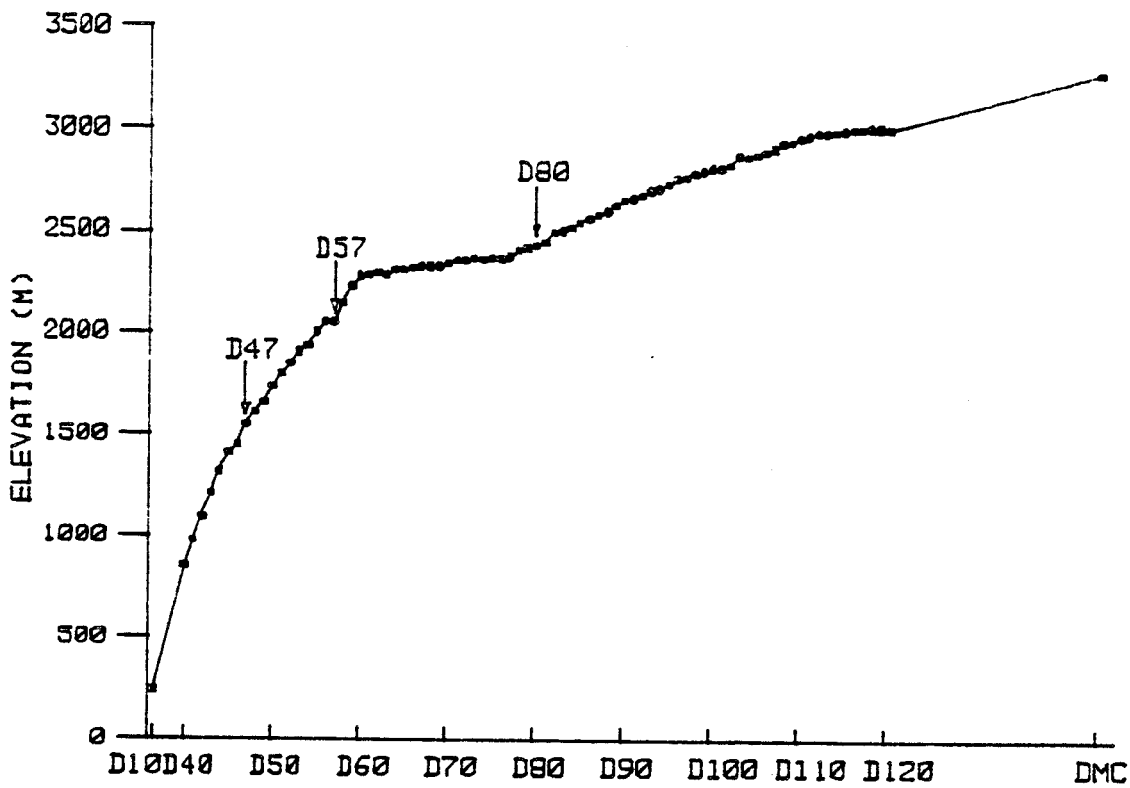

Fig. 1.4 The elevation profile of Adelie Land ice sheet on the line from D10 to Dome C.

Table 1.1 The geographic setting of the Automatic Weather Stations in Adelie Land, Antarctica. The distance is measured along the line between Dumont d'Urville and Dome C.

STATION	LOCATION	HT. (m)	DISTANCE FROM COAST (km)	SLOPE	AZIMUTH MAX. UPSLOPE
D10	66°42'S 139°48'E	240	5	2×10^{-2}	210°
D47	67°23'S 138°43'E	1560	110	5.5×10^{-3}	210°
D57	68°11'S 137°32'E	2103	210	6.5×10^{-3}	210°
D80	70°01'S 134°43'E	2450	440	1.8×10^{-3}	210°
Dome C	74°30'S 123°00'E	3280	1080		

it is extremely difficult to calculate an exact slope angle. The uneven terrain in the vicinity of D10 presents an additional difficulty. The direction of maximum slope also depends on local features in the area, but is approximates 210^{o} from true north.

Dome C is located at the highest point of its surroundings, and the area is flat. D10 is on the ice, about 5 km inland from the coast, while Dumont d'Urville is located on an island about 5 km from the coast.

1.3 Instrumentation

A better understanding of the katabatic wind in Antarctica has been hampered by the lack of observational data, although the phenomenon has been described and studied for many years, e.g., in the classic work of Mawson (1915). Data in the past were generally recorded either at manned stations at fixed points on a year-round basis or, during a number of field trips in summer, at different places on the same slope, but at different times (Weller 1969). Automatic Weather Stations (Renard and Salinas, 1977; Stearns and

Savage, 1981) have changed these procedures by providing simultaneous measurement at different fixed places on the same slope on a year-round basis.

In the late 1970s, A. Peterson at Stanford University developed AWS, which are able to record meteorological information on a year-round basis. In contrast to earlier versions of such stations which recorded the data in place (Sumner 1965, 1966), these newer stations are interrogated by satellite. This interrogation is carried out by polar orbiting satellites (NOAA 6, 7) which pass at intervals of less than two hours over the station. Normally, two satellites are used. Data are transmitted to Toulouse, France (Argos System), where they are recorded on magnetic tapes. The data tapes are sent to Stanford University, and, since 1981, to the University of Wisconsin at Madison, where they are transcribed into meteorological units, and sent on to us at Fairbanks for further analysis, usually about two months after the initial reading.

Dome C station, powered by a radioisotope thermoelectric generator (RTG), can run a full year without servicing, as do each of the other stations, powered by an array of automobile batteries charged by solar cells.

Four AWS were installed between 5 km and 440 km inland from the coast on the slope of Adelie Land (Wendler and Poggi, 1980) at altitudes ranging from 240 m to 2500 m above sea level. Another station, called Dome C, 1080 km from the coast, was installed on the top of an ice dome (3280 m) (Fig. 1.3). Their geographical settings are given in Table 1.1. The stations, sending information on meteorological conditions along the slope of Adelie Land on a year round basis via satellites, provide more comprehensive information than can be obtained by sporadic traverses. No manned stations exist in the area except Dumont d'Urville on the coast.

The data collected by the AWS are temperature, atmospheric pressure, wind speed and direction. Also recorded for maintenance purposes are the temperature in the instrument boxes and the voltage of the power supplies. The station has a storage capability of four consecutive values of all meteorological parameters, sampled at 10 minute intervals. Therefore, under the best conditions, with two satellites in orbit, a steady data flow at ten minute intervals can be obtained. Notwithstanding the harsh environmental conditions in which they operate, i.e. temperatures below -80^{o}C and

wind speeds of nearly 40 m/s, the AWS in Adelie Land transmitted data successfully during 60% of the time of the study. Of these data, the satellites missed roughly 10% due to periodic low angles of reception. Hourly data were compiled by using the observations closest to the hour. The air temperature was measured with a platinum resistance thermometer (Weed Instrument Co.), the atmospheric pressure with a digi-quartz pressure transducer system (Paroscientific Inc.), and wind speed and direction with a Bendix aerovane. The limits of accuracy of these sensors are as follows:

Temperature	$\pm 0.3^{\circ}C$
Pressure	± 0.1 mb
Wind Speed	± 0.2 m/s (0 ~ 4.4 m/s)
	± 0.5 m/s (8.6 ~ 89.6 m/s)
Wind Direction	$\pm 2^{\circ}$ over the full 360° range

2 GENERAL CLIMATE OF ADELIE LAND

To set the stage for the main topic discuseed in this dissertation, namely the factors affecting the katabatic winds, the climate of Adelie Land will be briefly reviewed in this chapter, especially the annual variation of mean monthly values of temperature, wind speed, and wind direction. All available data obtained by AWS were used to analyze these components.

In section 2.1 the AWS are classified according to geographic location, temperature, wind speed, and degree of slope. The annual variations of temperature and wind are discussed in sections 2.2 and 2.3, respectively, followed by a discussion of their combined effect in section 2.4. In section 2.5, the importance of blowing snow on the climate of Adelie Land is introduced. Finally, the questions, which are brought up in this chapter and are discussed further in following chapters, are summarized in chapter 2.6. Our motivation for choosing the topics discussed in subsequent chapters will also be explained.

2.1 Classification of the Stations

Mather and Miller (1967) classified the geographical location of stations on the antarctic slope into three groups; high plateau, intermediate plateau, and coastal region, reflecting differences in mean annual temperature and wind speed (Fig. 2.1). Radok (1973) also defined three zones on the antarctic continent in terms of surface slope. The latter classification system results in groupings similar to those defined by Mather and Miller.

The high plateau stations, Dome C and D80, show relatively low temperatures ($-50^{o}C$), light winds (5m/s), and slopes less than $2.0x10^{-3}$.

D47 and D57, the intermediate plateau stations are located closer to the coast and have stronger winds (10 m/s), higher temperatures ($-30^{o}C$), and steeper slopes ($2.0x10^{-3}$ to $7.0x10^{-3}$) than the high plateau stations.

The wind speed at the coastal stations varies greatly depending on the station's location (Parish 1980), such as near the foot of an ice slope or on an offshore island, etc.. However, the observed mean

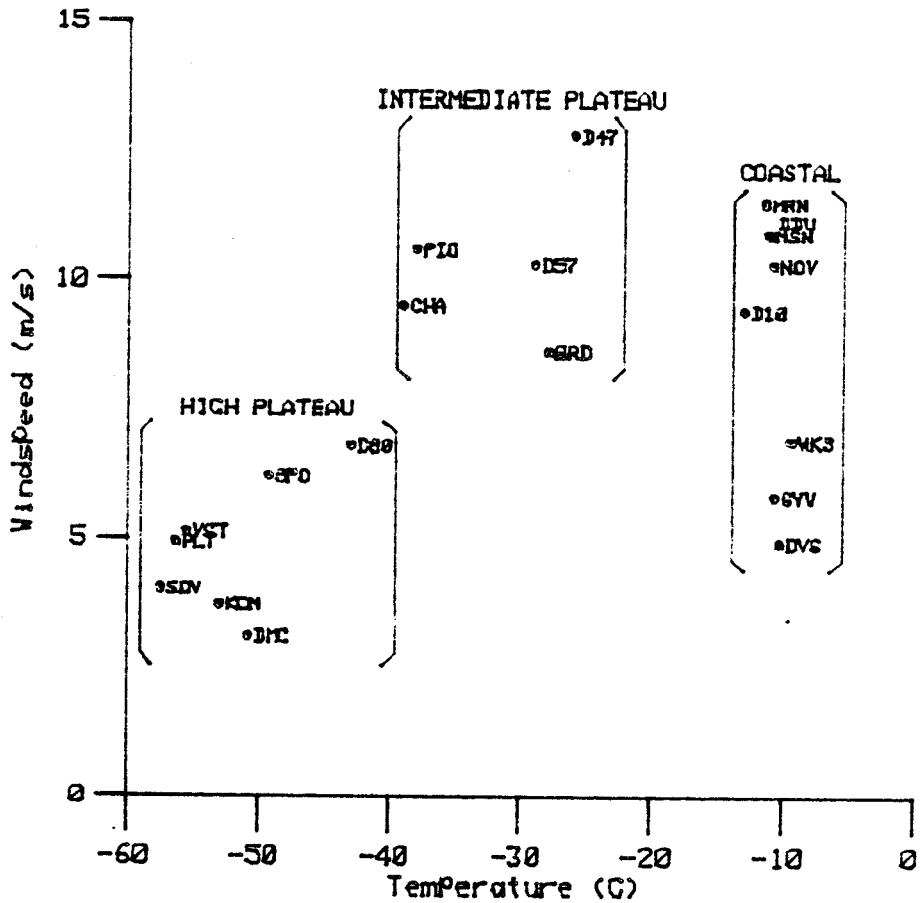

Fig. 2.1 Mean annual wind speed versus temperature for antarctic stations. The data are from Mather and Miller (1967) and Schwerdtfeger (1970) except for the stations in Adelie Land, Antarctica. The abbreviations are; MRN-Mirny, DDU-Dumont d'Urville, MSN-Mawson, WKS-Wilkes, SYW-Syowa, DVS-Davis, BRD-Byrd, PIO-Pionerskaya, CHA-Charcot, SPO-South Pole, VST-Vostok, PLT-Plateau, SOV-Sovietskaya, KOM-Komsomolskaya, DMC-Dome C.

annual temperature of all the coastal stations is close to -10°C, much warmer than the other two zones. D10 belongs to this group and is located on the ice 5 km from the coast.

2.2 Temperature

The graph in Fig. 2.2 shows the annual variations in temperature at the stations. The temperatures of D47 and D57 are combined, as they are similar. As would be expected, however, the average annual temperature at station D47, the lower of the two, is 4.0°C warmer than station D57. The month-to-month variations at D80 are larger than those at the other stations, because the measurements at D80 were only for one year, while those at the other stations were averaged for 2 - 3 years.

The coldest temperature in AWS of Adelie Land ever observed was -84.6°C at Dome C. Temperatures at Dome C always stay well below the freezing point, while the coastal station D10 has temperatures above the freezing point in midsummer.

Fig. 2.2 shows the typical "coreless" winter temperature pattern, the flattening of the temperature

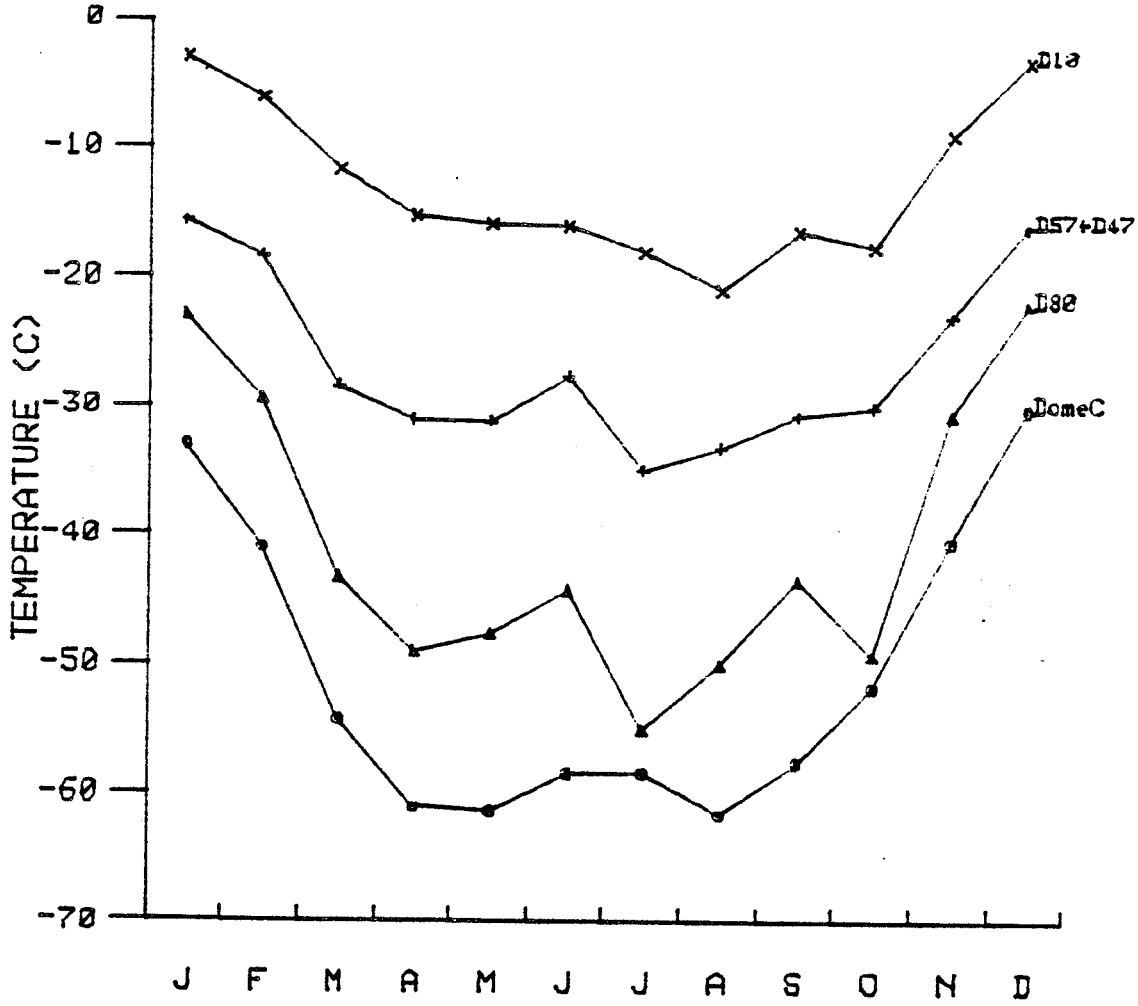

Fig. 2.2 Annual variation of temperature of Automatic Weather Stations in Adelie Land. Data for stations D47 and D57 were combined. The measurement at D80 was only for one year, while those at the other stations were averaged for 2 - 3 years.

curve in winter. This pattern will be discussed in chapter 4 in relation to the synoptic pressure pattern.

The large temperature differences between Dome C or D80 and the rest of the stations in winter indicate a strong surface inversion at Dome C or D80 relative to the other stations. The lower temperatures at Dome C and D80 are more pronounced than would be suggested by an adiabatic temperature gradient. Note that the elevation difference is smaller between, for example, D80 and D57 than between D57 and D10 (Table 1.1). This implies an above-adiabatic temperature gradient between D80 and D57 for all months but midsummer. This phenomenon will be discussed in chapter 5 in relation to the katabatic winds.

2.3 Wind

The annual variations of mean monthly wind speed are shown in Fig. 2.3. The wind speed at Dome C is very light, with a mean value of 3.2 m/s and no pronounced annual cycle. Compared with other inland stations, Dome C experiences the lowest wind speeds of

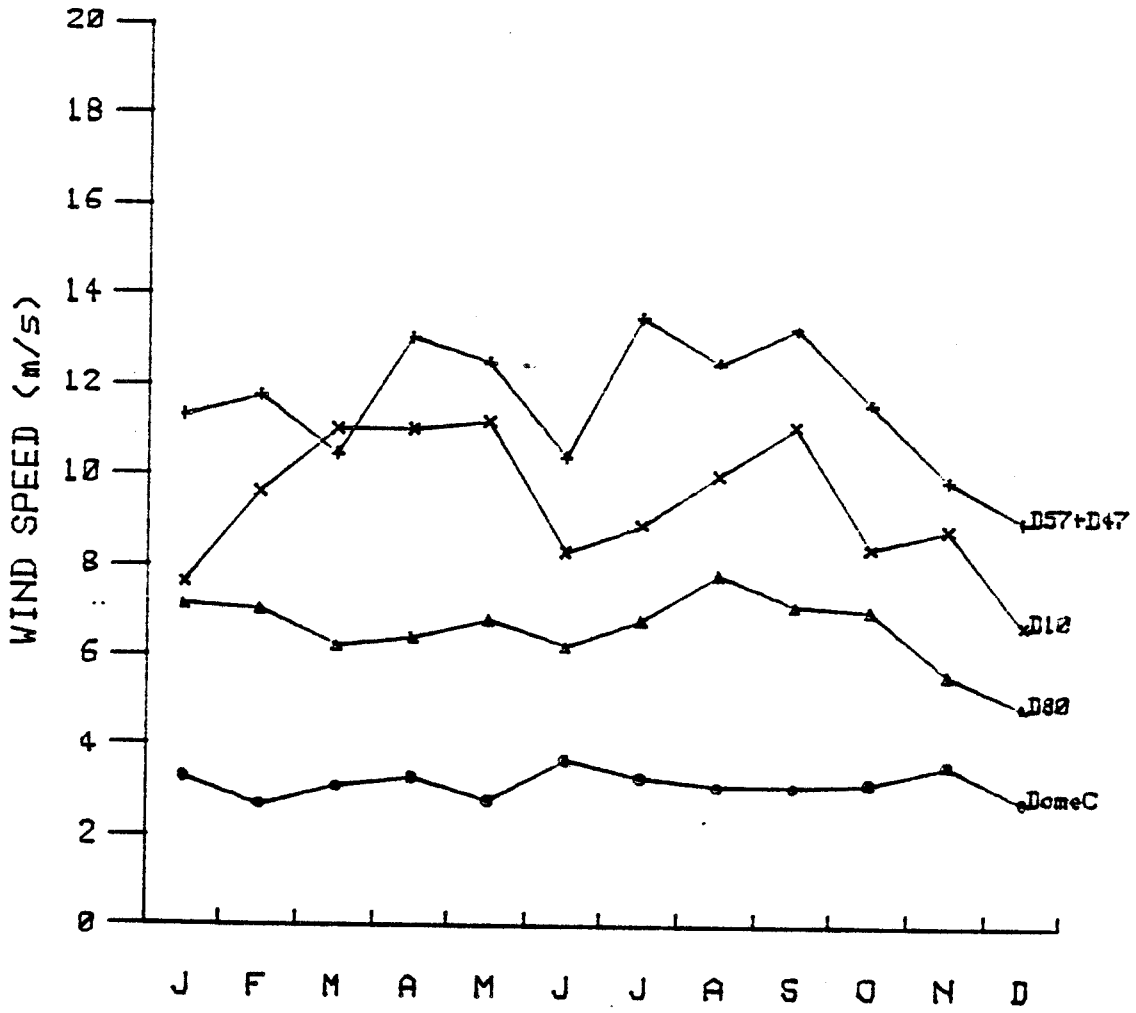

Fig. 2.3 Annual variation of monthly mean wind speed of Automatic Weather Stations in Adelie Land. Data for stations D47 and D57 were combined. The measurement at D80 was only for one year, while those at the other stations were averaged for 2 - 3 years.

all inland stations of Antarctica (Wendler and Kodama 1982). This is unique, as an exposed station at a height of 3280 m on any other continent would have higher wind speeds than those at lower elevations.

The wind speed steadily increases farther down the slope towards the coast (Fig. 2.3). Data for D57 and D47 are combined in the graph as they have similar annual patterns. On the average, however, the lower-lying station D47 had a 19 % higher wind speed than D57. The increase in wind speed from D57 to D47 and the decrease from D47 to D10 suggests a wind maximum somewhere around D47. The decrease in wind speed at D10, where the slope is greater than at D57 or D47, can be explained by hydraulic jumps (Ball 1956) and uneveness of the terrain. When hydraulic jumps occur upslope from D10, tranquil flow is observed at D10 rather than shooting flow (Streten 1963, Gosink 1983). Another explanation for the lower wind speed at D10 is its position on a ridge in the uneven terrain of the coastal area. The extremely strong wind on the Adelie coast experienced by Mawson was explained by Parish (1981) as a funneling effect often found in uneven terrain. The flow at the top of a ridge is characterized by a lower wind speed than that at the bottom of a valley.

Fig. 2.4 shows the monthly resultant wind vectors for all stations except Dome C, where the magnitude of the vectors is small and no systematic variations are found. The x-axis of the graph represents the down-slope component of the wind vector and the y-axis represents the cross-slope component. Arrows show the mean annual wind vectors. Each of the integers represents an average of wind vectors for each month of the year. Generally, the wind blows about 45^{o} to 60^{o} to the left of the fall line, and the monthly resultant wind vectors veer away from the down-slope in summer and toward the down-slope in winter. This veer in winds indicates the presence of a stronger thermal wind in winter than in summer. Compared with the mean annual resultant wind vectors of the other stations (arrows in Fig. 2.4), the vector at D10 points most closely in a down-slope direction. The angle between the vector and the down-slope direction increases from D10 to D57, which is expected, because the angle is inversely proportional to the steepness of the slope (Ball 1960). However, the angle between the resultant wind vector and the down-slope direction decrease from D57 to D80. This phenomenon will be dicussed in conjunction with the temperature gradient along the slope in chapter 6.

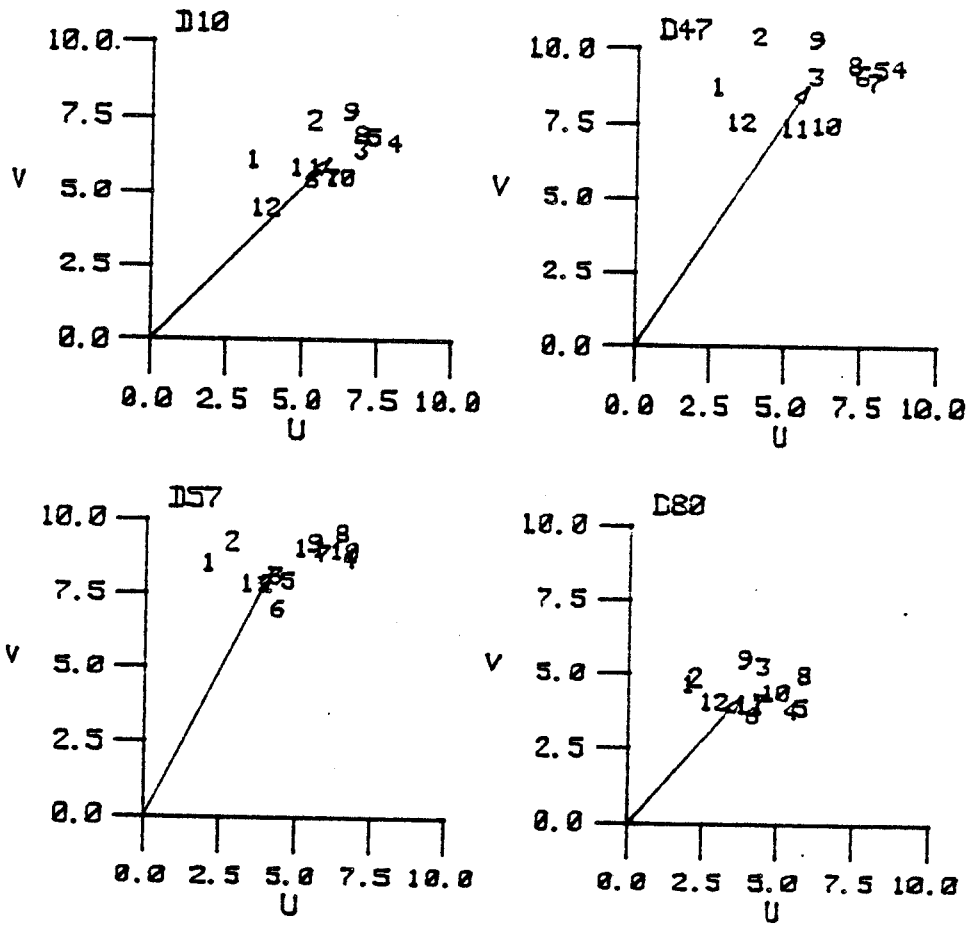

Fig. 2.4 The monthly resultant wind vectors for D10, D47, D57, and D80. Each of the integers represents an average of wind vectors for each month of the year. Arrows show the wind vectors, which are the resultant of all data available for each station.

With the exception of Dome C, all other stations show a strong constancy (q) in wind direction (Table 2.1). q is defined as a ratio of the resultant wind speed to the mean wind speed. A value of q=1.0 means that the wind blows only from one direction, whereas a value of q=0.0 means that the winds blow from all directions with equal strength and frequency. There is, of course, no place where q=0.0 is found, since the general circulation also has preferred directions. The strong directional constancy indicates that gravity is the most important factor in determining the direction of flow at all slope stations. However, two questions remain: 1) Why does q stay high during summer when the inversion is weak or destroyed? and 2) Why is the lowest value of q observed in winter instead of in summer? These questions are addressed in chapters 3 and 4, respectively.

2.4 Temperature and Wind

Lettau et al. (1977) showed that the inversion strength increases with decreasing temperature in Antarctica. This also holds true for the arctic and

Table 2.1 Wind direction constancy of Automatic Weather Stations in Adelie Land, East Antarctica.

Month	D10	D47	D57	D80	Dome C
Jan	0.93	0.98	0.96	0.93	0.43
Feb	0.92	0.93	0.95	0.90	0.54
Mar	0.95	0.96	0.93	0.94	0.47
Apr	0.94	0.95	0.91	0.98	0.50
May	0.93	0.96	0.83	0.99	0.28
Jun	0.86	0.93	0.73	0.84	0.56
Jul	0.90	0.95	0.90	0.83	0.36
Aug	0.94	0.95	0.94	0.96	0.67
Sep	0.93	0.89	0.92	0.90	0.41
Oct	0.93	0.94	0.94	0.97	0.55
Nov	0.87	0.88	0.93	0.90	0.72
Dec	0.88	0.90	0.92	0.79	0.60
Annual	0.92	0.94	0.91	0.92	0.51

subarctic areas (Wendler and Nicpon 1975). Further, the driving force of katabatic winds is proportional to the inversion strength on inclined surfaces. Hence, with lower temperatures, stronger winds are expected in areas dominated by katabatic winds. Fig. 2.5 shows this well for D10 and D57, whereas Dome C does not show any systematic relationship between temperature and wind speed.

The combination of an increase in wind speed with decreasing temperatures results in an environment extremely hostile to humans. The lower the surface temperature, the stronger the wind becomes, resulting in extremely low 'equivalent chill temperatures.' An opposite condition, for example, is found at Fairbanks in the flat interior of Alaska (Fig. 2.5). As the inversion builds up over this flat area, no gravity flow is experienced and the inversion layer suppresses transmission of the wind aloft to the surface. Hence, during cold spells no winds or very weak surface winds blow. Occasionally stronger winds aloft partly destroy the inversion layer and bring warmer air to the surface.

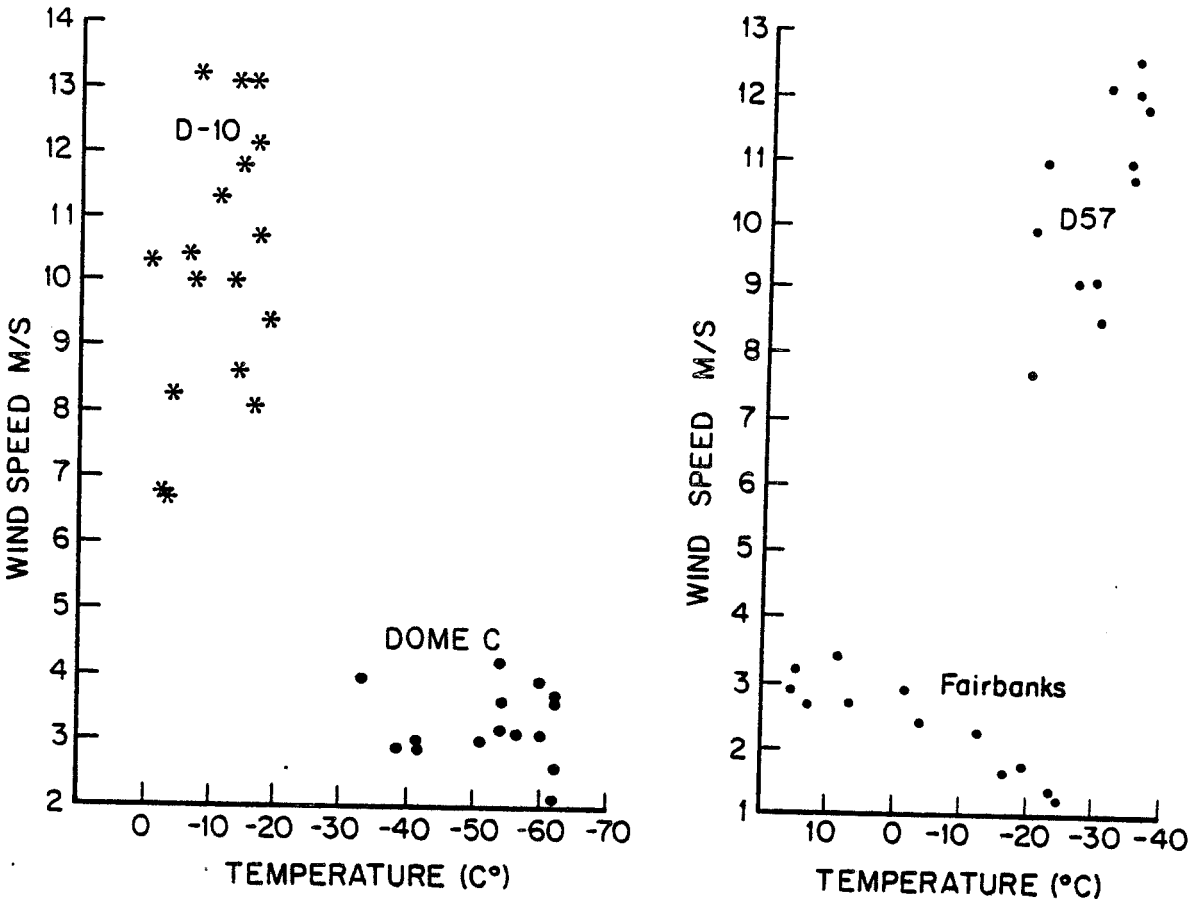

Fig. 2.5 Mean monthly values of temperature are plotted against the wind speed of the same station. For Dome C no relationship was found. For the coastal (D10) and the intermediate plateau (D57) stations the wind speed increases with lower temperatures, whereas for Fairbanks, Alaska, just the opposite trend was observed.

2.5 Blowing snow

Katabatic winds with blowing snow are common phenomena in Adelie Land. Mawson (1915) nicknamed the area around Cape Denison "Home of the Blizzard." Prudhomme and Valtat (1957) observed high-reaching or strong blowing snow at Port Martin for 45 % of the time with mean visibility of 350 m; for a quarter of the time snow drifts reduces the visibility to a mean of 35 m. Ball (1957) characterized katabatic winds carrying vast quantities of suspended snow as "large scale avalanches of low density."

Ball (1957) also estimated that a snow load of 10 g/m^3, which is not rare with strong winds (Loewe 1956, Budd et al. 1966), means an increase of density equivalent to a cooling of $2^{o}C$. He further stated that blowing snow in katabatic winds acts to keep air saturated or near saturation with respect to the ice, and to increase the surface friction. Loewe (1974) stated that blowing snow contributes to the high velocity of katabatic winds in Adelie Land. Yamamnouchi and Kawaguchi (1985) studied the effect of blowing snow on the radiation balance at Mizuho Station in East Antarctica.

We will treat the effect of blowing snow on katabatic winds in depth in chapter 6.

2.6 Summary

The climate of Adelie Land is heavily influenced by the steepness of the slope. Strong katabatic winds and low temperatures at the slope stations produce an inhospitable environment for human life, whereas Dome C, on a flat area at the top of an ice dome, has the lowest wind speeds of the interior plateau stations and the lowest temperatures among the AWS of Adelie Land.

The following questions are raised in this chapter:

1) How can the high directional constancy of winds in summer, when the inversion condition is weak or totally destroyed, be explained?

2) Why is the directional constancy sometimes low in winter? Is this phenomenon related to the coreless winter temperature pattern?

3) Does the temperature difference between the interior and the coastal area , which is larger than the adiabatic temperature change, affect the katabatic winds?

4) Is there any effect of blowing snow, which occurs frequently on the antarctic coastal slopes, on the katabatic winds?

These questions will be discussed in the following chapters.

3 DIURNAL VARIATION OF KATABATIC WIND IN ADELIE LAND

3.1 Introduction

The diurnal variation of katabatic winds in summer is one of the most frequently studied fields in antarctic meteorology, mainly because summer expeditions providing meteorological information have outnumbered winter expeditions. Changes in the diurnal variation of katabatic wind as a function of the steepness of the slope and the distance from the coast had seldom been investigated previous to the present time. Earlier Mather and Miller (1967), from data gathered from most of Antarctica's weather stations, showed that maximum wind speeds occurred in the morning in coastal area, and at midday on the interior plateau. Loewe (1974) analyzed the winds over the interior of Antarctica and Greenland, and found a mechanism to explain why stronger winds frequently occur near midday rather than during the colder part of the day.

In this chapter, using the data from AWS, the behavior of the wind in summer on the slope of Adelie Land is analyzed. Also, the change in the diurnal

variations of the meteorological components with respect to the steepness of the slope is discussed.

3.2 Mechanism of Diurnal Variation of Wind

The surface wind vector on a slope is a result of a summation of three acting forces: the pressure gradient force PF, the Coriolis force CF, and the stress force SF, resulting in a non-zero local acceleration of wind. In this section, for convenience, we treat the problem only for the steady state during daytime and nighttime, although it is in non-steady state for the transition periods from day to night and vice versa. The balance of the three forces is based on the steady-state momentum budget, which can be written in the form:

$$\underset{SF}{-\frac{\partial \vec{\tau}}{\partial z}} = \underset{CF}{-\vec{k} \times f\vec{U}} + \underset{PF}{\vec{k} \times f\vec{G}} \qquad (3.1)$$

where $\vec{U}$ and $\vec{G}$ are the wind vector and the total geostrophic wind vector including the thermal wind, respectively, $\vec{U}=(u,v)$, $\vec{G}=(u_g,v_g)$; $\vec{\tau}$ is the stress

vector, $\vec{\tau}=(-\overline{u'w'},-\overline{v'w'})$; f is the Coriolis parameter; $\vec{k}$ is the unit vector of the z-axis. The x-axis of the coordinate system is oriented down the slope.

Above a sloping terrain, the thermal activity of the underlying surface generates an additional component of the geostrophic wind (thermal wind), $v_T=\beta\theta'\psi/f$, where β is the buoyancy parameter, ψ is the slope angle, θ' is the difference in potential temperature between the boundary layer and the free atmosphere. The slope-induced thermal wind v_T is z-dependent and oriented perpendicularly to the slope vector. In this case, the total geostrophic wind is expressed in the form:

$$\vec{G}(z) = \vec{G}_t - [0,v_T(z)] \qquad (3.2)$$

where $\vec{G}_t$ is the synoptic geostrophic wind. Since v_T is positive at night, and very small and positive, or negative during the daytime, the geostrophic wind vector $\vec{G}$ at a height turns to the left or to the right with respect to the vector $\vec{G}_t$ at the top of the boundary layer. If we assume that both $\vec{G}_t$ and SP are constant, the change in the thermal wind v_T from day to night modifies the balance of forces (Eq. 3.1).

As a result, the wind vector $\vec{U}$ near the surface would turn toward the down-slope direction at night and more toward a cross-slope direction during the day.

In the special case Loewe (1974) discussed, the daytime maximum of $\vec{G}_t$ could be observed when the magnitude of v_T is comparable with $\vec{G}_t$. Fig. 3.1 shows an example of Loewe's case. The condition Loewe derived is:

$$(v_{Tn} + v_{Td}) < 2G_t \cos\gamma \qquad (3.3)$$

where v_{Tn} and v_{Td} are the thermal winds during the day and at night, respectively. γ is an angle between the thermal wind and $\vec{G}_t$.

The SF also varies with the time of day. Since the stability changes mainly as the result of changes in the heat budget at the surface, the diffusivity and the gradient of the Reynold's stress also vary. The stability, higher at night than during the day, reduces the turbulent mixing and allows the flow near the surface to decouple from $\vec{G}_t$. This stability also helps to develop a low level jet (Wipperman 1977). During the day the turbulent mixing increases, and therefore,

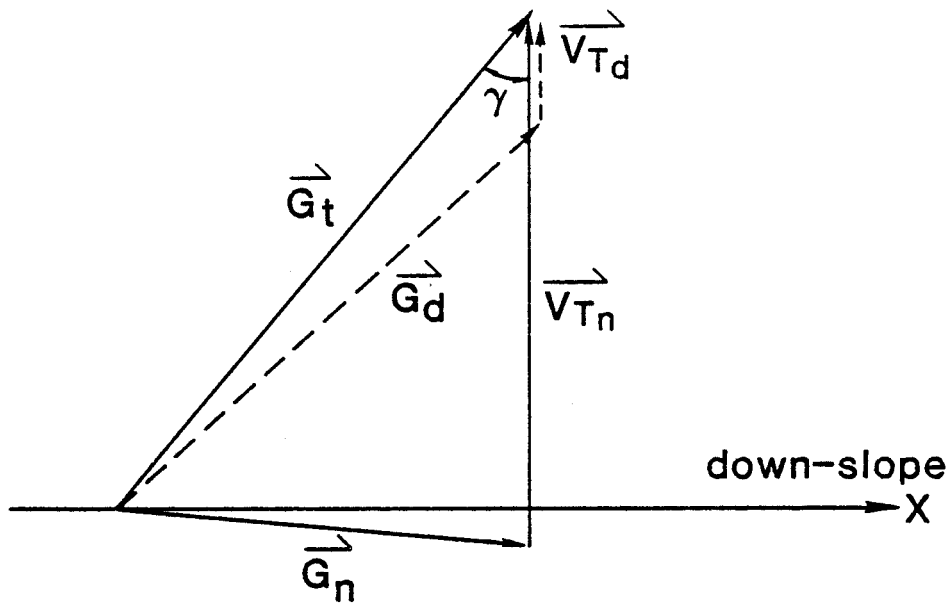

Fig. 3.1 The schematic diagram of the geostrophic wind vectors and the thermal winds for day and night. Note that the suface geostrophic wind for day, $\vec{G}_d$, can be larger than $\vec{G}_n$ for night. $\vec{G}_t$ is the synoptic geostrophic wind. $\vec{v}_{Td}$ and $\vec{v}_{Tn}$ are the thermal winds during day and night, respectively. γ is the angle between $\vec{v}_T$ and $\vec{G}_t$.

the transfer of energy from the upper wind into the surface layer is facilitated by the low stability within the boundary layer. Thus, the flow in the boundary layer is closer to $\vec{G}_t$ (Loewe 1974).

3.3 RESULT

Figs. 3.2a - e show the diurnal variations of temperature, pressure, wind speed, wind direction, pressure gradient force, friction coefficient, and the number of observations at D10, D47, D57, D80, and Dome C, respectively. Fewer transmissions are received around local noon than at other times, as is shown at the bottom of the graphs.

At station D10 (Fig. 3.2a), the temperature variation is a smooth sinusoidal curve with its maximum at 1500 LST and its minimum at 0300 LST. The pressure variation is somewhat irregular, possibly due to the variation of the number of observations. The wind speed has its maximum at 0400 LST, which is about the time of the lowest temperature observed. The weakest wind is observed a few hours after the time when the

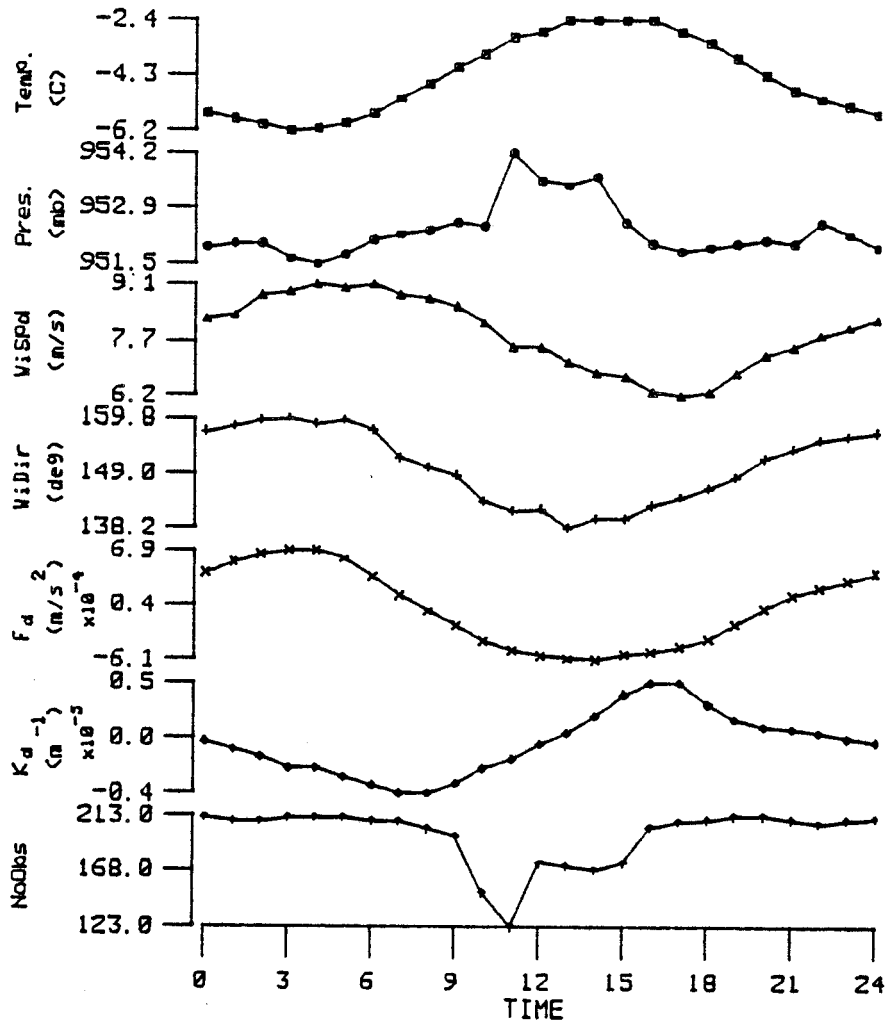

Fig. 3.2a The diurnal variations of temperature, pressure, wind speed, wind direction, pressure gradient force, friction coefficient, and the number of observations at D10. The method for calculating the diurnal variations of pressure gradient force and friction coefficient is explained in Appendix A.

highest temperature occurs. The variation of wind direction correlates well with the inverse pattern of the temperature graph.

The fifth curve in Fig. 3.2a shows the diurnal variation of the pressure gradient force, which is calculated from the diurnal oscillation of the wind vectors (see Appendix A). Since the pressure gradient force divided by the Coriolis parameter is a thermal wind, the diurnal component of the pressure gradient force arises only from the horizontal temperature gradient which is induced by the heating or cooling at the surface of the slope. In other words, it indicates the diurnal variation of the slope-induced thermal wind. According to Fig. 3.2a, the graph for the pressure gradient force agrees well with that of the wind direction.

The sixth curve in Fig. 3.2a is the diurnal variation of the friction coefficient, which is also calculated from the diurnal variation of the wind vectors assuming that the cross-slope component (y-direction) of the pressure gradient force is negligibly small and that the friction coefficient is constant in any horizontal direction. The friction coefficient indicates the stability of the boundary layer as well

as the intensity of the turbulent mixing. According to Fig. 3.2a, an inverse reading of the friction coefficient graph matches well with the graph of the wind speed variation.

From these graphs of wind speed, wind direction, pressure gradient force, and the friction coefficient, the following statements concerning D10 can be made:

1) At night the wind speed is greater and the wind direction is directed more toward the fall line than in the day because of the stronger thermal wind and stability.

2) During the day the wind speed is at a minimum when turbulent mixing is strongest, and the wind blows in a maximum cross-slope direction when the thermal wind is weakest.

3) As a corollary to 2), the daytime direction of $\vec{G}_t$ could be quite constant in a direction close to the cross-slope direction. Since both the stability and thermal wind are weak during the day, the only factor which controls the surface wind direction is $\vec{G}_t$. The small change in the surface wind direction from night to day can not be explained without

assuming a directional constancy in $\vec{G}_t$.

The diurnal curves of the parameters at D47 and D57 (Figs. 3.2b and c) are very similar to each other. The temperature variation is similar to that at D10. The pressure curve is also irregular as at D10. The patterns for wind speed and pressure gradient force, and the inverse pattern of temperature match each other quite well, and also the pattern of wind direction and the inverse pattern of the friction coefficient are similar to those observed for D10.

The phase difference between the temperature and wind speed curves is small at D10, and it becomes larger at D47 and D57 in Figs. 3.2a-c. At D10, the difference between the times of the minimum temperature and the maximum wind speed, or the maximum temperature and the minimum wind speed is one hour, whereas at D47 it is about 4 hours and at D57 about 5 hours. Because the wind speed varies with the friction coefficient, the stability of the boundary layer reacts a few hours later to the inversion strength (assuming the temperature at the upper boundary layer to be constant), depending on the steepness of the slope. The following phenomena help to explain the higher

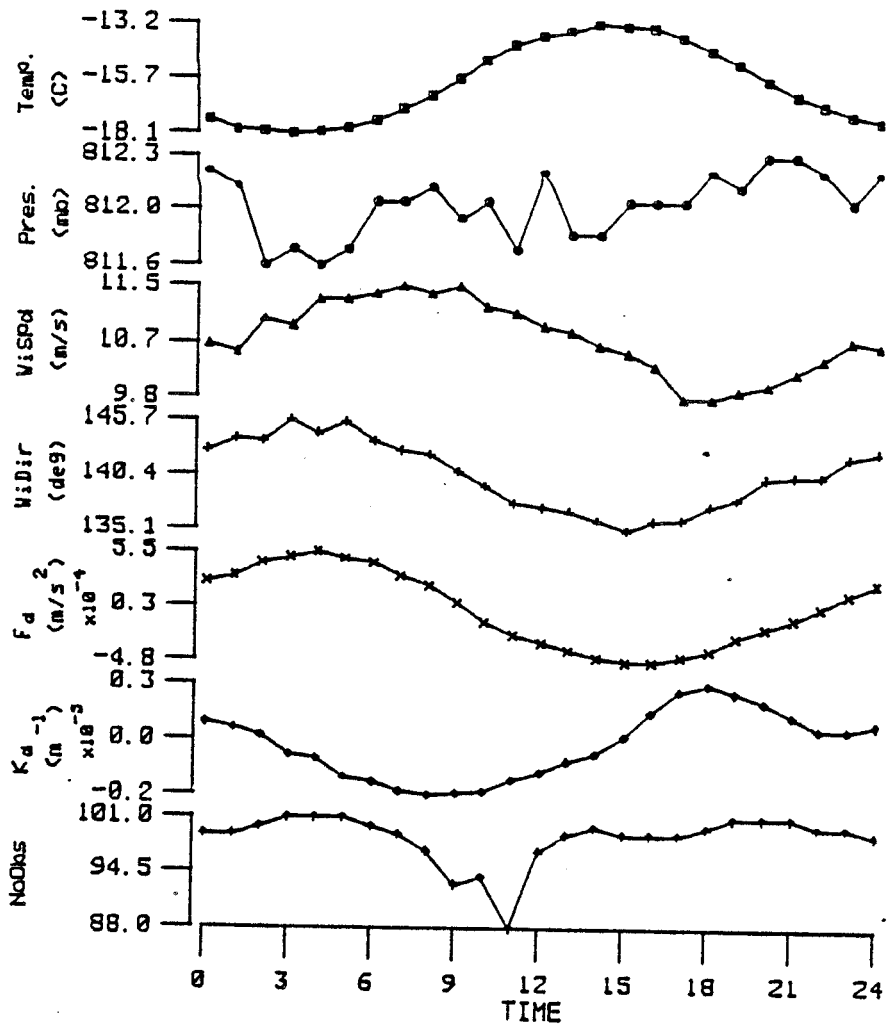

Fig. 3.2b The diurnal variations of temperature, pressure, wind speed, wind direction, pressure gradient force, friction coefficient, and the number of observations at D47. The method for calculating the diurnal variations of pressure gradient force and friction coefficient is explained in Appendix A.

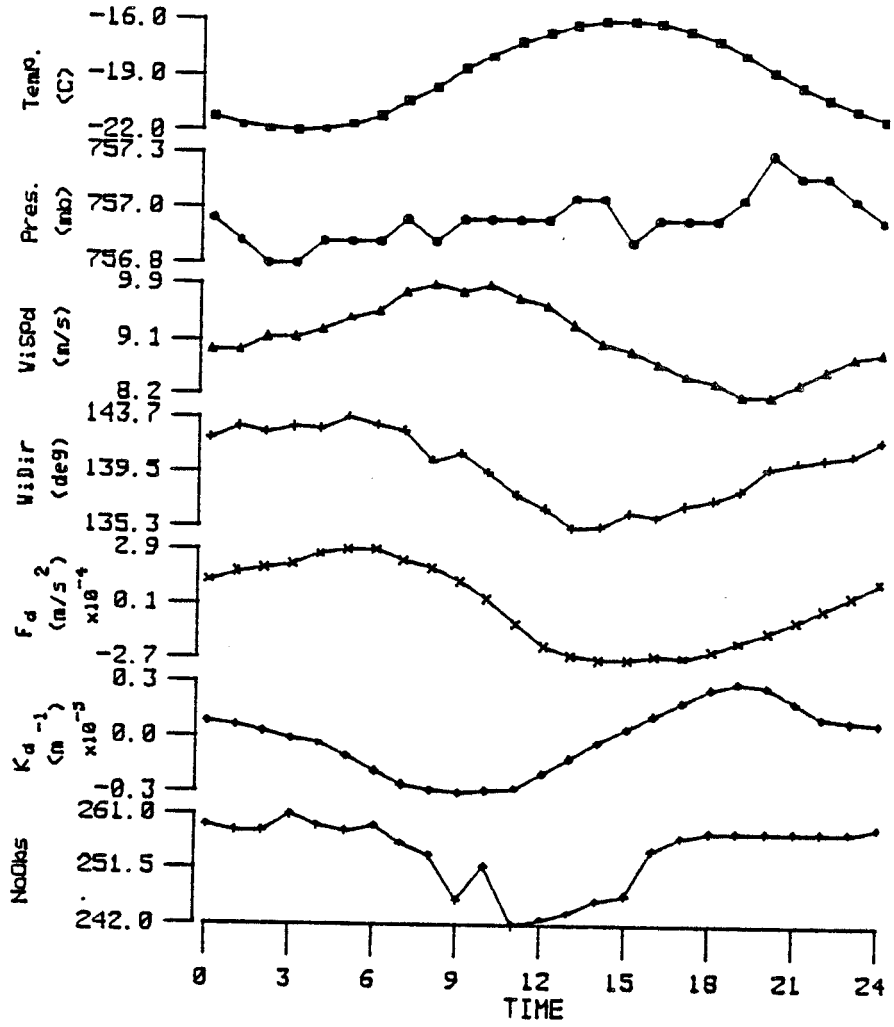

Fig. 3.2c The diurnal variations of temperature, pressure, wind speed, wind direction, pressure gradient force, friction coefficient, and the number of observations at D57. The method for calculating the diurnal variations of pressure gradient force and friction coefficient is explained in Appendix A.

stability found a few hours after the occurrence of a minimum temperature: 1) Temperature variations aloft lag behind the surface temperature variations. Riordan (1977) reports a phase lag of 5 hours between temperature at 32m and the surface in February at Plateau Station. 2) A decrease in the inversion depth due to the entrainment at the top of the boundary (Yamamoto, et al. 1979, Caughey et al. 1979), increases the temperature gradient. Mahrt (1981) suggested the existence of a nocturnal mixed layer, which is the remains of a daytime mixed layer. This nocturnal mixed layer, which is more turbulent than the layer beneath, might contribute to the decay of the stable boundary layer.

At D80 (Fig. 3.2d), the relationship between the diurnal curves of the wind vector, pressure gradient force, and the friction coefficient are different from those at D10, D47, and D57. Although the number of observations is very small relative to the rest of the stations, the mean deviation for each parameter is comparable to that found at the other stations (Table 3.1).

The diurnal pressure pattern (Fig. 3.2d) is semidiurnal, suggesting the influence of solar tides, a result of the global solar heating pattern (Chapman and

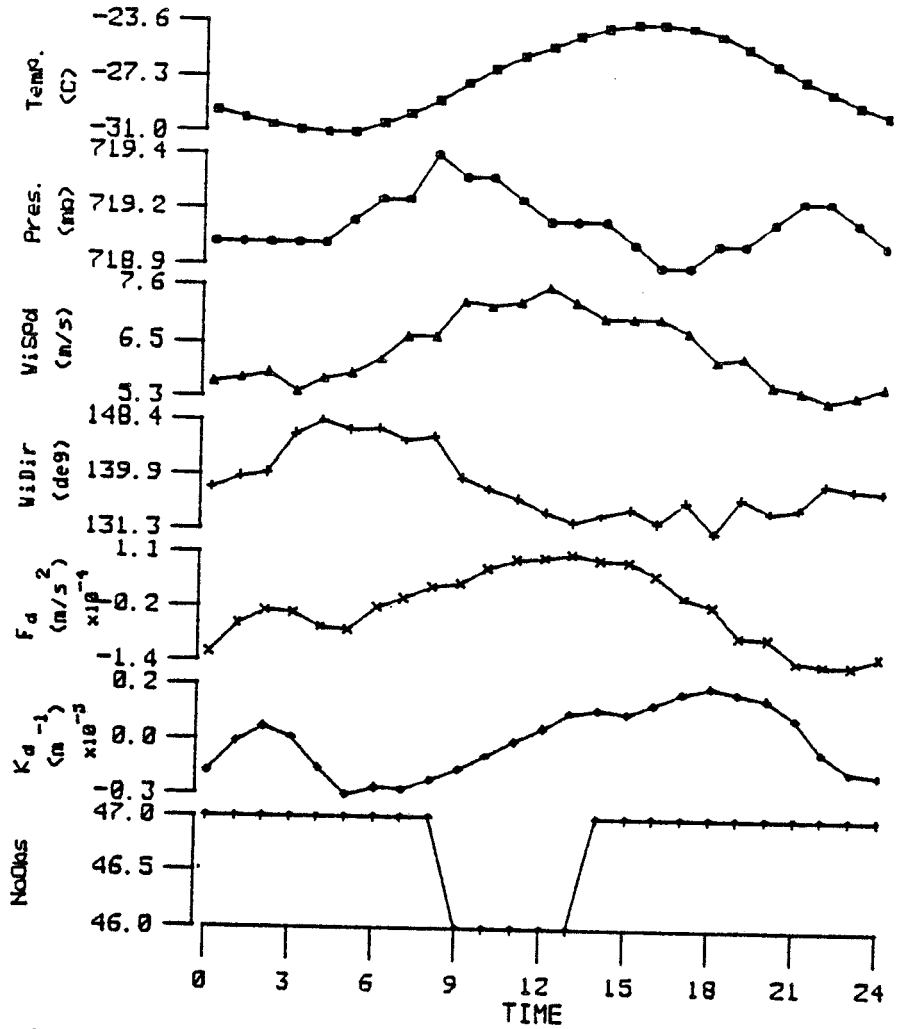

Fig. 3.2d The diurnal variations of temperature, pressure, wind speed, wind direction, pressure gradient force, friction coefficient, and the number of observations at D80. The method for calculating the diurnal variations of pressure gradient force and friction coefficient is explained in Appendix A.

Table 3.1 The average summer values for data from Automatic Weather Stations in Adelie Land.

Station	D10	D47	D57	D80	Dome C
Mean Temp.(^{o}C)	-4.4	-15.8	-19.0	-27.4	-35.0
Mean Dev.(^{o}C)	0.23	0.48	0.27	1.17	0.43
Mean Pres.(mb)	952.3	812.0	757.0	719.1	651.0
Mean Dev.(mb)	0.93	0.48	0.42	0.91	0.41
Mean Speed(m/s)	8.5	11.3	9.7	6.9	2.7
Mean Dev.(m/s)	0.34	0.42	0.24	0.40	0.11
Mean Dir.(deg)	151.4	140.4	139.9	143.4	199.5
Temp.Var. (^{o}C)	1.9	2.5	3.0	3.7	6.5
Dir. Constancy	0.91	0.95	0.94	0.91	0.48

Lindzen 1970). Such tidal variations are, however, both of inadequete magnitude and of the wrong phase to explain the wind variation. Because of the small number of observations (47 or 46) and the large deviation (the mean deviation averaged for 24 points is 0.9mb), the influence of the tidal wave on the wind vector cannot be proven.

The diurnal oscillations of temperature at D80 (Fig. 3.2d) and at the other stations have the same shape. Typical of interior plateau stations in Antarctica (Mather and Miller 1967), D80 has a maximum wind velocity at midday. In contrast to the stations mentioned above, at D80 the wind speed pattern matches the pressure gradient force pattern, and the wind direction pattern matches the inverse pattern of the friction coefficient. The larger total surface geostrophic wind at midday is explained by Loewe (1974) as mentioned in section 3.2 (Fig. 3.1). Although the pressure gradient force is large at midday, the wind direction is more cross-slope than at night due to the weak thermal wind at midday.

At Dome C, the diurnal curve of temperature variation is the same as that found at the other stations, but the variation is the largest among the

stations (Fig. 3.2e). At midday, the wind speed is at its maximum and the wind direction is closest to a cross-slope direction. The diurnal curve of the pressure gradient force fits well with the wind speed curve. The inverse pattern of the friction coefficient fits well with the wind direction pattern. Since Dome C lies in a flat area, the thermal wind must be negligible, even though there might be some effect from the slope leading towards Vinson Massif, the highest point in East Antarctica. Therefore, an explanation of the increase of the pressure gradient force at midday must be that it is the same as that found at D80 and in section 3.2 (Fig. 3.1).

Fig. 3.3 shows the diurnal variations of the wind vector. Each point is the average of values taken one hour before and after the hour indicated. The arrows show the mean wind vector. The shape of the diurnal variation of wind vectors is dependent upon the phase difference between the wind speed deviation and the wind direction deviation from the mean wind vector. The shape also depends on the changes in the thermal wind and the stability of the layer. At D10, the shape is almost oval stretching along the fall line, indicating the small phase difference between the wind speed and

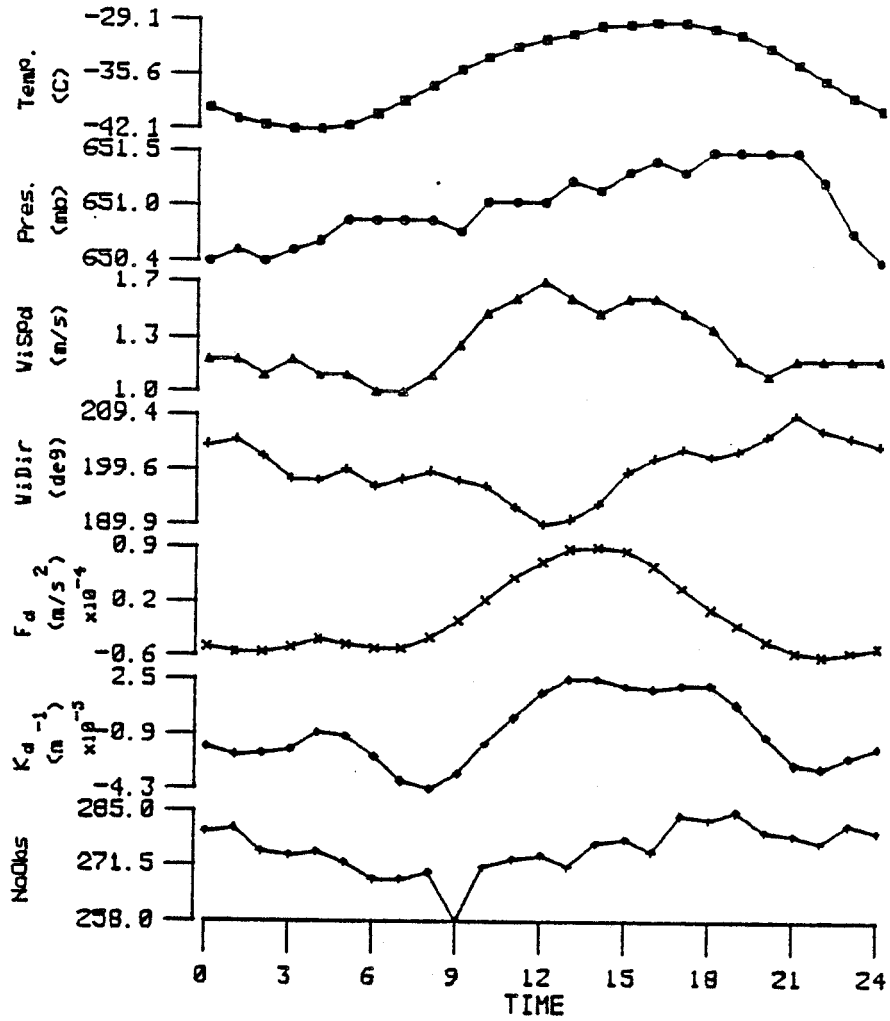

Fig. 3.2e The diurnal variations of temperature, pressure, wind speed, wind direction, pressure gradient force, friction coefficient, and the number of observations at Dome C. The method for calculating the diurnal variations of pressure gradient force and friction coefficient is explained in Appendix A.

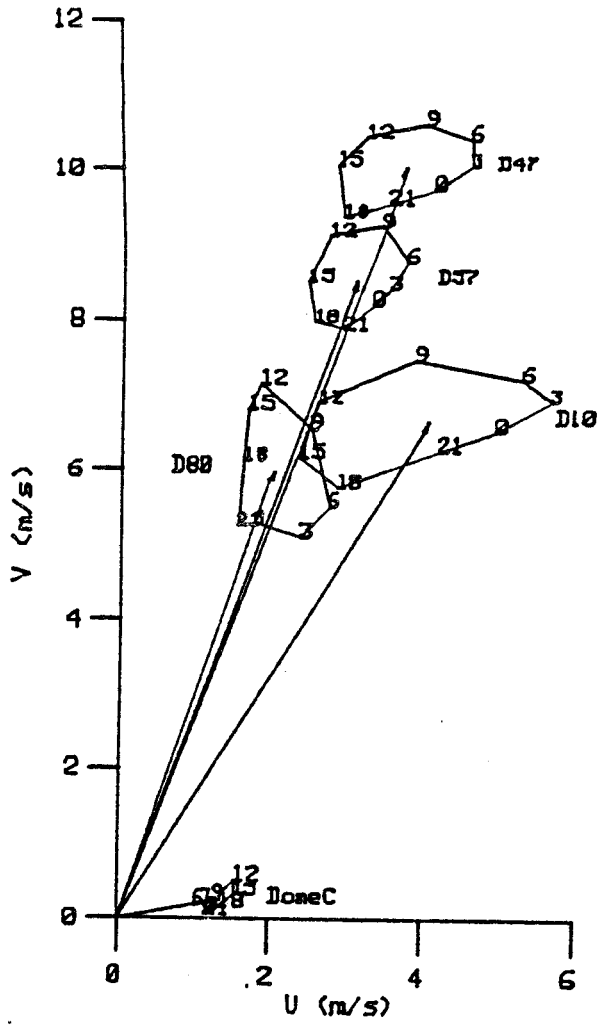

Fig. 3.3 The 3-hourly diurnal variations of wind vector for all Automatic Weather Stations in Adelie Land. The x-axis is the down-slope component of wind velocity and the y-axis is the cross-slope component of wind velocity. Each arrow shows the mean wind vector for each station. The number indicates the local solar time. Each point was averaged with the values one hour before and after.

wind direction. It becomes almost round at D47 and D57, and at D80 it becomes oval again stretching along the cross-slope direction. These changes are a result of the delay of the phases in the thermal wind and the stability in the boundary layer, which do not respond equally to the temperature variations at the surface. The same anticlockwise cyclic variations of the wind vector were reported by Riordan (1977) and Dabberdt (1970) for Plateau Station. At Dome C, a clockwise variation is found. However, since the variation is very small and the mean deviation is relatively large (Table 3.1), observational uncertainties can not be eliminated.

Fig. 3.4 shows the diurnal variation of the directional constancy of the winds, q. Table 3.1 shows that the mean constancy is very high for all stations except Dome C, where the value is almost half that of the other stations. Fig. 3.4 shows that, for D10, D47, and D57, the directional constancy is at its maximum in the early morning, indicating that the slope-induced thermal wind is important for the directional constancy of wind. At D80, in strong contrast, the directional constancy is low in the morning and reaches its maximum in the afternoon.

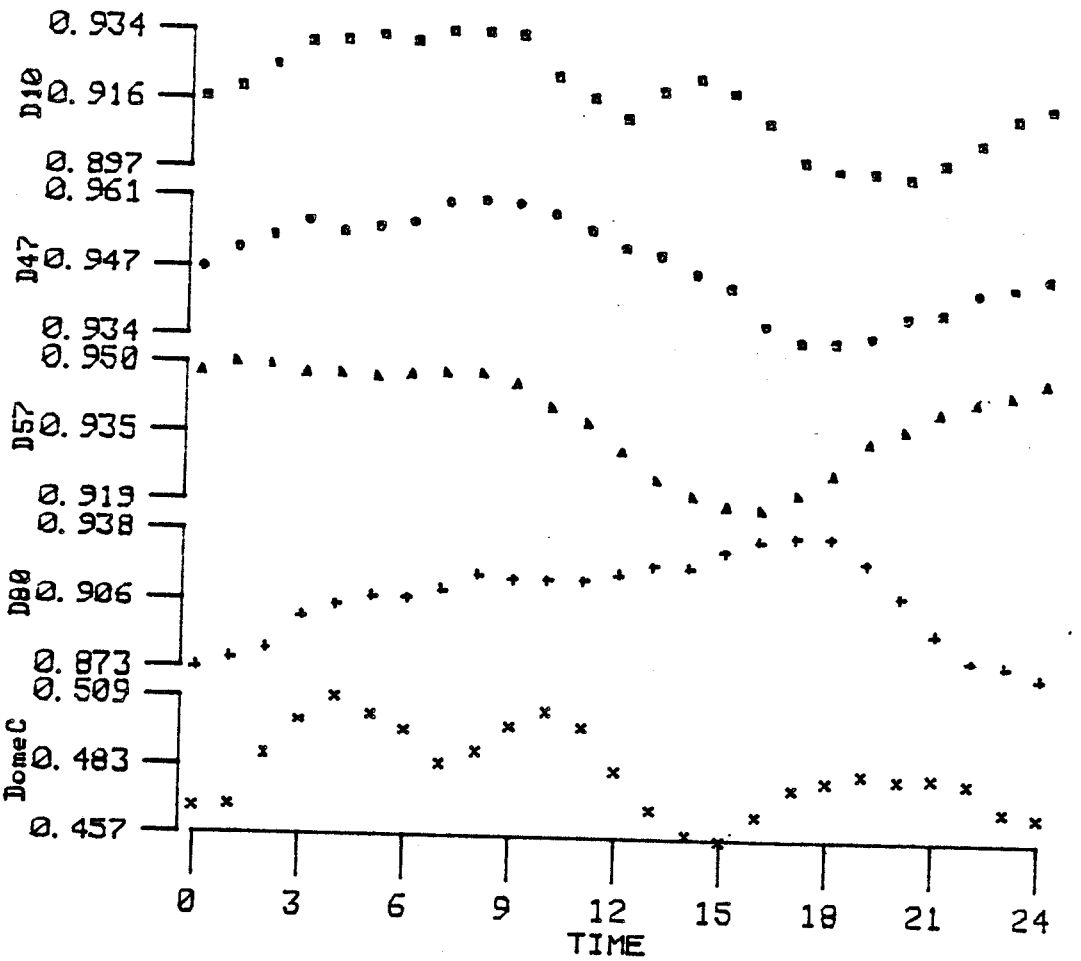

Fig. 3.4 The diurnal variation of the directional constancy of the winds, q, for all Automatic Weather Stations in Adelie Land.

These observations suggest that the direction of $\vec{G}_t$ is very consistent.

3.4 A Simulation

A simple time- and height- dependent model, developed by Sorbjan et al. (1985), is modified to simulate the diurnal variation of katabatic wind. The model is explained in Appendix B. The equations used in the model assume a balance of the Coriolis, frictional, and pressure gradient forces, which include components generated by a slope and by synoptic baroclinicity, resulting in a non-zero wind acceleration. Simple time- and height- dependent parameterizations are developed for the eddy viscosity and the slope induced thermal wind v_T. The values of v_T are allowed to vary as a sinusoidal function of time.

The tests for four different orientations of $\vec{G}_t$ are performed using the steady-state version of the model for the different parameterizations. The results are shown in Fig. 3.5. The figure at the left is obtained using a relatively large thermal wind and a small eddy viscosity. Note that the surface wind direction does

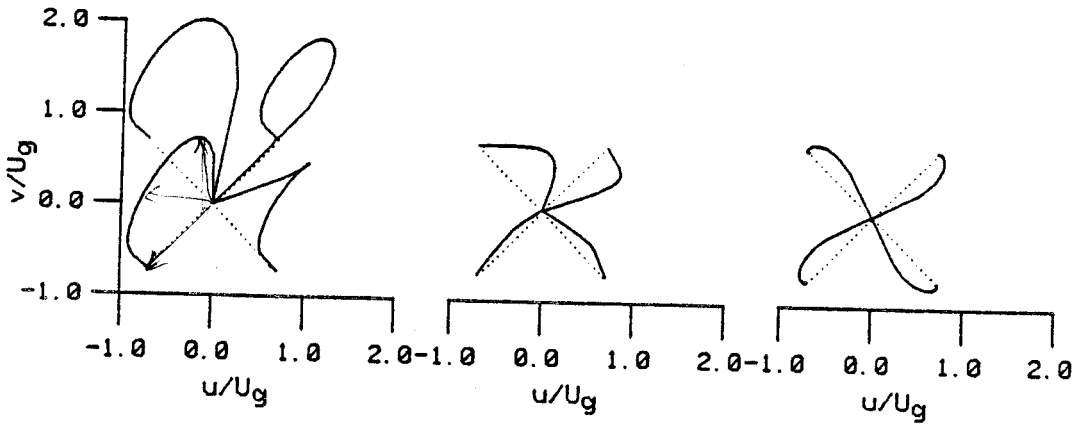

Fig. 3.5 Hodographs of the wind vectors obtained from the steady-state version of the model, for different orientations of the geostrophic wind vectors. A test of the role of the main factors influencing the flow over Antarctica:

1. v_T = +15 m/s; k_o = 1 m^2/s
2. v_T = +15 m/s; k_o = 20 m^2/s
3. v_T = +1 m/s; k_o = 1m^2/s

Dots indicate the direction of the geostrophic winds at the top of the ABL. x-axis of the coordinate system is oriented downslope. Eddy viscosity, $k = k_n$.

not change much for any of the four directions of $\vec{G}_t$, varying by less than 70^{o}. Mahrt and Schwerdtfeger (1970) obtained almost the same result, which was used to explain the high directional constancy in the katabatic wind in Antarctica. However, from the center figure and the right figure, it is obvious that the surface wind direction is dependent on the direction of $\vec{G}_t$ when, respectively, the eddy viscosity is large, or the slope-induced thermal wind is small. These results lead to the conclusion that the relatively high directional constancy in summer or during the day, when the thermal wind is weak at the slope stations in Adelie Land, must be caused by $\vec{G}_t$ having a constant direction.

Wind hodographs obtained from a 24 hour simulation of the model are shown in Fig. 3.6. Nighttime simulated hodographs have a spiral shape. The strongest low level jet is obtained about 9 hours after the beginning of the simulation, which is equivalent to 3:00 A.M. local time.

Fig. 3.7 shows two simulated diurnal variations of wind speed and wind direction. Note that a smaller value for wind direction denotes a more down-slope

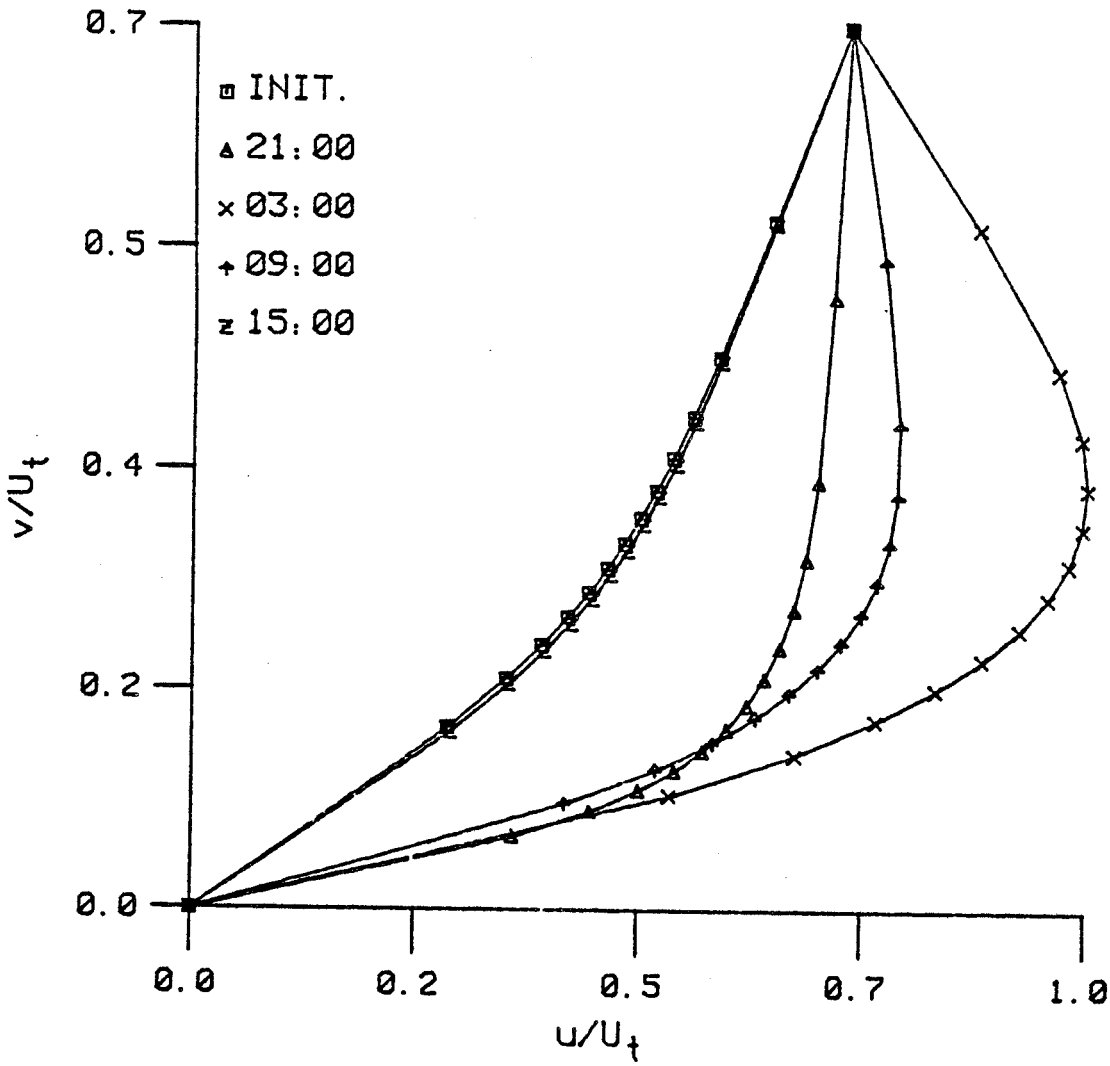

Fig. 3.6 Wind hodograph obtained by 24-hour simulation of the model, U_t - wind velocity at the top of the boundary layer. v_T = 15 m/s, k_o = 30 m^2/s.

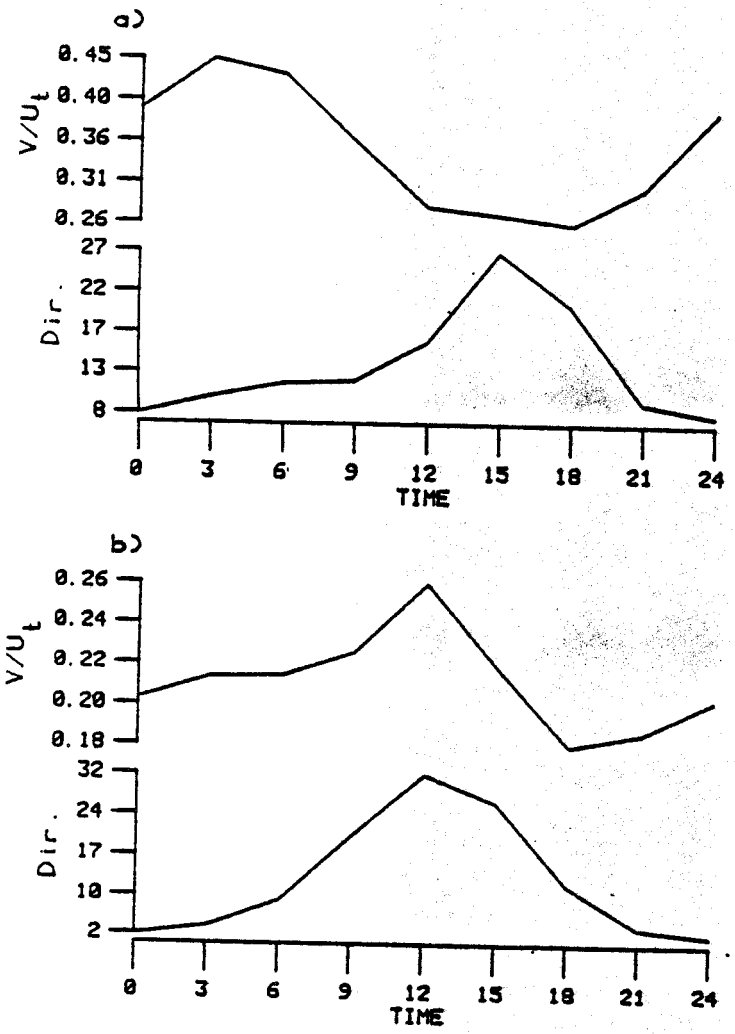

Fig. 3.7 The simulated diurnal variations of wind speed and wind direction. Note that the smaller values of wind directions indicate greater down-slope directions of the flow. The parameters are: a) v_T = 15 m/s, k_o = 20 m^2/s, and b) v_T = 4 m/s, k_o = 30 m^2/s.

direction of flow. $\vec{G}_t$ is kept equal in both cases, but eddy viscosities and thermal winds differ. In each case, the variation in wind direction is quite similar. However, the curves of wind speed variation differ, that in Fig. 3.7a having its maximum in the early morning and that in Fig. 3.7b at midday. The curves in Fig. 3.7a are similar to the curves of wind vector variation at D10 (Fig. 3.2a). The same comparison can be made between curves in Fig. 3.7b and Fig. 3.2d at D80. We can conclude from Fig. 3.7 that,

assuming $\vec{G}_t$ to be consistent, the diurnal variation of wind vectors depends on the variation in eddy viscosity and slope-induced thermal winds. The phase difference is controlled by these two factors.

3.5 Summary

Mather and Miller (1967) first documented the occurrence of maximum wind speeds at midday at the stations on the interior plateau of Antarctica. In this chapter, the diurnal wind vector variation was analyzed. The wind speed curves at D10, D47, D57, and D80 showed a similar pattern, but the time of maximum

wind speed shifted from early morning (D10) to midday (D80). Data from AWS and a simple model simulation showed the influence of slope-induced thermal wind, eddy viscosity, and geostrophic wind at the upper boundary on the diurnal variation of wind vectors in Adelie Land.

4 CORELESS WINTER IN ADELIE LAND

4.1 Introduction

As noted in Fig. 2.2, a 'coreless' or 'kernlose' winter temperature pattern is obvious. In April it is already nearly as cold as in the following six months. A longer period of observation would show a smoother than the irregular pattern shown in Fig. 2.2 caused by a single warm period in the winter.

The historical background for the theories of coreless winter are reviewed in section 4.2. In section 4.3, the extremes of temperature in Adelie Land in winter are analyzed in relation to the other meteorological components, followed by a new explanation of the cause of the coreless winter temperature pattern in section 4.4. This chapter is summarized in section 4.5.

4.2 Theories of the Coreless Winter

In the middle of the 19th century the famous Baltic-Russian explorer von Middendorf noted that the

temperature, the "core", or "kern". Hann, quoting Middendorf, stated that a "kern" is not found in the European part of the Arctic. Pollog later studied the winter temperature patterns in Europe and called the prolonged period of uniform winter temperatures, "kernlose", a modification of Hann's term (Loewe 1969). Before Pollog, Simpson (1919) had already noted the existence of a very developed coreless winter in the Ross Sea area of Antarctica. The following is a short historical note by Schwerdtfeger (1984) concerning Siple's observations:

> "When Paul Siple came to the South Pole on 30 November 1956, the first scientist to stay for a full year at that far-out place, he did not hesitate to dig, in 4 days of hard work, a 5.5 meter-deep pit. The purpose was to measure the temperature which at that depth comes close to the mean annual value. Knowing about the summer temperature on the plateau from Amundsen's and Scott's reports, and assuming the temperature of the coldest month should be as much below the annual mean as the summer values are above it ("like it is in

most other places"), he concluded the average temperature of the coldest month might drop below -84°C (-120°F), a possibility he considered "half in apprehension and half in excitement" (Siple 1959). Ten months later, he was surprised as well as relieved to find that the winter of the Antarctic Plateau is different. In 1957, the coldest month was September with a mean temperature of -62.2°C and the lowest minimum of -74°C."

Schwerdtfeger (1970) pointed out that the tempearture inversion strength in the atmosphere never exceeded a limit of 40°C, and in his model he assumes the existence of an equilibrium state in which long wave radiation loss in winter is balanced by atmospheric back radiation, vertical eddy flux of heat, heat conduction from the ground, and heat of sublimation. Also, he speculated that warm air advection is an important item in this heat balance.

Wexler (1958) attributed the reversal of the temperature trend to warm air advection associated with increased cyclonic activity during these months. According to his hypothesis, this cyclonic activity was

caused by baroclinic instability resulting from the great temperature contrast between the cold Antarctic continent and the surrounding oceans. This zone of high temperature contrast moved northwards later in the season as the Antarctic pack ice formed, leading to the eventual return of colder temperature. However, van Loon (1967), in considering the Ross Sea region, noted a shortcoming in Wexler's theory by pointing out a wintertime rise of mean pressure over the other southern hemisphere continents. This causes an amplification of the planetary wave pattern which is apparently greatest in that half hemisphere in which Australia is centered and results in an increase in warm air advection.

Loewe (1969) stated that Wexler's explanation for advection of warm air is correct for coastal areas but does not apply to inland areas where more pronounced warm spells are found, and that van Loon's explanation is correct for the Ross Sea area but does not apply all over Antarctica or the Arctic. He, as well as Thompson (1969), concluded that radiation is the main reason for coreless winters in high latitudes. Heat transport, a consequence of radiation, is probably only a contributory cause for coreless winters. The outflow

of cold air along the dome-shaped ice surface in Antarctica and in Greenland leads to descent of the warmer air above. The larger the cooling by radiation, the stronger will the outflowing wind be, and the more vigorous the mixing with the warmer air above. This mixing, extended over a period of time and tending to halt a drop in temperature, produces a coreless winter.

However, the supply of warm air aloft to the surface is limited unless warm air advection from lower latitudes is assumed. Loewe's explanation for coreless winters would be true for each episode of warm spells, but, without a horizontal influx of warm advective air, the temperature would generally decrease. This temperature decrease has never been observed.

Sinclair (1981) studied the extremely high summer temperatures of December 1978, and reported that advection of exceptionally warm, maritime air by strong winds from lower latitudes is an important heat source. He suggested that cyclogenesis at the high latitudes and simultaneous intensification of anticyclonic flow seem to be necessary conditions for the intense poleward advection.

4.3 Results

Fig. 4.1 shows the monthly mean air temperature for three stations on the slope of Adelie Land in 1983. The three stations were chosen because a large set of data was available. This figure shows the coreless winter temperature patterns with their distinctive reversals of the expected curve in June and September. If the mean of temperatures over a long period were taken, one would expect the curve to be U-shaped and to have less pronounced reversals (Schwerdtfeger 1970). Although average potential temperatures in summer are similar for all stations, in winter the potential temperature at D80 is much lower than at D10 or D47. The temperature curves, however, are very similar for the three stations, indicating that the warm spell is a phenomenon throughout Adelie Land. From February to April the drop in temperature is steep and in the months of May and June a warming of the temperature is observed. In July all stations recorded the coldest monthly mean temperatures. Warm spells are seen in August and September and a cold spell is again observed in October.

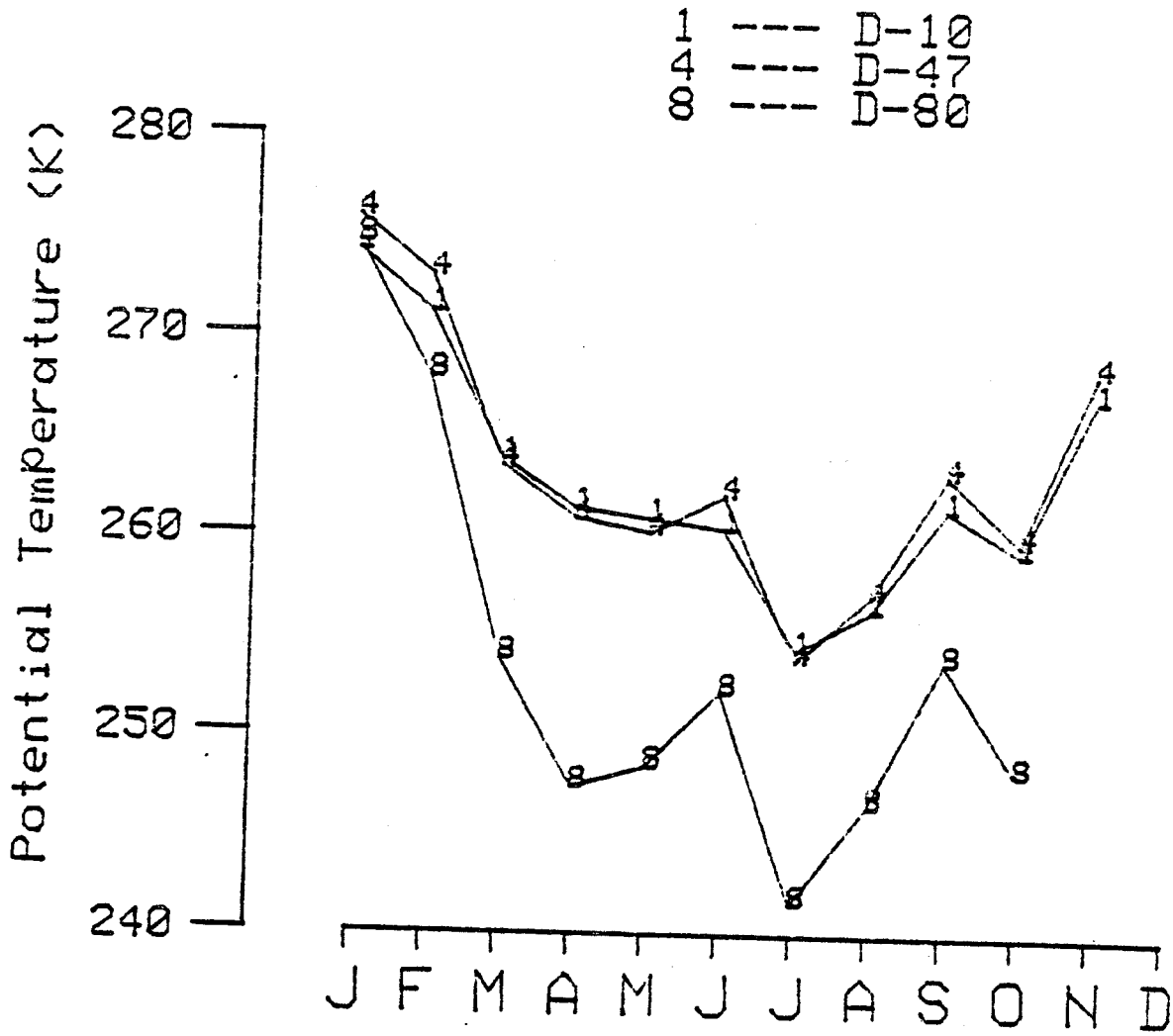

Fig. 4.1 Monthly averages of potential temperature for the stations in Adelie Land in 1983.

To define warm and cold spells objectively, all data from April to September were taken and absolute temperature deviations larger than one standard deviation from the mean were defined as warm or cold spells, depending on the direction of the deviation.

Table 4.1 shows the differences of the mean pressure, resultant wind speeds and directions from the overall averages and the chances of falling and rising pressure for warm and cold spells. Surprisingly, during warm spells the atmospheric pressure is higher than the averages for all three stations, and lower during cold spells. This is just the opposite of Wexler's (1958) explanation that: a) warm spells are caused by increased warm air advection, which is normally connected with increased cyclonic activity; b) cold spells are expected to be caused by decreased warm air advection and decreased cloudiness, both typical of an anticyclone.

In Fig. 4.2 the pressure is plotted against temperature. Correlation factors of 0.22 to 0.25 were found, which are significant at the 99% level.

Table 4.1 shows that wind speeds and also the directional constancy (see also chapter 2.3) are usually lower than average during both warm and cold

Table 4.1 The mean deviations in pressure, wind speed, directional constancy, and resultant wind direction, from their averages and the chances of pressure tendency for the cases of the temperatures which deviate more than one standard deviation (σ_T) from the average, for three stations in Adelie Land, Antarctica.

Station	Temp.	$\overline{P'}$ (mb)	$\overline{WS'}$ (m/s)	$\overline{q'}$	$\overline{WD'}$ (deg)	Chance rising pres. (%)	Chance falling pres. (%)
D80	$>+\sigma_T$	+12.4	-1.3	-.206	-12.0	62	38
	$<-\sigma_T$	-8.3	-0.6	-.144	+4.0	33	67
D47	$>+\sigma_T$	+9.7	-0.8	-.036	-12.0	62	38
	$<-\sigma_T$	-5.8	+0.5	+.012	+10.0	29	71
D10	$>+\sigma_T$	+9.2	-0.5	-.095	-4.0	63	37
	$<-\sigma_T$	-4.0	-2.1	-.054	+3.1	28	72

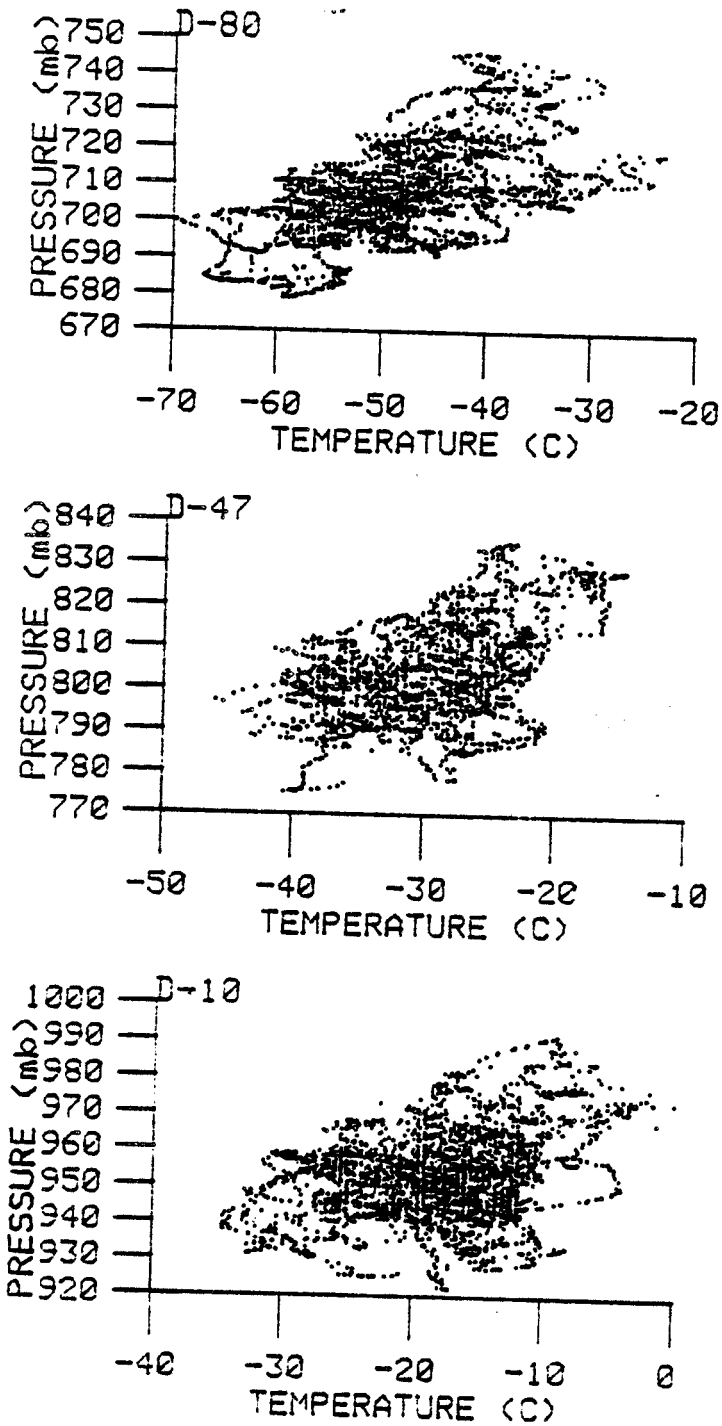

Fig. 4.2 Pressure versus Temperature, for D80, D47, and D10.

spells, except in the cases of the cold spells at D47. The deviations for wind speed and directional constancy at D47 are small relative to those at the other stations. The variations of mean monthly wind speed and directional constancy at D47 during winter months (Table 2.1) are also smaller relative to the other stations. The resultant wind directions during warm spells are more cross-slope and more down-slope during the cold spells. Table 4.1 also shows that the pressure was falling when two-thirds of the warm spells were observed, and rising when about 70% of the cold spells were observed.

The weather maps of the surface and 500 mb level were examined in order to find pressure distributions related to warm and cold spells. Figs. 4.3a and b show the typical pressure distribution at the surface and at 500 mb during warm and cold spells. Although the number of meteorological stations is only 25 in an area of 35×10^6 km^2 south of 65°S, compared to 340 such stations on the 9.5×10^6 km^2 of the U.S.A., they are sufficient to approximate the synoptic pressure distribution during cold and warm spells. Fig. 4.3a is the pressure map at 00Z, 20 June, 1983, exemplifying a warm spell. Temperature deviations of greater than two

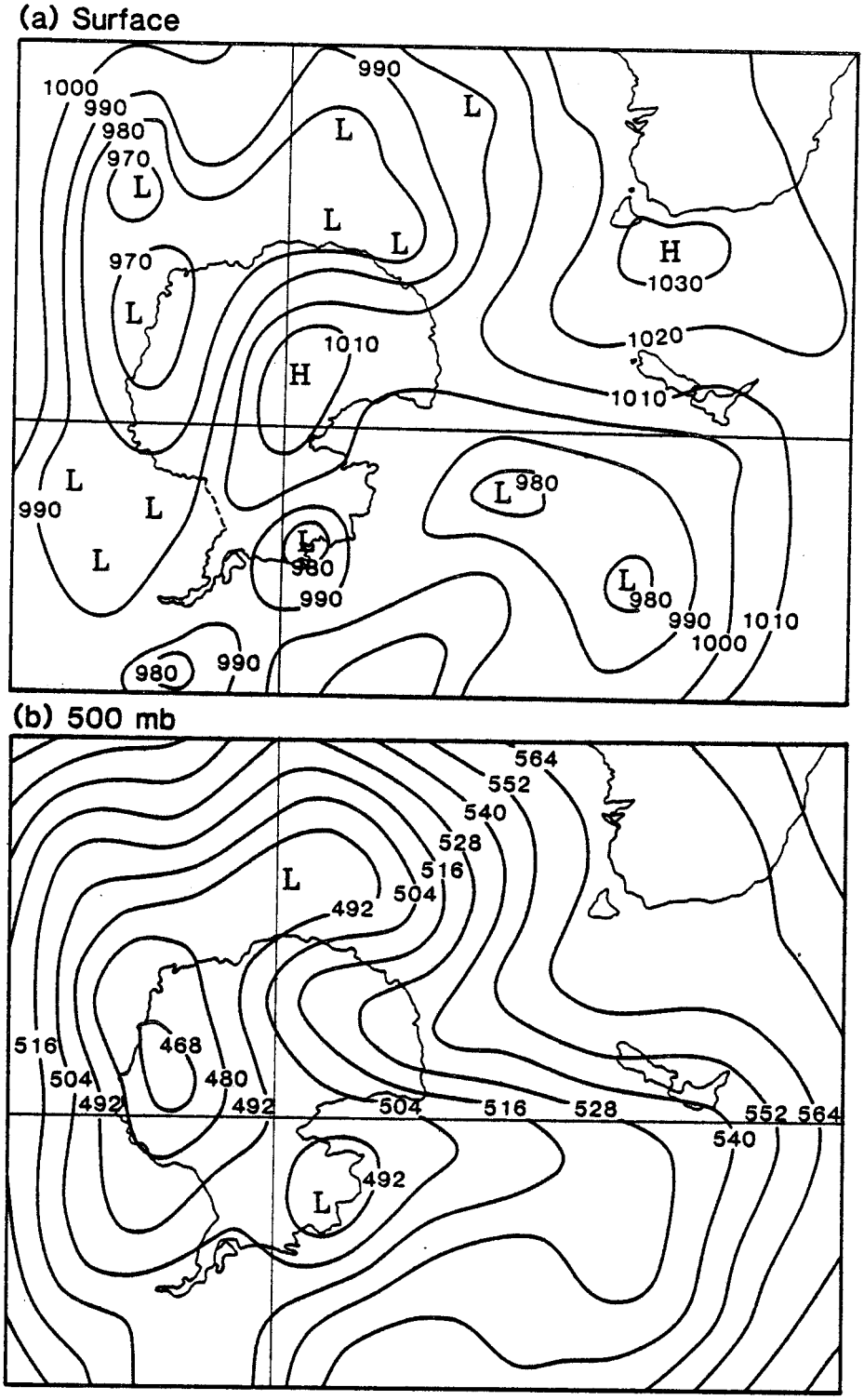

Fig. 4.3a Sea-level (a) and 500 mb (b) pressure charts for 00Z 20 June 1983.

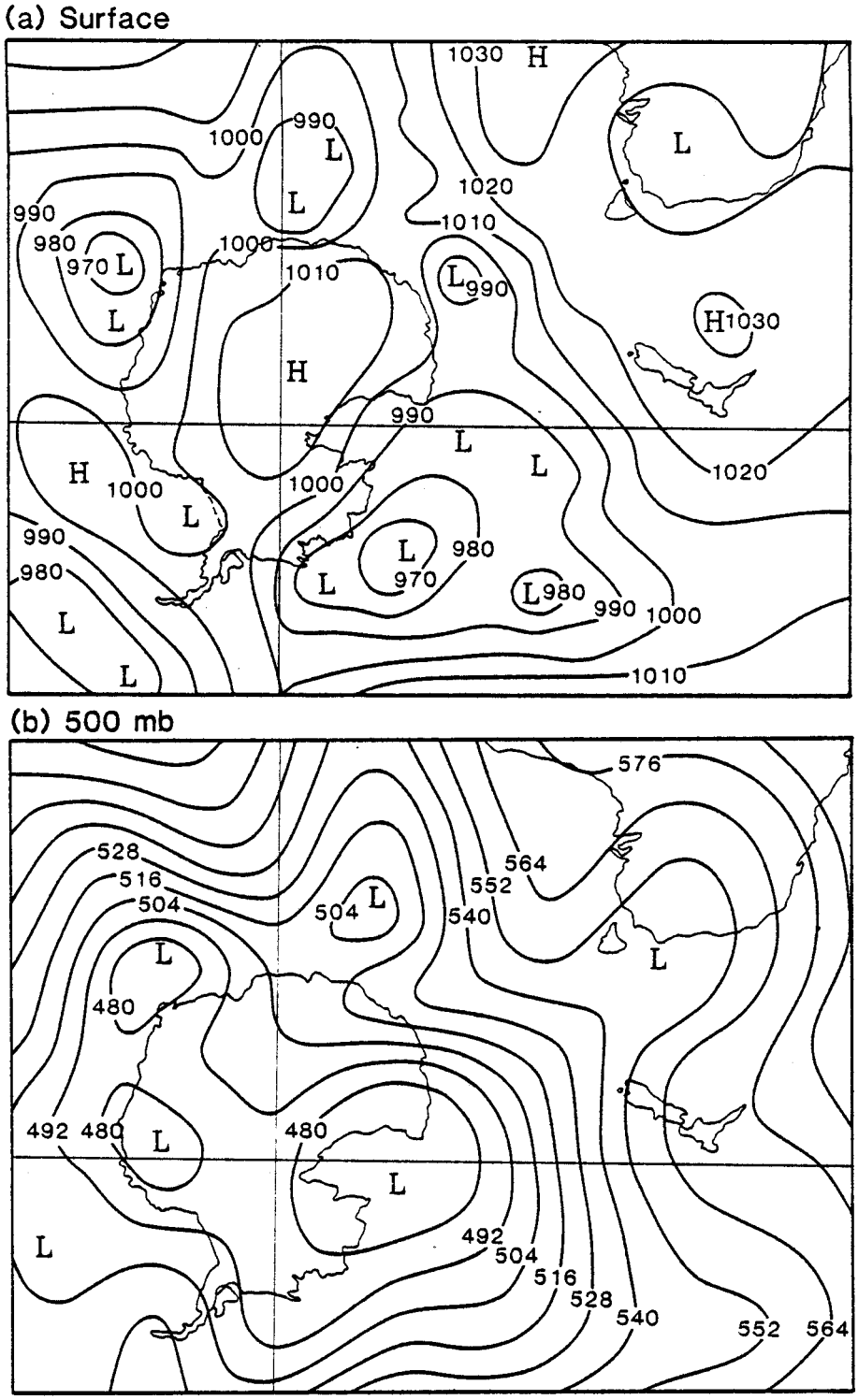

Fig. 4.3b Sea-level (a) and 500 mb (b) pressure charts for 00Z, 6 July, 1983.

standard deviations were observed at all stations. On the surface map, the antarctic continental anticyclone is connected with the high pressure to the east of Tasmania. The ridge connecting these two highs lies to the east of Adelie Land, which causes maritime air to enter the antarctic continent. In the 500 mb map, the ridge intrudes into Adelie Land, and the south-north air mass exchange is pronounced.

In contrast, during a cold spell (00Z, 6 July, 1983) the ridge in the pressure map (Fig. 4.3b) lies to the west of Adelie Land, now under the influence of the cyclone centered over the Ross Sea to the east. Similarly, the 500 mb map shows that the direction of the flow is from the south, indicating a cold continental air mass coming into Adelie Land.

4.4 Discussion

To find one explanation for the high atmospheric pressure associated with above-normal temperatures, the effect of the continental anticyclonic ridge can be examined. High atmospheric pressure at the stations in Adelie Land indicates that the anticyclone over the

Antarctic plateau is stronger than normal. This extends and intensifies the pressure ridge between the two semi-permanent cyclones which are situated at 100°E and 170°W just off the coast of the antarctic continent (Schwerdtfeger 1970). Since this pressure ridge normally moves eastward and the pressure usually falls at the stations during warm spells (Table 4.1), the ridge must be located to the east of the stations (Fig. 4.3a). Because northernly maritime air flows on the west side of the ridge, high temperatures can be the result of the warm air advection explained above. If this holds true, a shortcoming of Wexler's explanation for the coreless winter would be overcome. He could explain the coreless winter temperature for the coastal stations by increased cyclonic activity. However, the pronounced coreless winter temperature pattern on the interior plateau is difficult to explain in this manner. The explanation which takes into account the warm air advection associated with anticyclones, makes the coreless winter temperature patterns more plausible for the inland stations. The subsidence of warm air aloft to the surface boundary layer is also more likely to occur under the influence of anticyclones than under the influence of cyclones.

Cold spells in Adelie Land are associated with low pressure areas lying over or to the east of the Ross Sea. When the cyclone intensifies, it also brings cold air from the central part of the continent toward the coast. At this time, the high pressure ridge from the continental anticyclone is frequently located to the west of the stations. Therefore, when the cold airmass flows out from the central part of the continent, it brings abnormally cold temperatures to the stations.

The above explanation for the extremes in temperature do not apply everywhere in Antarctica or in the Arctic. However, it can be applied to the areas where the anticyclonic ridge is frequently located. According to Berson and Radok (1960), there are preferable areas for the formation of an anticyclonic ridge along the meridional lines of 0^{o}, $60^{o}W$ (Antarctic Peninsula), $120^{o}W$, and $140^{o}E$ (Adelie Land). In these areas, the same relationship between temperature and pressure found in Adelie Land can be observed.

4.5 Summary

The temperatures at the stations in Adelie Land are controlled by the heat budget of the boundary layer, especially by the radiation balance and by the latent and sensible heat fluxes. However, in order to explain the high temperatures associated with high pressures and the low temperatures associated with low pressures, it is necessary to seek the reasons in advection. During warm spells, the continental anticyclone extends its ridge to the east of Adelie Land, connecting at times with New Zealand or Australia anticyclones, and brings maritime air into Adelie Land. On the other hand, cold spells are mainly controlled by the semi-permanent cyclone over the Ross Sea, which acts on the continental anticyclonic ridge situated to the west of Adelie Land, and increases the flow of continental cold air towards the periphery of the ice dome.

5 THE TEMPERATURE GRADIENT OVER ADELIE LAND

5.1 Introduction

Radok (1973) first pointed out the importance of the effect of the vertical gradient of surface temperature on the magnitude of the true horizontal temperature gradient, which determines the actual thermal wind. The vertical gradient of surface temperature is defined as the surface temperature change between two stations divided by their difference in elevation. This factor is usually ignored in model and simulation studies. For example, Dalrymple et al. (1966) neglected this term, and as a result, the magnitude of the thermal wind estimated from the model using the wind observations was found to be twice that estimated from the inversion strength (Radok 1973). The pronounced variations in temperature existing on the surface of the antarctic ice sheet have been reported by many glaciologists, e.g. Budd et al. (1971) and Kane (1970), who analyzed 10m firn temperatures. Vertical gradients of surface temperature on the slope as large as $-2^{\circ}C/100m$ were reported by Budd et al. (1971). This means that if the vertical gradient

of surface temperature is less than -1°C/100m, an air parcel going down the slope is experiencing warmer air around it. This could cause acceleration down the slope or an increase in the magnitude of the thermal wind.

Several different assumptions have been used by modelers to describe the temperature structure in the inversion layer along the slope. Mahrt and Schwerdtfeger (1970) assumed the isotherms to be parallel to the inclined surface and temperatures to be constant along the slope surface. Schwerdtfeger (1975) discussed the effect on the inversion strength of the product of the inversion height variation and the average change of temperature along the fall line, but found it to be negligible. Radok (1974) mentioned the importance of surface temperature change along the slope plus the inversion strength on the slope in estimating the total horizontal temperature gradient. Ball (1960) assumed an isothermal condition for both the inversion layer and the free atmosphere with a discontinuous temperature jump at the interface. Parish (1982) used Ball's assumptions, but extended them to include variations in the inversion height and the effect of entrainment of air at the top of the inversion layer.

In this chapter, utilizing the data from AWS, we will discuss the wind and temperature of Adelie Land, making particular reference to the vertical gradient of surface temperature along the slope.

5.2 Results

As mentioned in chapter 2.1, the annual mean temperature distribution could be characterized by three zones: high plateau, intermediate plateau, and coastal. The differences in mean annual temperatures between the high plateau stations and the intermediate plateau stations and between the intermediate plateau stations and the coastal stations are the same, about $20^{o}C$ (Fig. 2.1). However, since the elevation difference between the high plateau stations and the intermediate plateau stations is less than 1500m (Table 1.1), the rate of change in temperature with respect to elevation is superadiabatic, whereas it is close to the value of the dry adiabatic lapse rate between the intermediate plateau stations and the coastal stations, where the elevation difference varies from 1500m to 2000m. This characteristic of temperature distribution

in Adelie Land is well illustrated in Fig. 5.1, which shows the monthly averages of potential temperatures for four stations on the slope and Dome C station for the years of 1982 and 1983. The differences in the potential temperature between D10 (coastal station) and D47 or D57 (intermediate plateau stations) are very small (<2K) throughout the year, whereas the differences between Dome C or D80 (high plateau stations) and D57 or D47 are very large (15K) during the winter months. Fig. 5.2 shows the variation of mean monthly vertical gradients of air temperature between the stations. The vertical gradient of temperatures between the coastal stations (D10) and intermediate plateau stations (D47 and D57) show the values to be very close to the dry adiabatic lapse rate throughout the year. This is also true for summer months between the intermediate plateau stations (D47 and D57) and the high plateau stations (D80 and Dome C); but in winter months, they reach over $2^{o}C/100m$, or twice the dry adiabatic lapse rate. Budd et al. (1971) found the same feature in the surface temperature - elevation gradient (the surface temperature measurements are taken from the firn 10 m below the surface, where they assumed that temperatures

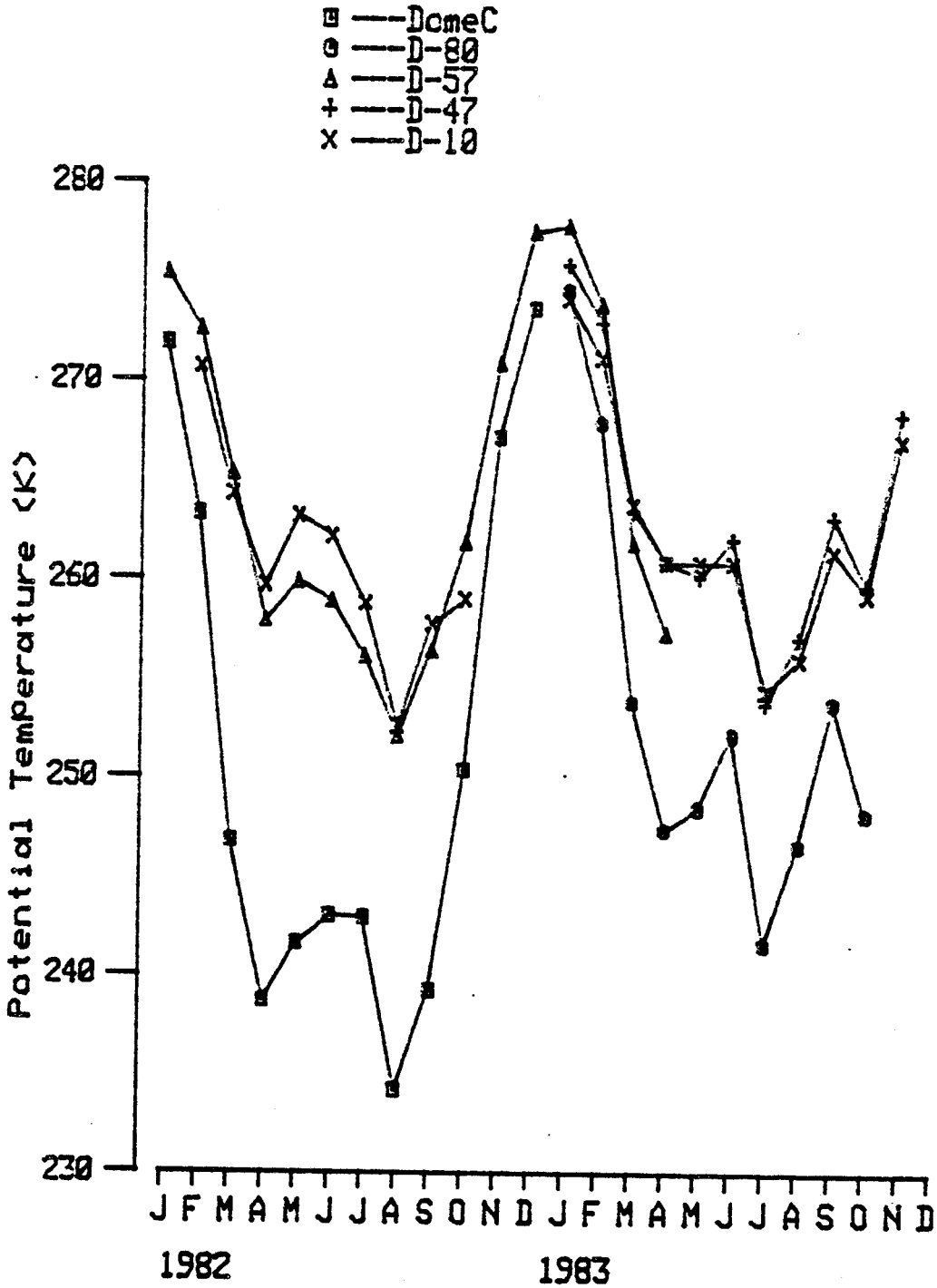

Fig. 5.1 Monthly averages of potential temperature for the stations in Adelie Land for 1982 and 1983.

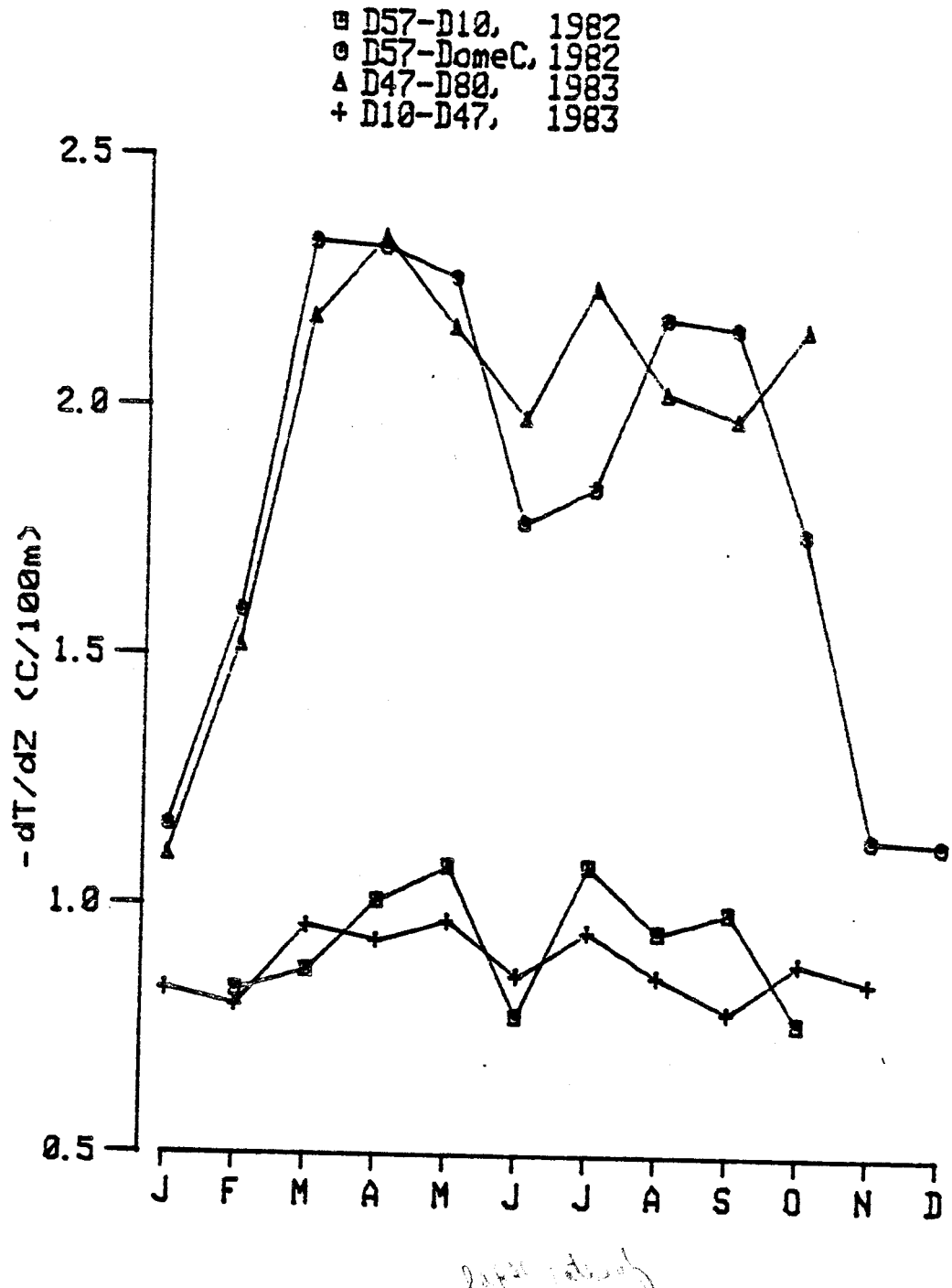

Fig. 5.2 The monthly mean vertical surface temperature gradient between the stations in Adelie Land, Antarctica.

correspond to the mean annual surface temperatures). The change in temperature gradient from the high plateau stations to the intermediate plateau stations is mainly due to the change in the surface heat budget, which reflects the transition from the low windspeeds on the high plateau stations to stronger katabatic winds on the intermediate plateau stations.

In Fig. 5.3, the wind speed, resultant wind direction, and potential temperature are given for summer and winter for each station. "Summer" is defined as the months of December and January, and "winter", as the months from April to September. In the top figure, except for D10, the wind speeds are proportional to the steepness of the slope, as predicted by Ball's model (1960). The lower wind speeds at D10, where the slope is greater than at D47 and D57, can possibly be explained by the hydraulic jumps and the uneven terrain, as discussed in chapter 2.3.

In the middle figure in Fig. 5.3 and Table 1.1, the flow is generally more downslope in winter than in summer. According to Gosink (1981), Ball's steady state uniform model predicts a deviation angle, α, from the fall line:

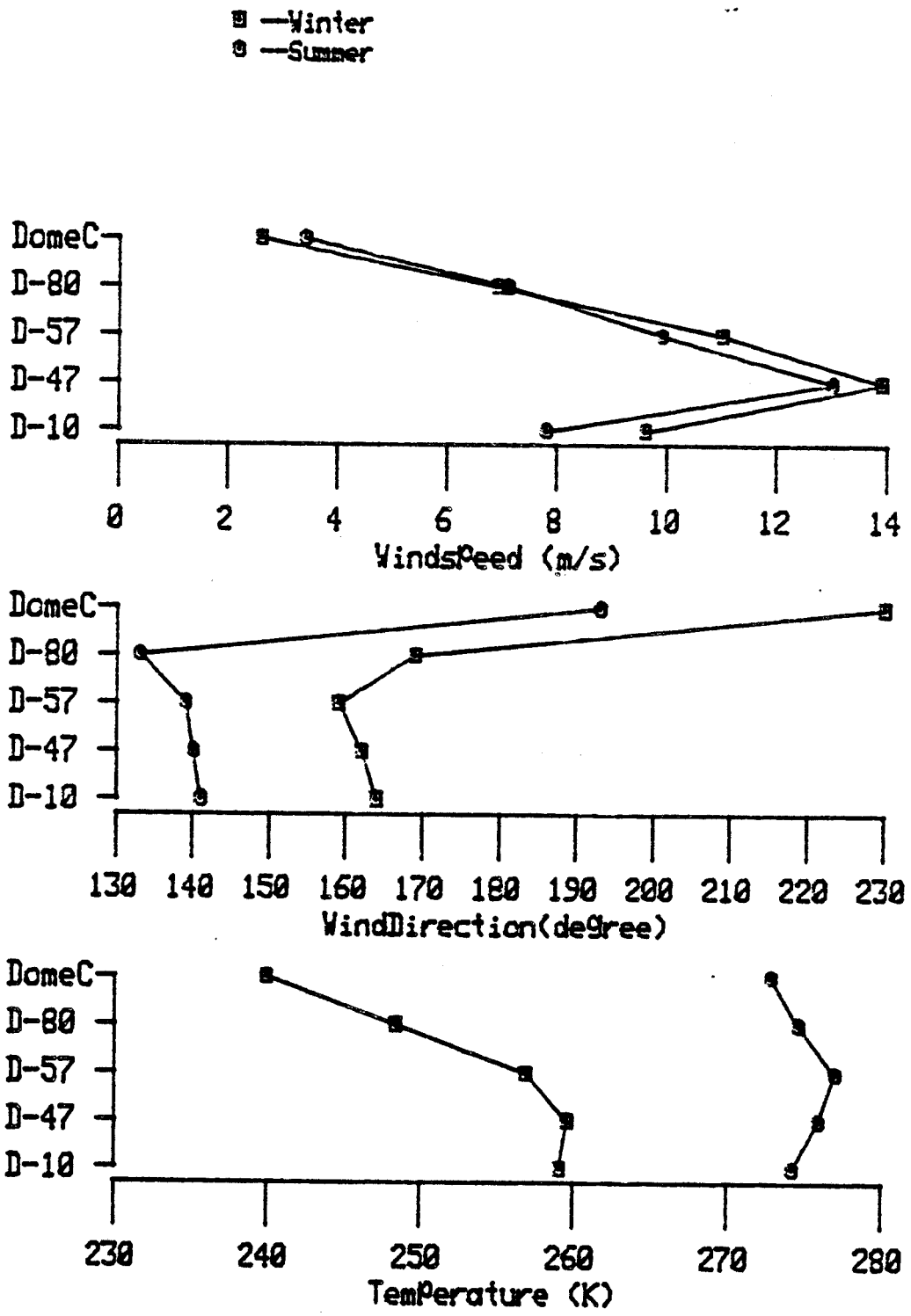

Fig. 5.3 The wind speed, resultant wind direction and potential temperature for summer and winter for the stations in Adelie Land, Antarctica.

$$\alpha = \arcsin\left[\left(\frac{fV}{F}\right)\right] = \arcsin\left[f\left(\frac{Q}{kF^2}\right)^{1/3}\right] \quad (5.1)$$

where $Q = uh$ expresses the net downslope transport of the medium; u is the down-slope component of wind speed; h and k are, respectively, the depth of katabatic flow and the friction coefficient; f and V are the Coriolis coefficient and the wind speed, respectively. V can be described as:

$$V = \left(\frac{FQ}{k}\right)^{1/3} \quad (5.2)$$

where F is the total pressure gradient force. With a negligible wind above the inversion layer, F can be expressed as:

$$F = \beta\theta'\psi \quad (5.3)$$

Eqs. 5.1 to 5.2 indicate that the deviation angle is inversely proportional to the 2/3 power of the inversion strength and the slope. Therefore, greater downslope flow in winter than in summer could be explained by the larger inversion strength in winter. For both seasons, the steeper slope stations show more downslope flow. An exception is at D80 where the

deviation angle in winter is smaller (more downslope) than at D57 where the slope is steeper. The reason for this may be due to a combination of smaller values of Q, and/or larger values of k and F. However, F is more likely to affect the deviation angle than Q and k, since F has the highest numerical power. According to Phillpot and Zillman (1970) the average inversion strength in winter (June, July, and August) at D80 is about 15^{o}C. The inversion strength calculated using Eqs 5.1 and 5.2 for D80 is 19^{o}C, i.e. 25 % larger than that predicted by Phillpot and Zillman. Therefore, the simple expression for F given in Eq. 5.2 will not adequately explain the small deviation angle there, and a more complete expression for total pressure gradient force must be found. From the bottom part of Fig. 5.3, it is obvious that the largest surface temperature gradient exists at D80. A scale analysis of total pressure gradient force will be done in the next section in order to determine the significance of additional terms in F, in particular the surface temperature gradient.

5.3 Discussion

As shown above, the vertical gradient of surface temperature along the slope can be one of the most important components of the total pressure gradient force which controls the surface wind in Antarctica. In this section, using a scale analysis of the forces composing the total pressure gradient force, we will discuss the conditions under which the force due to the gradient of surface temperature along the slope is dominant. The method of scale analysis is used to determine the relative importance of the forces. This technique involves the estimation of order of magnitude through the use of representative values of the dependent variables and constants that make up the forces. This method is widely used in model simulation in order to alter the complex general equations to easier and more economical forms for a specific application.

The total pressure gradient force can be written as follows (Mahrt and Larsen, 1982):

$$F = \beta\theta'\psi - \beta h \frac{\partial\bar{\bar{\theta}}}{\partial x} - \beta\bar{\bar{\theta}} \frac{\partial h}{\partial x} - \frac{1}{\rho} \frac{\partial p}{\partial x} \qquad (5.4)$$

where $\bar{\bar{\theta}} = \frac{1}{h} \int_0^h \theta' dz$ is the vertical average of potential temperature deficit in the inversion layer, and h is the depth of inversion layer. The x-direction coincides with the fall line. The z-direction is perpendicular to the plane of the slope. Fig. 5.4 demonstrates the schematic diagram of the distribution of equivalent potential temperatures in the inversion layer. The first term of the four terms on the right hand side of Eq. 5.4 is the pressure gradient force due to the inversion (buoyancy term). The second term is the pressure gradient force due to the change in the temperature profile in the inversion layer. In this study, this change is assumed to be due mainly to the surface potential temperature change along the slope (temperature gradient term). The third term is the pressure gradient force due to the change in the depth of the inversion layer (depth change term). The last term is the pressure gradient force in a free atmosphere. This pressure gradient force above the inversion layer is assumed to be small in this study,

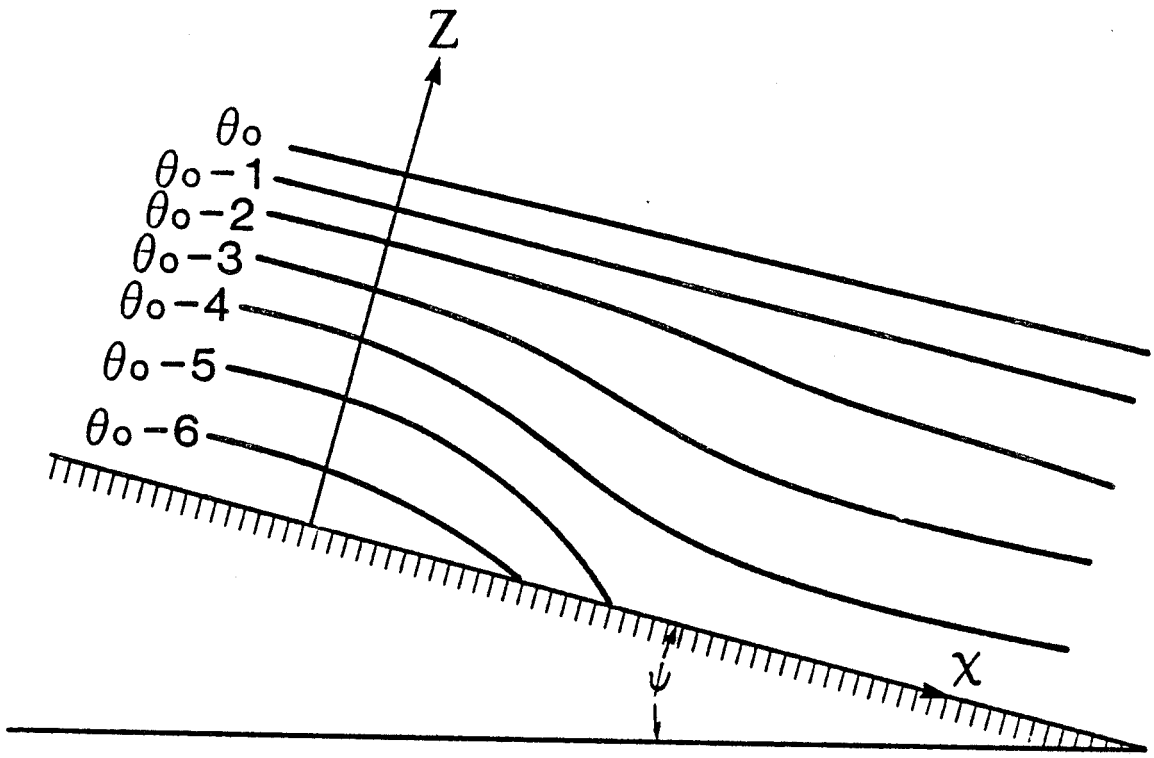

Fig. 5.4 The schematic diagram of the distribution of equivalent potential temperature in the inversion layer.

as the wind speed at Dome C, which is an indication of the pressure gradient in a free atmosphere (Parish 1982), is generally small (Wendler and Kodama 1984).

According to Mahrt and Larsen (1982), the first three terms on the right hand side of Eq. 5.3 can be expressed by the scales as:

$$\beta\theta'\psi \sim \beta\psi dT$$

$$-\beta h\frac{\partial\bar{\bar{\theta}}}{\partial x} \sim \beta H\frac{d\theta}{\iota} \sim \beta\psi Hd\theta/\Delta Z$$

$$-\beta\bar{\bar{\theta}}\frac{\partial h}{\partial x} \sim -\beta d\theta\frac{dH}{\iota} \sim -\beta\psi dTdH/\Delta Z$$

where dT is the scale for equivalent potential temperature deficit for the flow, H and dH are the scales for the depth and depth change of the inversion layer, $d\theta$ is the scale for surface equivalent potential temperature change along the slope, and $\Delta Z(=\iota\psi)$ is the scale for the surface elevation drop over the x-direction length scale ι. dT is a temperature difference normal to the surface, while $d\theta$ is a potential temperature change along the fall line. It is obvious that the change of depth of the inversion layer cannot exceed the value of the depth, that is, $H > |dH|$. We consider only positive values of dT and $d\theta$

for the purpose of this study, whereas dH can be either positive or negative. The positive sign denotes an increase of any value in the downslope direction. The relative scales for the three terms are obtained by dividing each scales by $\beta\psi$. They are:

$$dT, \quad Hd\theta/\Delta Z, \quad dTdH/\Delta Z. \tag{5.5}$$

No slope wind or gravity flow occurs if

$$d\theta/\Delta Z \simeq (dT/H)((dH/\Delta Z)-1). \tag{5.6}$$

$d\theta/\Delta Z$ represents the scale for vertical surface temperature gradient, dT/H is the scale for temperature gradient in the inversion layer, and $dH/\Delta Z$ is the ratio of the depth change scale and the elevation drop scale. Eq. 5.6 is the condition for which the buoyancy term is balanced by the temperature gradient term and depth change term. Under this condition there is no katabatic flow even if an inversion exists above the slope.

The condition in which the vertical gradient of surface temperature along the slope is dominant in determining the total pressure gradient force can be expressed as follows:

$$d\theta/\Delta Z >> (dT/H)(1-(dH/\Delta Z)). \qquad (5.7)$$

Eq. 5.7 simply means that the scale for the temperature gradient term should be larger than the sum of the other two scales.

There are two critical cases in Eq. 5.7. 1) $\Delta Z \simeq dH$, in which the depth change term is numerically equal to the buoyancy term but with an opposite sign. These terms cancel each other leaving the temperature gradient term alone in Eq. 5.4. Under this condition the top of the inversion layer is horizontal. According to the scales obtained from the data at D80 and at D57 for summer and winter (Table 5.1), this conditon is not realistic. 2) $dH \simeq 0$, in which case the temperature gradient term has to be larger than the average lapse rate in the inversion layer. In Table 5.1, the scale values for summer and winter are shown based on the data from D80 and D57. From Eq. 5.7, Table 5.1, and the condition $H > |dH|$,

$$0 < dH < 400. \qquad (5.8)$$

Table 5.1 The scales for the katabatic wind in Adelie Land.

PARAMETERS	SCALE	UNIT	REFERENCE
SUMMER			
$d\theta$	6	^{o}C	AWS
ΔZ	400	m	
dT	3	^{o}C	Wendler and Kodama (1982)
H	200	m	Wendler and Kodama (1982)
WINTER			
$d\theta$	10	^{o}C	AWS
ΔZ	400	m	
dT	15	^{o}C	Phillpot & Zillman (1970)
H	350	m	Kawaguchi et al. (1982)

The phenomenon which leads to a positive dH can be found in a deceleration of the flow associated with the entrainment of momentum from above the inversion layer. Since the wind speed becomes progressively stronger from D80 to D57 and to D47, Eq. 5.8 might not be realistic. The entrainment mechanism is suggested by many researchers, e.g. Parish (1980), Monin and Sawford(1978), but no data are available to verify this hypothesis for Antarctica. In winter, the wind at D80 tends to be directed more down-slope than that at D57 where the slope is less than at D80 (Fig. 5.3). Using the values in Table 5.1, Eq. 5.7 requires dH to be greater than 150 m, thus suggesting a large entrainment of momentum from above the inversion layer. Overall, the temperature gradient can be an important part of in theA total pressure gradient force. However, to better justify the importance of the temperature gradient term, an increase in the flow layer depth downward on the slope is required. Also the entrainment mechanism at the top of the layer needs to be investigated.

5.4 Summary

Station D80 on the high plateau showed a distinct flow pattern in winter, which suggested the importance of three components of the total pressure gradient force: the inversion strength, the slope angle, and the surface potential temperature gradient along the slope. The direction of the flow at D80 is more downslope than at D57 despite a less steep slope at D80. A scale analysis demonstrated the conditions under which the surface potential temperature gradient becomes more important relative to buoyancy in contributing to the total pressure gradient force. These conditions also require an increase of the thickness of the layer further down the slope, which suggests that the entrainment mechanism is important.

6 THE EFFECT OF SNOW ENTRAINED IN KATABATIC WINDS

6.1 Introduction

Katabatic winds with entrained snow are a common phenomenon in Adelie Land. There are, however, few experimental or model studies which consider the effect of snow entrained in katabatic winds, although both blowing snow and katabatic winds have been studied frequently and independently (e.g. Ball 1956, Schwerdtfeger 1970, Parish 1982, Loewe 1953, Budd et al. 1966, Kobayashi 1972, Schmidt 1982). The only study combining these two subjects was done by Mather and Miller (1964), who investigated the role of the direction of surface winds in Antarctica on the formation of sastrugi. Ball (1957) and Loewe (1974) mentioned the possible influence of drifting snow on katabatic flow.

Snow particles entrained into the katabatic flow layer have three possible influences on the character of the boundary layer flow: 1) an increase in density by entrainment of snow from the surface, 2) a decrease in temperature (i.e. increase in density) by

sublimation of snow particles and 3) an increase in surface friction. This paper discusses 1) and 2), as 3) can be assumed to be negligible compared with the influence of the density increase just by entrainment of snow particles, according to Ball (1957). Budd et al. (1966) reported that, in a wind profile under snow drift conditions at Byrd station, no evidence had been found of any significant deviations from the logarithmic wind profile. A slight tendency for the roughness height to increase with wind speed apparently cannot be explained by friction due to the drift snow itself.

In the next section, the theoretical relationship between katabatic force and the speed of wind with entrained snow is derived. The estimation of the katabatic force using the altimeter correction method is explained in section 6.3. In section 6.4, katabatic force due to the entrainment of blowing snow is obtained by the relationship derived in section 6.2 using the data from AWS. This chapter is summarized in section 6.5.

6.2 Katabatic Force and Blowing Snow Density

The cooling at the surface of sloping terrain generates an additional horizontal pressure gradient force (katabatic force), due to horizontal temperature differences (Sorbjan 1983). Details are given in Fig. 1.3. The increase in flow density due to the entrained mass of blowing snow is equivalent to an additional cooling, and therefore, increases the katabatic force. The graph in Fig. 6.1 plots the equivalent amount of cooling due to the entrainment of blowing snow against the blowing snow density. This graph does not consider any latent heat change associated with the sublimation of the blowing snow. For example, the increase in density of air to which 10 g/m^3 of snow have been added is equal to the density increase of air cooled $2^{o}C$ (Loewe 1974). This cooling is comparable to the average inversion strength during the summer months in Antarctica (Phillpot and Zillman 1970). The cooling equivalent of blowing snow of a few grams per cubic meter becomes an important factor in wind velocity. This density and higher ones were frequently observed at wind speeds above 18 m/s at the 10 m level at Byrd station in Antarctica (Budd et al. 1966).

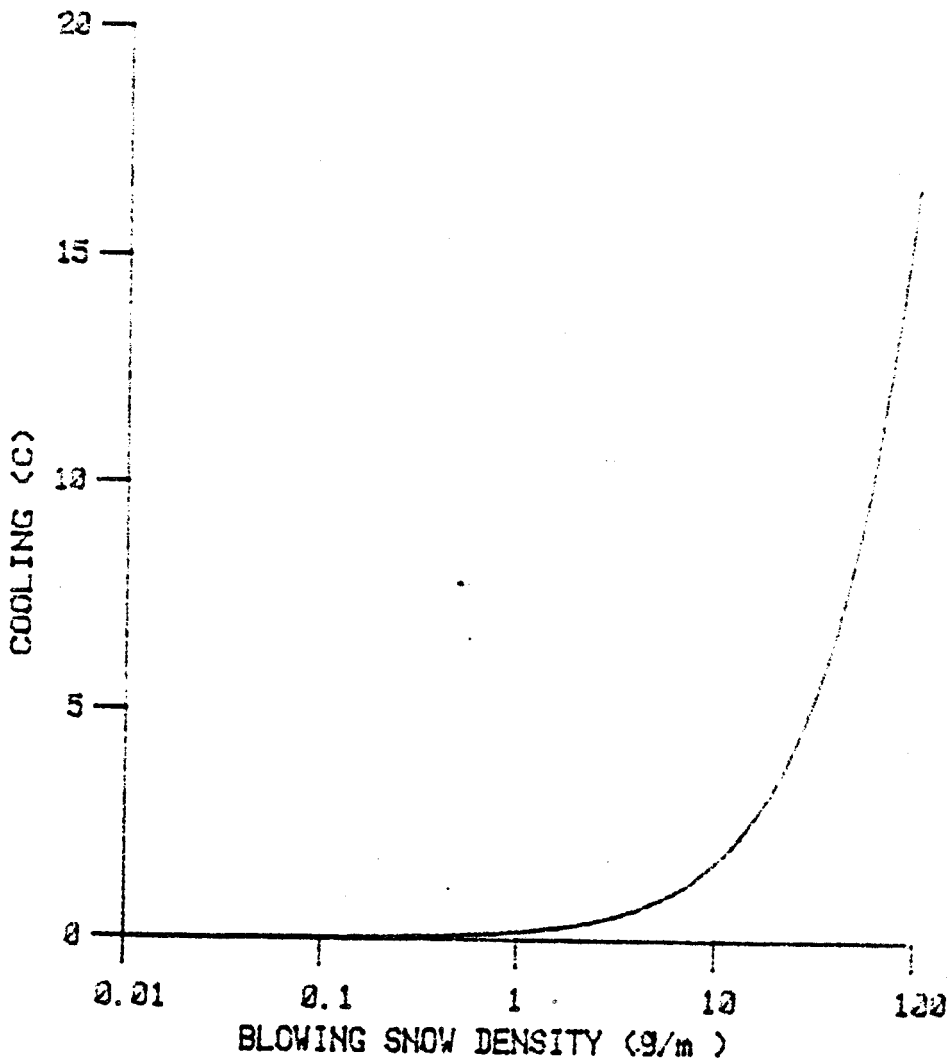

Fig. 6.1 The equivalent amount of cooling by the density increase due to the blowing snow with respect to the blowing snow density. The curve was calculated after Ball (1957) for the surface temperature of -20°C and the inversion strength of 10°C.

The increased density in the katabatic flow layer due to the entrainment of blowing snow particles leads to stronger wind speeds as the result of an increased katabatic force. Temperature and atmospheric pressure are, however, not directly affected by the entrained snow particles, if no sublimation from snow particles is assumed. The katabatic force, KF, in the case of blowing snow can be expressed in the following equation;

$$KF = KF_a + KF_{bs} \qquad (6.1)$$

where $KF_a = \beta\theta'\psi$, $KF_{bs} = g\rho_{bs}/\rho$. KF_a is the katabatic force due to the temperature difference between the surface and the free atmosphere without the blowing snow component, and KF_{bs} is an additional force due to blowing snow. g and ρ are gravitational acceleration and density, respectively. KF_{bs} cannot be calculated from the temperature and pressure because these two parameters are not directly changed by the entrainment of blowing snow.

According to the slab model of katabatic wind (Ball 1956), wind speed is proportional to the cube root of katabatic force, i.e.,

$$V^3 = (KF)Q/k, \qquad (6.2)$$

as in Eq. 5.2, where KF=F. For this derivation Ball assummed: 1) a negligible synoptic pressure gradient, and 2) a quadratic shear stress. Since the effect of snow particles entrained into the flow does not affect the values of temperature and pressure, KF_a with blowing snow present becomes;

$$KF_a = kV^3/Q - KF_{bs} \qquad (6.3)$$

The transport rate of snow by wind, $\rho_{bs}Q$, is proportional to the cube of wind speed (Kobayashi 1972, Dyunin 1967). Since KF_{bs} is proportional to ρ_{bs}, KF_{bs} is, as a result, proportional to V^3/Q. Thus, from the Eq. 6.3, it follows;

$$KF_a = (k - c)V^3/Q \qquad (6.4)$$

where c is a constant. The slope of the relationship of KF_a and V^3 is expected to be smaller in the case of blowing snow.

6.3 Katabatic Force and Altimeter Correction Method

Since AWS collect only surface data, information on the free atmosphere is needed to estimate the katabatic force. Therefore, the altimeter correction method, which is frequently used to estimate the surface

geostrophic wind (Bonner and Paegle 1970, Pinty and Isaka 1982), was introduced. The katabatic force, KF_a, normal to contour lines of the sloped terrain can be expressed by the following equation:

$$KF_a = gS^*\psi \qquad (6.5)$$

where $S^* = (T_s - T_{sp})/T_{sp}$. T_s is virtual temperature at the terrain surface. T_{sp} represents temperature in the standard atmosphere corresponding to the surface pressure.

6.4 Results

In Fig. 6.2 KF_a is plotted against the cube of wind speed for D47 for the period from 1 June to 10 July in 1983. The solid circles indicate averages for wind speed intervals of 2 m/s. The height of wind velocity and blowing snow density is the height of the AWS wind sensor, approximately 3 m from the ground. Wind speeds cited in this chapter from the other papers are converted to this height. The length of the line attached to each circle represents twice the standard deviation. The numerical values above the abscissa give the number of observations for each interval.

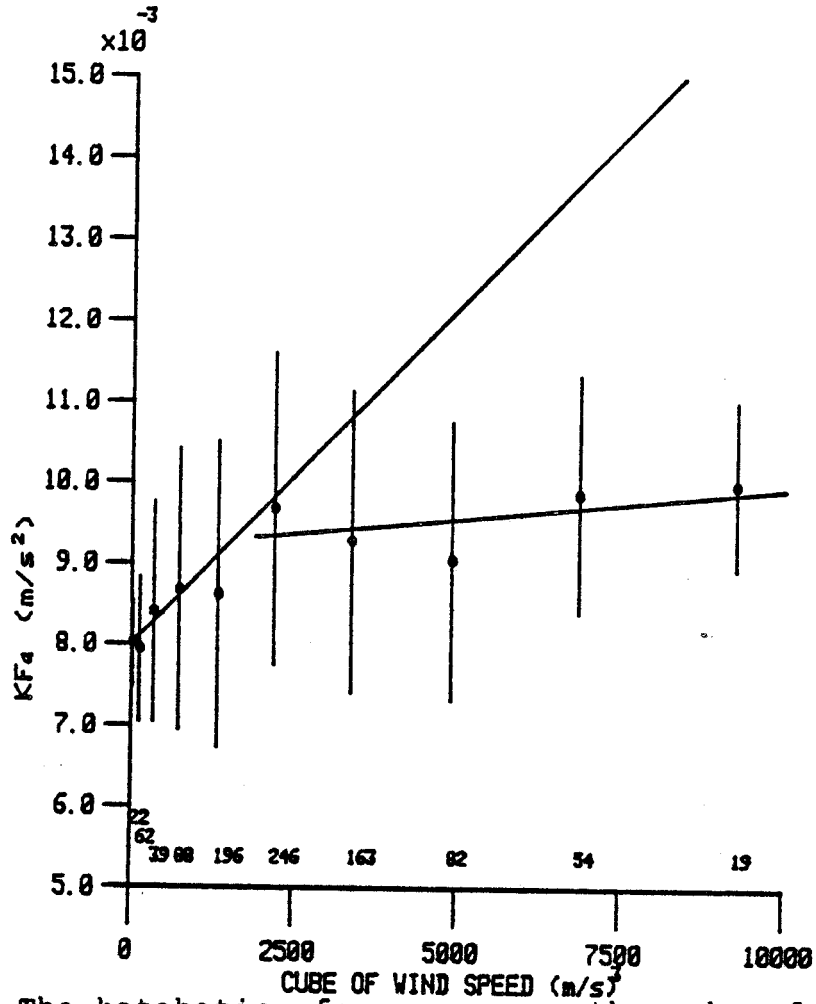

Fig. 6.2 The katabatic force versus the cube of wind speed. The solid circles indicate averages for wind speed intervals of 2 m/s. The length of line attached to each circle gives twice the standard deviation. The numerical values above the abscissa are the number of observations. Two linear regression lines were drawn using the lower six points and the upper five points.

Two linear regression lines are drawn using the lower six points and the upper five points. It is obvious from Fig. 6.2 that the slope for weaker wind speeds is steeper than that for stronger wind speeds. This may indicate the effect of blowing snow, as the stronger wind speeds, which reflect the effect of blowing snow, are increased by a relatively small increase in KF_a, which does not take into account the effect of blowing snow. The wind speed at the terminal point of two regression lines (12.4 m/s) agrees quite well with the wind speed at which blowing snow density can be more than 1 g/m^3 according to Budd et al. (1966).

In order to test whether the increase in wind velocity which occurs at wind speeds exceeding 12.4 m/s could be due to the increased density of the air with the entrained blowing snow, we will compare the measured intensification of the wind with the theoretical intensification of the wind due to entrained blowing snow. KF_{bs} is defined by Eq. 6.3 and is calculated as the difference in the two regression lines in Fig. 6.2 for wind speeds stronger than 12.4 m/s. K_{bs} is plotted against the wind speed (solid line in Fig. 6.3). The ordinate at the right side of the figure is the amount of suspended snow required to

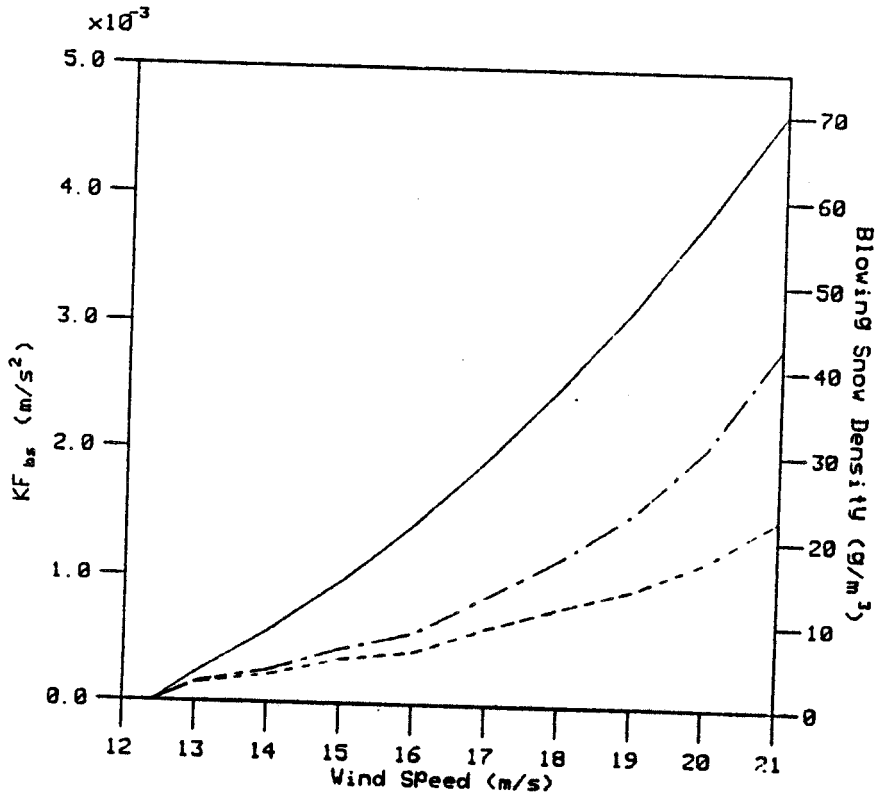

Fig. 6.3 Katabatic force due to the entrainment of blowing snow particles against wind speed. The right ordinate shows the density of suspended snow required to explain the increase of wind speed. The solid line is KF_{bs}. The broken line indicate the blowing snow density at the height of the AWS sensors for the corresponding wind speed according to Budd et al. (1966). The mixed broken line shows the total effect of blowing snow including the sublimation from the suspended snow particles.

explain the total increase of wind speed. This ordinate may be determined from Fig. 6.1. For a wind speed of 18 m/s, for example, an amount of suspended snow of 39 g/m^3 would be required. However, for the same wind speed, Budd et al. (1966) measured, 13 g/m^3, one third of the snow particle density (broken line in Fig. 6.3) needed to explain KF_{bs}. Hence, there must be an additional accelerative force.

Cooling due to sublimation of blowing snow particles may provide the additional accelerative force. Sublimation from blowing snow particles occurs due to the difference in vapor pressures at the surface of snow particles and the ambient air. It is difficult to achieve an accurate estimate of sublimation without knowledge of the moisture in the katabatic flow. However, a rough estimation was done by assuming the following conditions. 1) the air is kept saturated with respect to ice, 2) flow is downslope and in a steady state, 3) sublimation occurs due to the temperature increase caused by compression-warming during descent, 4) time of travel for an air parcel is fixed to a time scale of gravity flow, $t_g = V/\beta\theta'\psi$, after Gosink (1981) so that the distance of descent depends on the wind speed, and 5) the average

sublimation of the whole layer is proportional to the depth of a blowing snow layer with densities of more than 1 g/m^3. The estimated cooling under these conditions is converted to the equivalent blowing snow density and added to Fig. 6.3 (mixed broken line). This effect adds another 20 - 30 % to the katabatic force. Hence, suspended snow and sublimation of the snow particles under the above assumed conditions can explain about two thirds of KF_{bs}. Complete agreement might not be expected due to the differences in the physical properties of snow surfaces and turbulence in the flow between D47 and Byrd stations. The blowing snow density depends mainly on the size of snow particles blown from the snow surface into the flow layer. The difference in nature of turbulence, especially due to the difference in the roughness parameter (which is also a result of removal and accumulation of snow particles by wind), would affect the blowing snow density in the flow. Another cause for these differences could lie in our assumption that the amount of snow transported is proportional to the cube of the wind speed. Takahashi (1985) reported that the amount of snow transported by wind at Mizuho station is proportional to the power of 4 to 8 of the

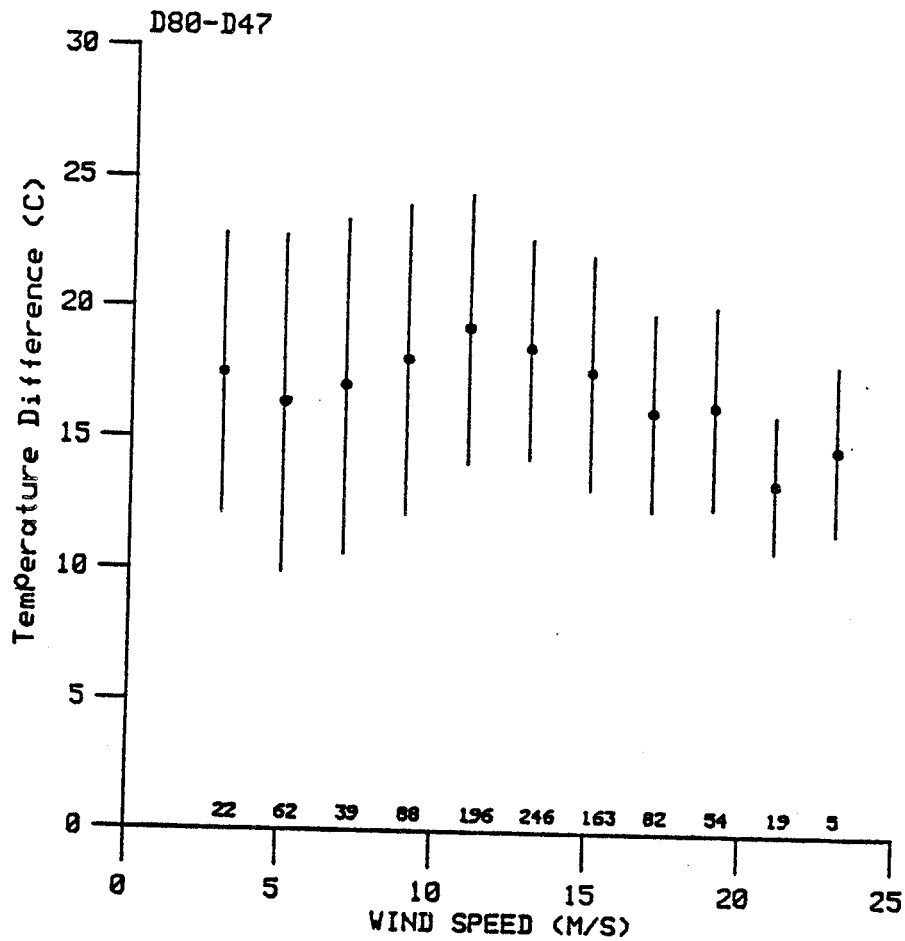

Fig. 6.4 The temperature difference between D80 and D47 against the wind speed at D47. The solid circles indicate averages for wind speed intervals of 2 m/s. The length of line attached to each circle gives twice the standard deviation. The numerical values above the abscissa are the number of observations.

wind speed, instead of 3, as we assumed. A full explanation for these differences must wait for a more detailed examination of blowing snow measurements.

In Fig. 6.4, the temperature differences between D80 and D47 are plotted against the wind speeds at D47. At about 11 m/s the relationship changes drastically. 11 m/s appeared to be about the threshold wind speed at which blowing snow starts to contribute substantially to the katabatic flow. The decreased temperature difference provides additional observational evidence for cooling caused by sublimation of the suspended snow at D47.

6.5 Summary

The entrainment of blowing snow particles increases the density of the katabatic flow layer by two mechanisms: first, by the addition of snow particles to the air column; and second, by the sublimation of the snow particles, with the corresponding loss of latent heat from the air, which decreases air temperature and thereby increases air density. This increase in density in the katabatic flow layer leads to increased

wind speed as a result of the change in air density in the boundary layer relative to the air density in the free atmosphere at the same height further down the slope. This accelerative effect occurs primarily at wind speeds exceeding 12 m/s, since at those high wind speeds there is usually a large amount of blowing snow entrained. Further intensive measurements of moisture profiles are needed to quantify more accurately the effect of sublimation of the blowing snow on the katabatic flow.

7 SUMMARY, DISCUSSION, AND GUIDELINES FOR FUTURE STUDY

Anlyses of katabatic winds were made from data collected from five Automatic Weather Stations extending from D10 to Dome C in Adelie Land. Data in the past were generally recorded either at sparsely distributed manned stations on a year-round basis or, during a number of field trips, at different places on the same slope, but at different times. AWS have changed this procedure by providing simultaneous measurements at different fixed places on the same slope on a year-round basis.

The AWS in Adelie Land are classified into three groups according to their location: high plateau, intermediate plateau, and coastal region, each having distinct annual temperature and wind speed patterns. The AWS locations can also be classified by degree of slope. From the flat area at Dome C, the slope increases in a parabolic curve through the other stations to the coastal station at D10. The coastal station, D10, on uneven terrain, has the highest mean annual temperature of the AWS but a somewhat lower wind speed than the intermediate stations, D57 and D47, where the highest wind speeds are observed. The high

plateau stations, D80 on a gentle slope, and Dome C on a flat area at the top of an ice dome in the interior of the continent, are characterized by the lowest wind speeds and the lowest temperatures in the groups. The mean annual wind speed at Dome C is the lowest of any of the Antarctic interior plateau stations.

The high directional constancy of the surface winds in Antarctica has previously been reported and explained by the inversion strength and steepness of the terrain. In summer, however, when the inversion is weak or destroyed, a high directional constancy of approximately 0.9, comparable to the mean annual value of 0.92, is found at the slope stations. An analysis of data, and model simulations of diurnal variations of katabatic winds in summer, shows that geostrophic winds blowing at the upper boundary of katabatic flow and eddy viscosity also affect the constancy of the wind direction in summer.

The consistency of geostrophic winds at the upper boundary of katabatic flow during daytime in summer was not confirmed due to the lack of data. The pressure maps, available from the few weather stations scattered over the large area of the Antarctic, are insufficient to prove the consistency in geostrophic wind direction.

The most realistic approach to confirm this point is to analyze vertical profile data taken from rawinsondes (or possibly remote sensing using satellites) simultaneously at each AWS. Sorbjan et al. (1985) analyzed some profile data in Adelie Land, and reached the same result as described in chapter 3.

Wind directional constancies at the slope stations in winter, when the inversion is expected to be stronger than that in summer, are sometimes lower than the mean annual constancies. These low constancies are associated with warm air advection from maritime air brought into Adelie Land when the continental anticyclonic ridge, connecting at times with the New Zealand and Australia anticyclones, lies to the east of Adelie Land.

The mechanism of entrainment of heat and momentum of the advected warm air into the katabatic flow layer, that changes its depth, has not been clearly understood. "Subsidence and adiabatic warming" is an easy and commonly used explanation for the warm spells by many researchers, e.g. Loewe (1969), but "subsidence" mechanisms and warming processes have not been explained clearly. It is also necessary to obtain vertical profile data showing the change in the depth

of the boundary layer in order to help understand the entrainment mechanisms.

There is a superadiabatic surface temperature change between the high plateau and intermediate plateau stations. Station D80, a high plateau station, showed a distinct flow pattern in winter, which suggested the importance of the influence of three factors on the total pressure gradient force: the inversion strength, the slope angle, and the surface potential temperature gradient along the slope. Total pressure gradient force is composed of three components: buoyancy, surface temperature gradient, and boundary depth change. Their relative importance was evaluated, and the results showed that the superadiabatic surface temperature change along the slope could be of importance when the buoyancy component is balanced or nearly balanced by an increase in depth of the katabatic wind layer.

One of the reasons for the superadiabatic surface temperature change between the high plateau and intermediate plateau stations could be found in a large entrainment of momentum and heat from above the katabatic flow layer between D80 and D57. A large change of slope exists between these two stations (Fig.

1.3). Although the entrainment of heat and momentum lead to an increase in depth of the boundary layer, and as a result, to a deceleration of flow, the observed increase in wind speed from D80 to D57, and to D47, would indicate the importance of katabatic force due to the increase in slope angle and to the surface temperature gradient along the slope rather than to the effect of the increase in the depth of katabatic flow.

The entrainment of blowing snow particles increases the density of the katabatic flow layer by two mechanisms: first, by the addition of snow particles to the air column; and second by the sublimation of the snow particles, with the corresponding loss of latent heat from the air, which decrease air temperature and thereby increases air density. This increase in density in the katabatic flow layer leads to increased wind speed as a result of the increase in air density in the boundary layer relative to the air density in the free atmosphere at the same height further down the slope. This accelerative effect occurs primarily at wind speeds exceeding 12 m/s, since at those high wind speeds there is usually a large amount of entrained snow.

After all this, two questions on entrainment mechanisms remain, one relating to the entrainment of heat and momentum at the upper boundary, and another to blowing snow at the ground. In addition to vertical profile measurements of temperature and wind in and above the katabatic wind layer, measurements of moisture profiles are necessary.

Also unknown yet are the mechanisms of turbulent mixing, entrainment and gravity waves in the strongly stable boundary layer. Even when the overall Richardson number (a measure of the stability in the layer) exceeds 0.25, turbulence may occur sporadically. The Richardson number of a part of the boundary layer temporarilly dips below the critical value of 0.25 in response mainly to internal wave motions. This sporadic turbulence is absorbed by the internal wave motions and therefore is extremely difficult to measure. High stabilities in which the Richardson number exceeds its critical number are observed even during night in summer in Adelie Land (Sorbjan et al. 1985). These mechanisms must be clarified in order to better understand katabatic winds.

Appendix A

Since the AWS do not include information on the vertical profile of the wind vector, the following equations were used to estimate the pressure gradient force F (Parish 1981):

$$\frac{\partial u}{\partial t} = F_x + fv - kVu$$

$$\frac{\partial v}{\partial t} = F_y - fu - kVv \qquad \text{(A1)}$$

where V is the wind speed, and u and v are wind components in the x- and y-directions, respectively. f is the Coriolis parameter (-1.3×10^{-4} s^{-1}) and k is a frictional constant (5×10^{-5} m^{-1}). The frictional force is taken as proportional to the square of the wind speed, a parameterization often used in turbulent fluid flows.

Each variable is separated into the stationary part and the diurnal variation part.

$$u = u_s + u_d$$

$$v = v_s + v_d$$
$$F_x = F_{sx} + F_{dx} \qquad \text{(A2)}$$
$$F_y = F_{sy} + F_{dy}$$
$$k = k_s + k_d$$

The stationary variables satisfy the steady-state version of Eq. A1:

$$0 = F_{sx} + fv_s - k_s Vu$$
$$0 = F_{sy} - fu_s - k_s Vv \qquad \text{(A3)}$$

and for the diurnal part:

$$\frac{\partial u_d}{\partial t} = F_{dx} + fv_d - k_s Vu_d - k_d Vu$$
$$\frac{\partial v_d}{\partial t} = F_{dy} - fu_d - k_s Vv_d - k_d Vv \qquad \text{(A4)}$$

The diurnal variation of the friction coefficient, k_d, is obtained assuming that F_{dy} is negligibly small:

$$k_d = (-fu_d - \frac{\partial v_d}{\partial t} - k_s Vv_d)/(Vv) \qquad \text{(A5)}$$

Then, F_{dx} is calculated using the following equations:

$$F_{dx} = -\frac{\partial u_d}{\partial t} - fv_d + k_s V u_d + k_d V u \qquad (A6)$$

APPENDIX B

A Numerical Model of Flows over Antarctica.

This simple model is based on the following set of equations which describes the distribution of the wind velocity in the non-steady atmospheric boundary layer (ABL) over a slightly inclined terrain (the non-steady version of the equations derived by Sorbjan, 1983).

$$\frac{\partial u}{\partial t} - f(v-v_{go}) + fz\frac{\partial v_g}{\partial z} + fv_T = \frac{\partial}{\partial z}K\frac{\partial u}{\partial z}$$

$$\frac{\partial v}{\partial t} + f(u-u_{go}) - fz\frac{\partial u_g}{\partial z} = \frac{\partial}{\partial z}K\frac{\partial v}{\partial z} \qquad \text{(B1)}$$

where
- u, v, -- components of the wind and the
- u_g, v_g, u_{go}, v_{go} -- geostrophic wind vectors at an arbitary height and the surface,
- f -- Coriolis parameter,
- K -- eddy viscosity,
- $v_T = \beta\theta'\psi/f$ -- slope generated thermal wind.

In Eq. B1, it is assumed that the geostrophic wind can vary with height (synoptic baroclinicity).

Our model is designed to describe qualitatively the time variation of the wind in the ABL. This is achieved by adopting a very simple and somewhat arbitrary closure of Eq. B1, for the eddy visocity K. Generally, the eddy viscosity can be parameterized as follows:

$$K = \begin{cases} \kappa u_* z(1-z/h)/(1+4.7\eta z/h) & \text{stable (Sorbjan 1984)} \\ \kappa u_* z(1-z/h) & \text{neutral (B2)} \\ 4K_{max} z/z_i(1-z/z_i) & \text{convective (Wyngaard 1981),} \end{cases}$$

where h, z_i -- height of the stable and convective ABL,

K_{max} -- maximum value of K in the convective ABL,

κ -- van Karman constant,

u_* -- friction velocity,

$\eta = h/L$ -- stability parameter, L - Monin-Obukhov length.

We generalize Eq. B2 concerning only the statble condition:

$$K(z,t) = K_n/(1-4.7\eta Z) \qquad (B3)$$

where $K_n = K_o Z(1-Z)$ (neutral case, $K_o = \kappa u_* H$), and $Z = z/H$, where H is the height of ABL. We assumed in Eqs. B3 that $H = 200m$.

The time forcing in the model is expressed by the function F, which describes a diurnal variation of the eddy viscocity and the thermal wind. We assumed $K_n(t) = [1+cF(t)]$ with $c = 20$, and $\eta(t) = -15F(t)$. The function F(t) is defined as:

$$F(t) = (COS((2\pi t/T))-1)/2. \qquad (B4)$$

where T = 24 hours.

The form of F(t) indicates that we assume the neutral condition to start with and stay in the stable condition changing its intensity.

In Eq. B1, we also assume that

$$v_T = v_T(0)(e^{-Z} - e^{-1})/(1 - e^{-1}) \qquad (B5)$$

where $v_T(0) = RF(t)$ and R is equal to the amplitude of the thermal wind multiplied by the Coriolis parameter. Notice that the thermal wind decreases exponentially

from the value $v_T(0)$ at the surface to zero at the top of the ABL. The exponential shape of v_T was also assumed by Mahrt and Schwerdfeger (1969). The other parameters in Eq. B1 are chosen to be u_{go} = 5 m/s, v_{go} = 5 m/s, f = -1.3×10^{-4} s^{-1}.

The boundary conditions are established as:

$$\text{for } z=0: \quad \begin{cases} u=0 \\ v=0 \end{cases}$$

$$\text{for } z=H: \quad \begin{cases} u = u_{go} + \dfrac{\partial u_g}{\partial z}h \\ v = v_{go} + \dfrac{\partial v_g}{\partial z}h \end{cases} \qquad \text{(B6)}$$

As an initial condition, we use the steady state solution of Eq. B1, with $K = K_n$ and $v_T(0) = 0$. To solve Eq. B1, we first transform it to the form:

$$\frac{\partial W}{\partial t} = \frac{\partial}{\partial Z}K\frac{\partial}{\partial Z}W - f(v_T+i\Lambda Z)e^{ift} \qquad \text{(B7)}$$

where $W = [(u+iv) - (u_{go}+iv_{go})]e^{ift}$

$$\Lambda = \left[\frac{\partial u_g}{\partial Z} + i\frac{\partial v_g}{\partial Z} \right]$$

and then express Eq. B7 in the finite difference form. The finite differences algebraic equations were solved by the "tridiagonal algorithm", described in Appendix A of Roache (1972).

We performed a numerical experiment with the non-zero synoptic thermal wind of the magnitude of 5 m/s/km in a 200 m deep layer, which is equivalent to the horizontal temperature gradient of about 1.5 K/100km. We found that synoptic baroclinicity modifies the wind hodographs very little in the ABL. Therefore, the Λ is assumed to be negligible in the study.

JAN 80 D-10

DATE	Temp.	Pres.	WSpd	WiDir
1	999.9	999.9	99.9	999.9
2	999.9	999.9	99.9	999.9
3	999.9	999.9	99.9	999.9
4	999.9	999.9	99.9	999.9
5	999.9	999.9	99.9	999.9
6	999.9	999.9	99.9	999.9
7	-4.9	999.9	56.2	180.0
8	-0.6	967.0	12.3	153.2
9	-0.3	968.9	6.7	160.2
10	-0.5	967.2	3.6	162.3
11	0.4	962.2	4.7	166.0
12	-3.6	959.4	7.8	124.2
13	-4.5	960.0	8.3	132.8
14	-5.0	956.3	9.6	145.5
15	-4.5	955.7	5.3	128.4
16	-4.8	958.7	7.8	170.1
17	-3.3	954.8	4.9	167.9
18	-2.2	955.3	2.2	184.9
19	-2.8	958.3	2.2	160.9
20	-1.8	952.0	7.0	136.9
21	-1.8	950.4	9.9	143.5
22	-2.2	955.0	6.0	161.8
23	-1.1	958.7	4.7	132.1
24	-1.3	962.8	4.7	147.8
25	-1.3	965.2	5.0	154.2
26	-1.8	960.7	8.0	141.6
27	-3.3	962.7	4.7	163.9
28	-0.8	960.8	5.7	179.3
29	-2.6	950.7	8.3	153.1
30	-4.1	948.2	6.1	150.9
31	-3.3	952.0	9.5	171.6
AVE	-2.4	958.6	6.3	152.9

FEB 80	D-10				DOME C			
DATE	Temp.	Pres.	WSpd	WlDir	Temp.	Pres.	WSpd	WlDir
1	-2.1	954.8	10.6	175.2	999.9	999.9	99.9	999.9
2	-2.5	951.4	10.0	165.7	999.9	999.9	99.9	999.9
3	-2.1	951.4	10.6	149.6	999.9	999.9	99.9	999.9
4	-5.9	956.1	12.9	168.3	999.9	999.9	99.9	999.9
5	-7.2	958.1	9.2	171.4	-42.4	647.7	2.3	274.1
6	-8.2	959.3	5.6	171.3	-41.0	647.0	2.8	278.1
7	-6.7	957.7	4.6	184.5	-42.2	644.5	2.5	254.6
8	-9.9	959.0	5.1	188.0	-42.4	644.5	2.3	253.4
9	-8.8	965.9	7.2	176.6	-40.8	650.6	3.0	297.1
10	-5.2	963.5	11.7	144.9	-34.6	656.8	0.6	278.7
11	-5.3	956.9	10.4	147.7	-36.0	655.4	2.2	247.4
12	-7.0	951.1	10.8	156.7	-35.3	652.8	3.3	192.8
13	-7.6	955.3	10.6	186.7	-37.8	656.1	4.1	178.9
14	-5.7	957.4	12.9	155.6	-37.0	659.2	2.8	199.7
15	-3.7	950.2	9.9	157.9	-36.4	656.2	2.2	181.5
16	-4.6	958.7	10.4	151.3	-33.6	656.0	0.8	212.7
17	-7.3	961.5	7.9	179.1	-39.1	654.6	2.9	244.4
18	-9.5	952.0	6.3	160.9	-39.7	649.4	6.9	205.8
19	-8.4	953.4	4.8	177.5	-41.8	648.9	6.7	160.1
20	-5.2	958.8	7.7	138.1	-40.3	649.9	0.9	264.0
21	-9.1	955.5	10.5	181.2	-42.9	647.3	3.8	245.8
22	-10.9	958.6	11.4	173.1	-45.8	649.3	3.5	169.7
23	-7.2	959.9	14.8	179.0	-45.4	652.4	1.8	229.5
24	-5.5	959.7	13.1	172.0	-46.6	651.5	2.1	249.1
25	-7.4	956.4	16.1	165.0	-47.2	650.2	1.8	228.7
26	-9.8	955.2	16.1	179.5	-48.7	648.5	2.2	251.6
27	-9.3	957.3	17.8	168.5	-50.1	652.5	2.7	184.1
28	-2.9	957.7	7.7	130.2	-45.5	656.9	2.4	137.4
29	-3.7	964.6	4.4	172.5	-40.9	653.5	0.4	176.1
AVE	-6.5	957.3	9.7	166.1	-41.4	651.6	2.0	216.1

MAR 80	D-10				DOME C			
DATE	Temp.	Pres.	WSpd	WiDir	Temp.	Pres.	WSpd	WiDir
1	-10.4	961.3	7.4	197.5	-47.3	648.3	3.4	264.7
2	-12.9	954.6	6.3	198.1	-52.5	642.4	2.5	225.6
3	-9.9	962.3	5.5	171.1	-54.5	644.6	2.5	197.4
4	-7.5	957.1	17.4	168.0	-54.1	651.5	1.9	258.9
5	-8.4	944.8	17.0	175.1	-53.3	651.3	1.5	174.5
6	-9.4	952.2	13.7	176.6	-50.0	651.2	1.4	179.2
7	-10.7	956.3	8.6	185.1	-52.7	648.9	3.8	252.9
8	-12.6	955.1	14.1	192.0	-56.5	651.1	5.3	234.9
9	-8.7	963.9	7.5	175.7	-51.2	654.1	3.5	233.2
10	-11.5	960.1	8.0	182.7	-44.4	653.7	5.0	237.2
11	-13.1	963.6	7.0	196.5	-49.5	652.2	3.3	249.9
12	-6.5	960.6	7.5	150.6	-49.2	653.7	1.6	182.6
13	-6.7	953.9	18.0	164.1	-47.4	657.2	2.4	142.3
14	-10.7	949.6	14.1	165.2	-45.9	654.9	2.2	197.2
15	-10.9	937.5	11.4	177.1	-45.9	645.7	3.7	221.5
16	-12.1	945.5	11.3	150.5	-52.9	644.2	2.2	228.1
17	-12.3	947.8	17.2	171.6	-56.0	648.2	2.1	181.9
18	-12.6	943.6	21.3	177.2	-56.8	647.8	2.5	194.2
19	-14.3	945.1	16.4	180.7	-57.3	641.9	3.8	233.7
20	-10.7	937.8	15.8	162.6	-59.9	636.3	3.4	222.7
21	-7.6	926.2	27.6	161.4	-59.4	640.4	1.2	161.9
22	-4.4	924.8	23.8	156.9	-48.9	646.1	4.6	130.8
23	-2.7	935.0	16.6	165.0	-41.1	650.6	5.9	107.7
24	-2.9	945.8	8.9	157.2	-45.9	654.7	3.1	123.5
25	-4.4	953.7	12.5	156.8	-51.2	652.3	2.7	150.7
26	-6.1	958.7	17.5	162.1	-48.5	654.3	0.5	63.8
27	-6.8	959.1	16.9	177.2	-51.6	656.6	1.7	80.7
28	-7.8	966.4	18.2	175.9	-47.5	657.0	1.5	319.7
29	-9.5	972.2	6.3	190.2	-56.6	654.2	4.3	263.7
30	-7.8	968.5	5.2	177.0	-58.0	657.1	3.4	238.3
31	-7.4	964.4	7.2	175.1	-52.0	658.1	2.1	180.9
AVE	-9.0	952.4	12.8	170.8	-51.5	650.3	1.9	208.7

APR 80	D-10				DOME C			
DATE	Temp.	Pres.	WSpd	WiDir	Temp.	Pres.	WSpd	WiDir
1	-8.6	963.6	7.5	160.8	-49.3	654.4	3.1	265.5
2	-10.1	959.9	5.4	208.7	-53.0	650.0	4.5	268.7
3	-9.6	961.3	5.1	155.6	-59.2	649.1	2.6	229.2
4	-12.8	961.6	6.1	160.6	-60.0	648.8	2.7	241.0
5	-13.8	965.3	6.0	176.2	-61.2	647.3	1.9	197.5
6	-14.5	968.5	4.4	192.9	-61.5	648.6	3.7	186.0
7	-10.6	961.4	11.6	148.1	-57.7	651.0	2.4	251.4
8	-12.0	957.2	9.6	177.0	-60.8	649.4	2.4	233.7
9	-13.8	955.4	11.3	173.2	-61.9	648.1	3.2	183.9
10	-13.0	952.2	16.8	185.1	-61.9	646.1	2.5	185.1
11	-13.5	967.2	6.9	168.9	-62.5	648.6	1.8	220.0
12	-12.6	959.3	19.0	168.4	-60.9	654.1	2.1	182.8
13	-13.7	957.4	23.9	176.8	-59.0	654.1	2.4	232.9
14	-15.7	961.2	14.7	181.3	-60.5	649.9	2.5	227.4
15	-16.3	965.9	13.8	177.5	-62.0	652.2	2.3	205.9
16	-15.7	971.6	15.1	183.8	-59.5	657.7	3.8	225.3
17	-16.1	965.6	9.9	181.7	-54.6	658.7	5.1	208.5
18	-17.3	956.2	8.0	177.5	-48.7	650.2	6.2	227.8
19	-21.2	954.2	15.1	186.5	-58.3	650.5	7.6	186.7
20	-15.2	959.7	16.5	177.2	-62.5	652.3	3.6	175.5
21	-14.5	953.5	14.2	176.1	-60.5	647.5	3.9	179.6
22	-17.2	943.2	12.7	177.7	-60.8	641.3	5.5	184.9
23	-16.1	954.8	14.7	176.6	-61.6	643.7	3.9	145.5
24	-13.7	950.4	25.7	177.4	-61.3	648.3	2.3	99.0
25	-15.0	948.4	21.0	184.2	-59.2	640.9	0.8	321.4
26	-17.7	950.4	7.7	191.3	-64.6	634.1	2.5	240.6
27	-15.3	943.5	9.9	159.1	-71.3	632.2	1.5	186.4
28	-17.1	947.1	5.7	167.3	-67.0	632.9	0.7	138.5
29	-15.5	948.4	6.4	154.2	-58.2	634.1	0.4	257.7
30	-15.9	949.3	9.0	143.8	-67.3	634.6	1.9	213.8
AVE	-14.5	957.2	11.6	175.6	-60.2	647.1	2.4	207.4

MAY 80	D-10				DOME C			
DATE	Temp.	Pres.	WSpd	WiDir	Temp.	Pres.	WSpd	WiDir
1	-19.8	940.1	9.1	177.5	-71.0	631.7	2.0	191.0
2	-20.7	941.4	8.6	200.4	-73.0	630.5	2.5	193.3
3	-18.7	943.9	6.7	181.3	-72.1	626.7	0.5	227.9
4	-24.2	949.6	6.8	215.7	-68.6	627.6	1.8	259.0
5	-19.7	942.6	9.3	180.7	-68.6	631.5	3.5	188.4
6	-21.2	947.1	10.4	198.5	-69.9	631.8	1.5	179.6
7	-12.7	951.6	17.5	158.5	-58.4	639.8	3.1	59.9
8	-7.9	939.8	15.6	147.2	-52.4	642.6	5.1	81.5
9	-5.0	945.3	12.2	138.0	-44.7	646.2	6.1	98.6
10	-11.2	966.9	10.1	180.4	-56.1	653.6	1.4	96.5
11	-9.8	962.4	13.5	181.4	-59.2	653.9	1.9	207.6
12	-13.7	955.4	6.7	203.3	-60.9	646.8	3.5	207.7
13	-17.0	946.4	15.9	180.9	-62.0	639.3	4.1	223.3
14	-18.0	948.7	15.1	177.0	-66.5	636.4	1.7	161.7
15	-18.8	963.5	13.0	188.7	-72.5	647.6	0.2	180.0
16	-21.3	961.9	7.2	189.2	-57.2	652.5	6.0	147.5
17	-18.4	963.6	6.0	156.0	-49.2	652.1	5.6	138.6
18	-15.5	968.7	8.2	174.9	-61.6	650.5	1.2	167.5
19	-18.2	966.9	8.4	185.8	-62.5	647.8	2.6	205.7
20	-22.7	963.0	12.4	187.0	-64.0	642.6	2.7	190.2
21	-20.9	959.2	9.9	179.9	-67.9	637.6	0.5	218.1
22	-23.2	958.9	8.2	190.6	-72.4	633.8	0.0	0.0
23	-20.6	960.4	4.1	169.4	-67.5	635.7	0.0	0.0
24	-15.7	947.9	17.7	162.0	-58.1	639.8	0.0	0.0
25	-16.1	939.0	17.8	176.9	-61.1	639.2	0.0	0.0
26	-18.8	939.9	9.1	177.7	-68.5	634.5	0.9	223.8
27	-25.5	945.2	7.8	201.8	-64.4	630.0	2.5	193.5
28	-24.1	951.1	15.3	210.7	-71.5	633.7	0.6	264.2
29	-18.5	969.0	14.4	208.7	-63.8	651.8	2.4	266.1
30	-8.8	976.9	6.7	166.6	-44.7	655.7	7.1	307.9
31	-7.3	969.1	3.2	156.7	-33.1	652.6	5.4	334.6
AVE	-17.2	954.6	9.9	179.3	-61.8	641.2	0.9	179.4

JUN 80	D-10				DOME C			
DATE	Temp.	Pres.	WSpd	WlDir	Temp.	Pres.	WSpd	WlDir
1	-8.0	954.9	3.6	222.6	-37.1	646.4	3.4	291.0
2	-12.2	948.6	10.0	206.7	-51.9	647.1	3.6	249.5
3	-8.3	953.6	11.1	138.1	-47.2	646.2	1.7	73.3
4	-6.7	957.0	6.2	144.7	-42.0	642.6	0.9	316.5
5	-11.6	964.5	6.1	203.5	-55.5	648.5	2.9	278.8
6	-14.7	955.1	5.3	215.8	-60.4	642.6	2.6	243.8
7	-15.2	948.9	7.2	154.6	-64.5	638.7	1.8	216.1
8	-19.7	953.2	12.0	175.0	-68.2	642.8	1.8	223.7
9	-17.9	956.7	8.5	155.2	-60.3	646.0	1.7	228.8
10	-20.6	943.0	6.5	188.5	-62.9	634.1	3.0	214.2
11	-29.4	936.9	4.6	216.5	-60.3	623.2	6.0	204.3
12	-30.4	945.2	3.6	198.0	-66.4	620.5	3.2	178.9
13	-22.1	947.3	4.3	141.2	-70.6	622.2	0.6	259.9
14	-21.4	954.0	5.5	216.3	-67.5	627.8	4.1	273.1
15	-18.4	965.9	7.1	168.7	-63.5	641.4	6.8	270.4
16	-12.7	962.2	16.7	156.6	-61.9	651.3	5.4	269.8
17	-16.3	949.9	18.6	175.1	-62.1	648.1	5.8	218.5
18	-20.1	939.7	16.3	168.3	-61.8	639.3	8.1	181.2
19	-24.1	942.2	11.1	181.8	-63.2	632.2	6.6	181.7
20	-24.3	941.9	15.7	178.5	-62.1	629.9	6.7	178.2
21	-20.9	944.7	8.6	178.4	-63.7	630.6	5.4	162.3
22	-24.4	948.2	6.7	184.0	-71.8	630.3	2.0	169.9
23	-23.3	953.4	10.1	178.9	999.9	999.9	99.9	999.9
24	-15.4	958.4	13.8	157.5	-71.4	637.0	1.5	182.2
25	-16.9	951.2	14.4	165.2	-68.2	643.7	1.5	159.4
26	-15.9	950.8	12.1	150.0	-61.9	644.7	3.2	147.4
27	-16.7	957.4	6.7	169.5	-64.4	643.3	2.8	183.9
28	-21.5	946.8	5.6	202.1	-64.4	631.9	2.6	225.3
29	-26.0	956.0	5.7	215.1	-67.0	632.3	3.2	186.0
30	-16.3	965.2	12.1	156.3	-73.0	645.7	1.4	150.3
AVE	-18.4	951.4	8.5	173.8	-61.9	638.3	2.5	210.6

JUL 80	D-10				DOME C			
DATE	Temp.	Pres.	WSpd	WlDir	Temp.	Pres.	WSpd	WlDir
1	-13.7	971.1	18.0	169.4	-62.5	654.1	0.5	121.8
2	-9.7	972.8	13.2	149.1	-51.7	659.8	1.9	112.7
3	-8.1	971.4	12.1	164.6	-54.3	659.6	2.2	109.6
4	-8.4	971.3	11.6	173.1	-57.7	657.5	0.2	190.8
5	-11.1	969.2	11.6	177.1	-59.8	659.0	1.5	193.5
6	-15.3	966.7	16.5	187.1	-60.3	659.2	2.4	216.2
7	-16.3	963.7	9.4	176.2	-58.5	656.2	4.9	222.1
8	-22.2	962.3	7.3	178.9	-62.3	650.6	3.2	194.1
9	-25.0	955.1	7.0	188.0	-60.2	647.0	6.2	204.4
10	-22.0	967.4	6.2	186.6	-62.1	649.3	2.2	233.2
11	-15.2	961.7	3.7	158.3	-50.9	644.8	1.7	42.4
12	-13.6	955.1	6.7	190.8	-51.2	640.7	3.1	346.6
13	-12.2	961.0	4.5	184.8	-55.4	637.7	2.8	322.9
14	-10.0	965.0	6.3	222.3	-58.9	637.9	3.2	314.3
15	-11.9	972.0	2.4	204.2	-62.5	645.1	3.0	285.5
16	-11.7	978.2	3.6	139.2	-41.3	653.1	3.0	55.7
17	-10.2	985.1	1.3	145.6	-32.4	656.6	7.7	330.9
18	-7.9	973.3	6.3	214.7	-42.3	656.0	6.0	290.9
19	-11.6	967.5	9.1	176.9	-61.3	653.2	3.9	245.8
20	-17.7	959.1	10.4	174.2	-60.2	647.6	4.3	246.2
21	-21.3	954.5	3.7	139.3	-62.3	641.1	1.8	202.9
22	-18.5	964.9	8.2	156.9	-61.0	643.5	0.9	13.5
23	-18.3	974.6	4.8	193.7	-60.3	650.0	2.3	281.3
24	-14.7	961.4	4.9	155.1	-61.1	645.1	3.5	269.9
25	-19.9	956.8	5.9	200.3	-60.2	642.2	1.6	231.2
26	-19.1	970.9	6.0	145.7	-59.1	645.2	0.7	350.5
27	-18.9	956.7	14.1	152.0	-61.8	645.6	1.4	143.7
28	-10.1	962.4	10.6	158.2	-54.8	643.4	4.9	74.9
29	-10.2	971.3	8.3	177.8	-56.1	650.7	3.2	352.8
30	-11.6	980.0	10.9	159.4	-53.2	661.3	0.8	340.2
31	-9.6	971.3	11.1	150.9	-59.7	661.8	2.7	261.4
AVE	-14.1	967.2	7.7	171.5	-56.6	650.1	1.0	273.8

AUG 80	D-10				DOME C			
DATE	Temp.	Pres.	WSpd	WlDir	Temp.	Pres.	WSpd	WlDir
1	-15.4	948.4	11.9	167.8	-57.9	650.6	6.4	228.5
2	-21.9	941.9	10.2	168.7	-61.5	636.4	5.2	200.3
3	-23.6	949.8	14.4	175.2	-63.2	633.2	3.9	167.9
4	-18.0	955.0	15.4	159.5	-65.8	638.9	1.0	200.0
5	-18.2	955.2	8.0	145.2	-65.0	638.1	1.2	210.9
6	-20.6	948.5	7.0	167.1	-66.2	634.6	2.1	186.6
7	-23.0	956.1	4.3	182.9	-66.8	638.1	1.4	163.4
8	-17.2	952.6	13.2	155.8	-67.8	637.1	0.7	339.0
9	-16.6	948.1	15.8	163.6	-68.9	635.5	1.0	193.5
10	-18.7	937.6	20.7	174.2	-71.8	637.2	2.2	173.4
11	-19.2	945.9	15.7	172.7	-69.5	637.4	2.0	177.0
12	-17.7	947.2	14.3	173.9	-71.4	635.8	0.9	190.0
13	-18.1	948.3	14.5	183.7	-65.4	640.1	3.1	181.2
14	-21.1	953.8	10.6	177.5	-68.0	643.9	1.9	202.4
15	-21.5	963.0	14.1	178.2	-65.0	648.5	2.0	245.3
16	-17.8	958.3	18.1	177.0	-61.1	649.0	2.1	219.5
17	-17.2	942.6	14.8	176.8	-60.4	643.5	2.1	207.8
18	-18.4	944.3	9.5	184.6	-64.3	636.0	2.3	243.3
19	-17.6	958.9	8.8	180.7	-69.7	640.0	1.4	189.9
20	-13.0	958.3	10.6	166.9	-62.2	648.0	1.5	194.4
21	-11.8	955.1	17.6	176.8	-60.5	653.8	1.5	208.3
22	-13.5	961.7	15.5	185.3	-59.6	658.4	2.2	223.8
23	-20.9	953.7	20.6	182.1	-58.5	657.1	3.3	190.3
24	-18.1	946.4	20.4	170.7	-60.4	654.0	2.0	169.8
25	-11.0	956.1	19.2	168.1	-57.0	654.9	1.1	321.8
26	-10.3	963.6	15.0	183.6	-48.4	657.7	1.5	298.3
27	-11.6	962.3	3.1	146.0	-47.3	655.3	1.5	279.6
28	-13.7	958.4	18.5	175.9	-48.2	648.9	1.3	297.0
29	-22.0	956.8	1.8	179.7	-54.4	631.3	0.5	26.9
30	-22.5	965.0	8.6	153.0	-54.2	635.1	2.4	76.8
31	-19.1	964.0	6.0	171.0	-61.4	640.1	1.0	140.8
AVE	-17.6	953.2	12.7	172.9	-62.0	643.5	1.5	202.4

SEP 80	D-10				DOME C			
DATE	Temp.	Pres.	WSpd	WiDir	Temp.	Pres.	WSpd	WiDir
1	-19.3	958.9	3.2	145.5	-65.6	641.1	1.2	163.8
2	-18.1	961.7	7.2	129.3	-61.5	641.1	3.5	145.6
3	-13.1	970.8	11.9	152.4	-47.2	645.0	7.3	53.2
4	-10.4	966.5	15.6	165.0	-41.8	647.0	5.6	8.1
5	-8.4	959.9	7.9	152.0	-38.9	645.6	3.0	349.9
6	-8.9	951.6	18.0	168.0	-56.7	649.6	1.5	243.4
7	-11.9	948.8	18.4	163.0	-60.2	651.2	2.0	231.2
8	-14.4	945.0	16.9	174.3	-62.2	646.5	2.3	187.7
9	-13.9	931.4	23.8	175.8	-64.3	641.2	1.7	186.7
10	-8.3	937.3	7.4	122.5	-56.5	640.6	4.8	136.6
11	-6.6	949.8	14.4	139.1	-51.4	649.2	3.7	76.9
12	-5.6	955.1	11.1	133.8	-38.2	655.9	5.3	68.4
13	-7.0	960.9	11.0	138.2	-39.2	657.1	3.0	67.0
14	-7.3	965.9	12.7	155.0	-42.6	656.2	1.4	26.0
15	-9.1	968.5	9.8	175.3	-48.4	654.2	3.0	284.5
16	-10.1	965.9	10.2	171.8	-60.0	655.9	4.4	241.7
17	-15.4	966.9	17.9	164.3	-57.9	660.4	2.3	216.2
18	-10.7	955.2	17.4	154.6	-52.8	656.7	2.7	228.2
19	-12.1	953.4	14.7	147.6	-56.7	652.2	2.4	177.8
20	-16.5	949.8	14.1	156.3	-55.7	649.3	3.6	182.9
21	-23.8	946.4	14.2	160.3	-55.5	640.1	6.3	196.8
22	-25.8	941.6	8.9	173.5	-53.7	627.3	7.1	174.1
23	-22.0	944.9	6.4	171.9	-57.7	632.3	6.0	120.5
24	-19.7	947.4	9.7	178.2	-60.1	634.1	3.1	98.9
25	-19.8	949.6	7.9	175.9	-59.9	630.2	0.8	21.6
26	-19.1	946.8	11.0	163.5	-60.9	627.0	1.9	339.6
27	-15.7	940.5	13.6	168.0	-62.3	623.6	5.2	307.4
28	-13.9	940.2	17.2	174.2	-58.4	631.1	1.5	321.9
29	-13.9	940.8	15.0	168.4	-49.6	630.3	2.5	341.7
30	-10.6	939.9	7.9	146.4	-52.0	629.4	0.9	345.0
AVE	-13.7	951.9	12.2	160.8	-54.2	643.3	0.5	138.1

OCT 80	D-10				DOME C			
DATE	Temp.	Pres.	WSpd	WlDir	Temp.	Pres.	WSpd	WlDir
1	-14.0	945.1	3.0	199.6	-57.7	628.0	1.6	145.8
2	-17.8	950.6	6.2	179.6	-62.5	625.3	3.1	158.4
3	-18.9	953.3	6.2	179.2	-66.6	628.4	2.8	250.7
4	-16.2	951.3	17.2	173.6	-62.8	625.5	5.0	231.9
5	-22.7	917.3	16.4	184.4	-60.3	619.8	7.2	194.3
6	-25.0	928.7	11.1	176.9	-63.1	619.0	5.1	197.6
7	-26.4	934.5	3.8	201.2	-63.9	618.4	4.2	221.9
8	-24.0	944.0	5.6	143.8	-62.6	625.3	3.4	168.7
9	-21.5	942.2	4.6	176.6	-59.6	632.9	4.3	167.5
10	-14.8	941.0	8.3	179.1	-51.7	635.5	2.4	103.9
11	-15.5	949.0	6.9	156.1	-46.3	636.8	4.4	55.0
12	-14.0	939.6	13.2	167.0	-46.1	634.1	2.7	18.3
13	-14.1	942.3	7.4	176.8	-44.3	630.9	3.5	347.1
14	-15.3	941.8	6.5	195.7	-55.0	650.6	3.5	262.5
15	-15.7	940.8	7.7	185.2	-60.3	650.0	5.8	230.2
16	-21.6	933.6	8.4	188.6	-56.9	629.?	8.1	201.3
17	-18.6	946.4	8.0	182.9	-54.9	635.5	3.3	203.1
18	-16.8	947.1	4.0	178.0	-54.3	635.5	2.7	210.4
19	-18.7	948.9	6.5	198.1	-55.7	637.6	3.1	228.8
20	-16.8	945.8	8.1	198.4	-53.1	636.2	2.6	240.4
21	-15.3	948.9	5.8	207.1	-54.3	633.6	3.7	247.6
22	-15.8	948.7	3.4	198.1	-58.5	631.2	3.2	218.9
23	-15.6	950.9	5.5	142.4	-47.6	631.7	0.0	180.0
24	-16.2	946.5	5.7	182.9	-53.8	632.3	3.3	189.9
25	-19.7	943.1	7.6	167.0	-48.9	642.0	8.8	186.6
26	-17.1	946.3	13.2	167.8	-44.5	646.2	8.8	199.1
27	-15.6	946.0	5.5	138.7	-45.1	654.0	6.1	179.7
28	-12.4	948.8	9.5	162.1	-43.6	655.2	6.3	178.5
29	-11.2	957.1	13.1	179.5	-46.1	652.5	2.9	170.9
30	-11.1	957.0	8.1	183.9	-43.7	653.9	1.5	127.2
31	-11.4	953.4	6.8	167.2	-45.9	650.2	3.1	210.5
AVE	-17.1	944.1	7.6	176.9	-53.7	634.8	2.9	200.0

NOV 80	D-10				DOME C			
DATE	Temp.	Pres.	WSpd	WiDir	Temp.	Pres.	WSpd	WiDir
1	-13.4	954.4	4.7	184.9	-44.5	644.4	3.0	208.5
2	-14.6	961.5	8.9	173.2	-44.4	645.7	1.3	106.3
3	-10.7	961.3	11.2	167.8	-37.2	648.7	0.6	274.9
4	-9.9	960.1	6.7	176.4	-44.9	647.6	1.6	195.5
5	-9.9	960.4	5.1	174.8	-44.2	647.0	1.2	191.2
6	-7.7	968.8	6.6	152.4	-43.9	652.4	1.0	35.2
7	-6.2	976.1	11.0	136.6	-36.3	658.8	1.2	40.9
8	-7.7	966.6	11.8	154.0	-39.0	658.0	1.5	161.0
9	-8.4	948.7	20.3	169.7	-41.9	655.9	3.2	171.0
10	-7.3	951.9	13.3	171.1	-39.8	654.2	3.8	180.9
11	-9.6	956.8	10.9	156.0	-39.2	656.4	4.2	174.1
12	-10.4	959.8	6.4	146.6	-37.2	655.7	5.5	168.2
13	-9.4	951.9	12.4	162.6	-38.2	651.5	4.4	178.6
14	-9.5	955.5	8.4	183.6	-39.6	648.7	3.0	181.6
15	-8.2	960.1	8.7	154.9	-39.5	649.3	1.1	159.4
16	-7.4	955.7	18.3	149.2	-37.3	652.1	1.2	79.1
17	-8.0	964.5	10.3	155.4	-37.8	655.9	2.3	122.7
18	-7.7	953.0	15.6	167.2	-39.3	654.8	2.7	208.4
19	-10.0	943.7	22.9	168.4	-37.7	651.7	5.4	177.8
20	-7.1	948.4	17.5	172.5	-35.9	652.8	5.7	174.3
21	-6.0	957.8	7.6	174.6	-35.0	655.2	4.6	140.6
22	-6.4	961.3	5.7	183.0	-35.1	658.1	3.2	148.9
23	-6.2	967.9	6.6	167.8	-34.7	660.7	1.8	219.5
24	-6.9	964.0	4.2	141.4	-34.3	658.2	5.6	227.7
25	-8.4	957.8	4.7	178.8	-35.1	652.8	4.3	214.6
26	-7.7	956.6	7.6	163.1	-35.6	651.3	3.2	208.0
27	-7.2	955.5	8.3	164.3	-35.6	647.3	3.3	224.1
28	-7.0	952.8	5.6	183.9	-35.1	644.8	2.1	229.1
29	-3.5	951.3	8.2	178.8	-34.8	646.7	1.9	269.5
30	-1.0	950.1	5.3	159.7	-31.7	648.9	0.8	281.6
AVE	-8.0	957.8	9.7	164.8	-38.1	652.1	2.2	185.1

DEC 80	D-10				DOME C			
DATE	Temp.	Pres.	WSpd	WiDir	Temp.	Pres.	WSpd	WiDir
1	-2.9	948.0	4.1	144.3	-25.6	649.2	0.3	138.3
2	-3.7	954.5	4.1	156.0	-29.3	650.3	0.7	91.5
3	-3.1	953.8	4.8	192.9	-29.7	650.9	1.1	141.2
4	-4.9	950.2	3.4	185.5	-32.3	648.1	2.1	141.1
5	-6.0	950.4	5.1	170.0	-31.4	649.0	1.5	135.0
6	-4.3	950.7	3.6	182.7	-31.3	648.3	1.2	177.3
7	-4.2	944.6	6.6	144.8	-32.3	644.2	1.7	165.3
8	-4.6	949.3	4.7	168.7	-31.0	645.5	1.0	156.3
9	-3.8	954.3	5.3	175.9	-22.7	648.4	0.0	127.9
10	-5.0	959.1	2.4	187.5	-30.2	649.7	0.9	281.2
11	-4.7	955.6	3.8	175.7	-25.5	649.5	0.1	196.9
12	-4.6	958.8	4.2	180.9	-22.1	651.0	0.0	309.0
13	-3.4	961.8	4.4	189.1	-31.3	653.2	2.1	194.1
14	-3.2	961.0	5.8	165.7	-33.8	655.3	3.4	207.1
15	-3.0	958.7	5.7	187.6	-31.7	654.1	5.1	222.4
16	-5.4	953.7	7.7	156.0	-32.8	651.7	6.1	184.1
17	-5.0	954.8	6.2	166.9	-32.4	650.0	5.3	182.9
18	-3.5	962.2	5.4	137.1	-31.5	650.9	3.5	180.8
19	-4.0	966.6	10.9	141.0	-24.4	658.9	0.6	172.5
20	-1.5	963.8	9.7	134.7	-24.7	662.0	1.0	198.4
21	-1.5	948.3	13.7	149.7	-25.7	658.8	1.9	148.3
22	-2.1	956.6	6.4	154.8	-26.4	658.7	1.7	202.8
23	-3.4	959.6	4.1	174.4	-27.8	657.3	2.8	201.5
24	-2.4	953.4	8.3	135.3	-27.1	653.9	2.4	191.8
25	-3.1	950.9	5.1	162.7	-23.8	652.0	0.9	192.5
26	-2.0	958.1	3.7	166.1	-24.3	654.6	2.5	187.5
27	-3.4	962.6	5.7	171.8	-27.9	653.2	4.9	262.7
28	-2.5	957.8	10.8	132.8	-26.3	654.8	1.8	215.1
29	-2.6	958.7	11.9	149.4	-26.5	658.0	3.5	93.5
30	-3.0	952.3	10.7	142.9	-27.7	657.3	2.4	95.8
31	-3.0	945.1	12.8	158.2	-28.1	652.6	2.6	203.8
AVE	-3.6	955.3	6.1	157.8	-28.3	652.6	1.6	186.5

JAN 81 D-57 DOME C

DATE	Temp.	Pres.	WSpd	WiDir	Temp.	Pres.	WSpd	WiDir
1	999.9	999.9	99.9	999.9	999.9	999.9	99.9	999.9
2	999.9	999.9	99.9	999.9	999.9	999.9	99.9	999.9
3	999.9	999.9	99.9	999.9	999.9	999.9	99.9	999.9
4	999.9	999.9	99.9	999.9	999.9	999.9	99.9	999.9
5	999.9	999.9	99.9	999.9	999.9	999.9	99.9	999.9
6	999.9	999.9	99.9	999.9	999.9	999.9	99.9	999.9
7	999.9	999.9	99.9	999.9	999.9	999.9	99.9	999.9
8	999.9	999.9	99.9	999.9	999.9	999.9	99.9	999.9
9	999.9	999.9	99.9	999.9	999.9	999.9	99.9	999.9
10	999.9	999.9	99.9	999.9	999.9	999.9	99.9	999.9
11	999.9	999.9	99.9	999.9	999.9	999.9	99.9	999.9
12	999.9	999.9	99.9	999.9	999.9	999.9	99.9	999.9
13	999.9	999.9	99.9	999.9	999.9	999.9	99.9	999.9
14	999.9	999.9	99.9	999.9	999.9	999.9	99.9	999.9
15	999.9	999.9	99.9	999.9	999.9	999.9	99.9	999.9
16	-22.4	761.0	10.4	166.8	-32.5	653.3	1.9	177.8
17	-22.7	756.2	10.5	171.4	-35.5	650.0	3.8	208.0
18	-22.1	747.7	7.1	162.0	-33.4	642.3	4.1	212.9
19	-21.3	757.1	4.4	155.0	-34.5	646.1	2.5	119.7
20	-20.3	760.6	9.1	172.8	-34.8	648.5	1.3	225.3
21	-21.3	755.5	9.8	148.0	-34.5	646.7	1.9	219.8
22	-18.5	750.5	18.6	137.4	-35.5	650.6	3.1	121.8
23	-14.2	748.7	15.9	137.1	-31.8	649.8	6.8	84.7
24	-14.1	751.2	13.6	139.6	-28.6	647.4	5.3	83.9
25	-15.7	754.0	6.3	146.1	-28.2	646.0	4.3	346.2
26	-17.1	751.0	10.8	141.7	-34.6	647.7	3.4	246.4
27	-21.0	748.1	15.0	155.4	-34.5	649.9	5.6	222.0
28	-23.2	748.7	17.7	144.1	-34.5	650.6	5.5	222.1
29	-22.6	754.6	10.6	168.6	-35.7	648.6	4.5	228.8
30	-21.7	752.7	11.9	141.0	-36.6	646.9	3.1	224.8
31	-22.9	752.7	14.9	142.3	-36.2	647.8	1.6	175.1
AVE	-20.1	763.1	11.3	149.7	-33.7	648.2	1.4	203.1

FEB 81	D-10				D-57				DOME C			
DATE	Temp.	Pres.	WSpd	WiDir	Temp.	Pres.	WSpd	WiDir	Temp.	Pres.	WSpd	WiDir
1	-6.7	953.7	5.9	177.1	-22.7	753.8	12.9	141.4	-38.4	648.2	1.2	160.4
2	-3.0	952.3	2.8	162.9	-18.4	753.3	6.3	132.2	-39.1	644.9	3.0	64.6
3	-3.1	953.8	5.1	135.6	-17.3	755.4	9.3	131.7	-37.0	647.7	3.9	18.2
4	-3.3	953.7	15.7	151.1	-16.9	757.7	19.6	132.8	-33.7	654.4	1.8	55.0
5	-4.7	954.2	12.2	160.2	-20.0	757.2	17.2	137.6	-32.1	653.6	2.1	331.1
6	-5.6	951.1	6.1	140.6	-19.9	752.3	15.2	139.3	-33.1	651.3	1.6	152.3
7	-6.1	948.2	8.9	155.2	-22.1	750.5	17.4	148.9	-40.0	654.2	3.1	148.3
8	-8.9	950.7	3.5	168.3	-22.1	749.2	12.8	158.9	-41.2	651.2	2.5	212.4
9	-7.9	952.8	6.7	179.0	-21.9	749.5	12.4	155.2	-39.5	650.2	4.5	265.3
10	-7.6	945.2	18.8	184.3	999.9	999.9	99.9	999.9	-36.5	653.4	4.9	231.2
11	-6.5	951.2	15.2	184.4	999.9	999.9	99.9	999.9	-37.3	652.3	3.9	226.4
12	-4.9	955.3	6.6	159.0	999.9	999.9	99.9	999.9	-36.2	651.4	3.4	235.9
13	-4.5	958.0	5.5	166.0	999.9	999.9	99.9	999.9	-37.5	652.3	3.9	260.9
14	-5.9	943.7	12.4	170.0	999.9	999.9	99.9	999.9	-38.2	647.1	1.8	214.9
15	-7.7	946.1	8.8	159.5	999.9	999.9	99.9	999.9	-43.2	644.5	2.1	207.2
16	-8.1	944.5	10.1	167.7	999.9	999.9	99.9	999.9	-44.6	642.8	2.6	182.4
17	-6.9	939.0	16.0	179.7	999.9	999.9	99.9	999.9	-45.2	642.3	2.0	172.3
18	-2.2	941.6	12.0	143.3	999.9	999.9	99.9	999.9	-41.5	645.2	2.1	81.6
19	-3.2	946.0	14.5	163.2	999.9	999.9	99.9	999.9	-39.4	650.0	2.6	16.9
20	-3.3	948.7	16.4	166.0	999.9	999.9	99.9	999.9	-41.3	652.4	0.8	152.9
21	-7.3	953.6	13.0	172.8	999.9	999.9	99.9	999.9	-46.6	651.6	2.9	191.8
22	-11.0	956.4	8.1	179.5	999.9	999.9	99.9	999.9	-45.3	645.2	3.7	225.8
23	-7.0	955.0	13.1	140.7	999.9	999.9	99.9	999.9	-47.5	646.7	1.7	165.5
24	-3.1	955.0	9.9	133.7	999.9	999.9	99.9	999.9	-44.2	650.4	1.2	74.6
25	-2.3	956.9	9.9	120.5	999.9	999.9	99.9	999.9	-39.2	652.8	0.6	108.1
26	-9.1	958.5	8.9	211.5	999.9	999.9	99.9	999.9	-48.0	651.9	2.5	220.7
27	-10.7	959.5	7.5	195.0	999.9	999.9	99.9	999.9	-52.1	650.2	4.9	200.3
28	-12.6	961.6	8.0	187.5	999.9	999.9	99.9	999.9	-50.8	652.7	6.1	182.8
AVE	-6.1	951.6	9.5	164.7	-20.1	753.2	13.6	142.2	-41.0	649.7	1.3	204.8

MAR 81	D-10				D-57				DOME C			
DATE	Temp.	Pres.	WSpd	WiDir	Temp.	Pres.	WSpd	WiDir	Temp.	Pres.	WSpd	WiDir
1	-14.3	969.3	13.6	183.2	999.9	999.9	99.9	999.9	-51.9	658.0	4.8	177.1
2	-10.0	979.4	6.1	168.1	999.9	999.9	99.9	999.9	-52.1	662.0	2.5	155.2
3	-6.8	980.8	5.0	157.9	999.9	999.9	99.9	999.9	-51.1	664.5	2.6	245.0
4	-7.2	968.3	10.5	162.5	999.9	999.9	99.9	999.9	-51.7	662.0	2.9	192.4
5	-7.8	961.2	6.1	165.2	999.9	999.9	99.9	999.9	-50.1	656.1	2.3	186.1
6	-9.9	961.3	6.5	175.8	999.9	999.9	99.9	999.9	-49.4	651.5	2.1	268.5
7	-9.0	969.8	4.1	154.9	999.9	999.9	99.9	999.9	-49.3	655.5	3.6	269.5
8	-7.5	958.1	15.0	156.2	999.9	999.9	99.9	999.9	-50.4	656.0	3.5	255.5
9	-8.3	956.7	12.8	163.6	999.9	999.9	99.9	999.9	-53.1	652.6	2.7	226.0
10	-11.6	959.5	13.0	172.8	999.9	999.9	99.9	999.9	-54.3	650.9	2.0	206.5
11	-10.8	954.5	14.3	176.7	999.9	999.9	99.9	999.9	-57.2	645.4	1.7	188.1
12	-12.9	957.1	10.4	183.2	999.9	999.9	99.9	999.9	-58.6	642.2	3.6	145.2
13	-15.0	944.2	9.7	176.5	999.9	999.9	99.9	999.9	-58.4	637.6	3.7	176.1
14	-13.2	945.0	14.4	182.7	999.9	999.9	99.9	999.9	-53.1	642.5	4.2	138.4
15	-9.0	949.3	17.6	173.2	999.9	999.9	99.9	999.9	-54.8	650.6	3.0	141.5
16	-8.1	951.6	16.4	183.1	999.9	999.9	99.9	999.9	-53.8	650.8	2.6	131.9
17	-10.5	954.5	11.5	178.9	999.9	999.9	99.9	999.9	-50.5	647.7	1.3	29.5
18	-9.6	955.7	16.3	171.8	999.9	999.9	99.9	999.9	-53.6	646.9	1.5	285.4
19	-9.6	954.0	18.0	178.8	999.9	999.9	99.9	999.9	-51.7	645.3	0.8	304.6
20	-11.4	950.3	13.1	183.8	999.9	999.9	99.9	999.9	-53.1	640.1	1.1	358.6
21	-11.6	953.0	5.3	185.0	999.9	999.9	99.9	999.9	-57.8	636.2	1.7	263.9
22	-11.6	961.2	5.2	184.5	999.9	999.9	99.9	999.9	-59.9	643.0	3.8	256.0
23	-9.0	964.7	12.5	142.5	999.9	999.9	99.9	999.9	-57.3	652.4	2.8	212.8
24	-10.3	957.8	10.5	164.3	999.9	999.9	99.9	999.9	-50.4	652.9	3.1	127.6
25	-13.9	953.0	9.1	185.0	999.9	999.9	99.9	999.9	-52.9	649.6	3.5	177.5
26	-14.9	951.4	10.9	172.6	999.9	999.9	99.9	999.9	-57.3	645.1	3.7	176.7
27	-16.8	965.2	7.1	191.8	999.9	999.9	99.9	999.9	-59.8	648.7	2.6	180.8
28	-14.6	961.1	12.3	174.6	999.9	999.9	99.9	999.9	-59.1	652.1	3.2	177.1
29	-16.5	960.0	15.9	177.4	999.9	999.9	99.9	999.9	-59.8	654.5	5.2	172.8
30	-18.6	961.6	13.6	186.5	999.9	999.9	99.9	999.9	-57.8	653.5	5.1	179.4
31	-19.6	954.8	8.5	194.0	-41.1	749.1	16.2	179.3	-59.0	649.1	6.9	176.7
AVE	-11.7	959.0	10.8	174.6	-41.1	749.1	16.2	179.3	-54.6	650.3	2.2	187.6

APR 81	D-10				D-57				DOME C			
DATE	Temp.	Pres.	WSpd	WiDir	Temp.	Pres.	WSpd	WiDir	Temp.	Pres.	WSpd	WiDir
1	-15.0	960.9	7.3	186.3	-35.8	758.0	14.1	178.0	-59.8	653.0	5.2	174.6
2	-10.2	959.6	15.2	176.1	-27.9	760.1	17.1	141.7	-49.1	658.6	6.3	113.1
3	-7.1	972.5	12.7	163.7	-23.5	770.6	16.2	138.9	-52.3	665.5	3.6	90.1
4	-9.3	980.1	11.2	175.8	-23.9	774.9	14.2	138.5	-52.5	667.1	2.4	9.4
5	-8.9	975.6	10.2	180.4	-25.9	773.3	12.8	161.1	-51.2	666.3	2.3	242.5
6	-11.8	961.9	17.9	167.2	-26.1	761.8	18.2	139.2	-51.2	658.7	2.9	107.9
7	-11.1	963.0	20.0	162.0	-23.9	761.7	17.3	137.3	-42.3	652.0	5.7	30.8
8	-7.9	973.6	7.9	166.8	-23.4	768.2	6.3	145.4	-53.2	648.1	5.6	340.1
9	-12.5	971.9	5.3	184.4	-27.9	764.3	5.4	181.5	-66.5	644.6	5.9	256.4
10	-14.5	968.2	13.7	184.9	-37.1	762.1	14.7	173.5	-61.3	654.4	4.0	183.7
11	-13.1	958.7	18.0	173.8	-32.9	758.3	15.6	146.9	-60.0	653.2	3.6	242.6
12	-14.3	940.5	14.8	177.5	-38.5	735.8	20.1	161.0	-59.8	637.8	4.9	265.8
13	-19.6	947.3	7.0	188.7	-36.9	741.5	8.3	164.1	-63.1	630.8	2.8	261.2
14	-20.6	952.5	4.5	191.7	-39.1	744.7	7.0	174.8	-64.0	629.6	2.3	224.2
15	-15.5	954.0	4.2	155.6	-29.7	749.0	4.7	139.6	-67.9	638.6	2.6	228.0
16	-14.0	940.0	14.3	174.5	-29.9	741.6	10.9	140.5	-65.6	628.2	2.9	297.4
17	-15.2	931.6	12.0	179.5	-30.9	734.1	12.2	133.5	-64.4	624.0	1.9	26.3
18	-13.8	943.4	5.9	184.8	999.9	999.9	99.9	999.9	-60.4	629.0	3.1	38.0
19	-14.9	950.1	16.7	186.1	-33.7	739.0	10.7	151.5	-53.7	631.0	6.2	352.5
20	-11.5	954.2	8.3	184.5	999.9	999.9	99.9	999.9	-64.2	633.4	0.9	106.1
21	-17.4	954.9	5.2	225.6	999.9	999.9	99.9	999.9	-65.6	627.0	2.7	331.9
22	-20.2	954.9	3.9	223.8	999.9	999.9	99.9	999.9	-74.3	622.6	4.0	265.8
23	-22.3	958.0	5.5	196.7	999.9	999.9	99.9	999.9	-76.3	628.2	5.1	263.7
24	-24.3	961.4	4.3	229.9	999.9	999.9	99.9	999.9	-75.5	628.6	3.2	234.7
25	-18.6	964.1	8.0	118.5	999.9	999.9	99.9	999.9	-67.7	632.5	1.5	186.6
26	-7.7	960.8	14.5	124.7	999.9	999.9	99.9	999.9	-49.8	642.7	4.8	51.8
27	-1.7	962.0	6.4	105.0	999.9	999.9	99.9	999.9	-44.1	652.0	2.9	351.6
28	-5.6	952.6	10.6	154.7	999.9	999.9	99.9	999.9	-51.1	655.8	2.6	241.3
29	-4.1	946.9	2.7	15.5	999.9	999.9	99.9	999.9	-54.9	643.7	1.1	108.3
30	-15.3	955.9	7.2	221.3	999.9	999.9	99.9	999.9	-58.9	639.8	1.2	204.7
AVE	-13.3	957.7	8.9	174.1	-29.6	758.1	11.7	150.3	-59.5	642.1	0.7	283.7

MAY 81	D-10				D-57				DOME C			
DATE	Temp.	Pres.	WSpd	WiDir	Temp.	Pres.	WSpd	WiDir	Temp.	Pres.	WSpd	WiDir
1	-13.9	961.3	13.4	173.0	999.9	999.9	99.9	999.9	-66.0	647.6	2.3	165.5
2	-13.7	956.1	15.5	170.5	-28.9	754.9	17.2	139.3	-55.7	648.0	1.5	321.3
3	-14.0	956.7	10.1	167.5	-31.4	753.4	14.9	141.2	-59.8	643.0	3.3	280.1
4	-16.4	957.5	6.8	166.4	-33.6	753.0	9.0	149.6	-62.1	640.5	3.2	263.6
5	-15.8	955.9	8.3	146.2	-34.9	750.1	8.0	157.7	-70.2	637.5	3.0	218.2
6	-20.1	943.0	20.3	178.2	-37.4	743.1	15.4	160.2	-66.3	639.0	4.4	182.9
7	-18.0	936.4	15.8	171.9	-36.6	736.5	18.6	142.5	-59.5	639.1	4.5	157.7
8	-16.8	939.8	17.6	175.2	-33.8	739.8	18.5	138.4	-64.1	637.4	3.1	160.3
9	-14.2	943.9	19.7	180.0	-30.7	747.0	17.6	139.4	-61.7	640.7	3.0	119.0
10	-15.3	957.7	10.5	170.2	-32.0	749.9	16.3	135.0	-59.6	643.5	2.1	32.8
11	-16.3	960.7	8.6	170.4	999.9	999.9	99.9	999.9	-61.1	641.5	1.5	6.0
12	-13.1	949.3	16.6	134.6	-29.2	744.2	25.0	90.0	-62.4	640.4	3.6	86.9
13	-12.5	961.6	14.3	151.0	-27.6	757.4	16.6	116.1	-50.4	647.9	7.7	79.8
14	-15.4	962.0	16.5	174.8	-31.5	759.1	16.8	138.7	-55.9	653.8	0.6	136.8
15	-15.6	945.3	18.8	186.8	-37.6	746.3	16.9	172.4	-61.2	643.2	4.6	231.1
16	-24.2	947.3	8.4	209.8	-50.1	740.4	18.4	177.3	-67.1	632.2	3.9	189.5
17	-24.6	954.2	8.8	190.0	-52.0	741.0	18.5	182.1	-71.8	637.2	2.7	165.0
18	-25.5	947.3	8.1	190.1	-48.7	735.2	13.3	175.5	-70.0	634.2	4.3	179.4
19	-26.1	941.1	8.9	184.6	-44.8	733.0	12.3	174.9	-67.2	630.2	3.0	164.3
20	-20.8	945.6	10.7	185.8	-39.6	740.8	15.1	174.5	-69.3	635.0	3.2	134.4
21	-16.5	962.9	6.1	162.4	-32.3	754.3	8.4	145.3	-60.8	641.7	3.6	92.5
22	-15.1	964.9	6.5	194.3	-34.8	757.9	7.2	178.3	-61.9	638.1	1.1	335.6
23	-15.7	962.3	7.1	193.4	-37.7	754.1	7.1	175.9	-71.4	636.0	5.1	198.0
24	999.9	999.9	99.9	999.9	-34.6	741.8	13.2	154.7	-61.2	635.1	7.2	183.0
25	999.9	999.9	99.9	999.9	-43.8	745.7	12.6	168.1	-62.6	634.6	5.7	150.0
26	999.9	999.9	99.9	999.9	-40.3	744.0	11.5	171.3	-63.3	638.4	5.2	184.3
27	999.9	999.9	99.9	999.9	-40.3	755.9	21.8	182.7	-59.9	655.4	4.9	227.5
28	999.9	999.9	99.9	999.9	-34.0	769.3	16.1	178.5	-56.8	658.5	4.5	268.8
29	999.9	999.9	99.9	999.9	-29.8	767.7	9.7	174.1	-47.8	651.7	2.3	332.1
30	999.9	999.9	99.9	999.9	-18.4	761.3	1.1	304.6	-58.8	642.5	3.1	309.0
31	999.9	999.9	99.9	999.9	-17.6	763.2	3.0	267.3	-55.9	644.5	2.2	308.0
AVE	-17.4	952.7	11.6	174.2	-34.4	751.5	11.4	159.5	-61.9	641.5	1.6	180.5

JUN 81	D-57				DOME C			
DATE	Temp.	Pres.	WSpd	WlDir	Temp.	Pres.	WSpd	WlDir
1	-16.5	769.8	4.7	273.1	-36.1	648.7	8.2	317.7
2	-23.8	773.8	8.5	177.2	-45.0	656.0	4.8	329.9
3	-16.8	777.0	1.5	162.4	-28.9	654.1	11.7	341.8
4	-19.0	770.8	3.2	263.3	-33.0	648.6	10.5	312.2
5	-23.1	756.4	4.4	191.8	-41.1	641.2	9.0	298.9
6	-32.6	760.5	8.9	174.8	-49.0	643.5	3.7	298.4
7	-25.0	747.3	1.8	235.5	-61.3	637.7	1.4	189.4
8	-39.1	746.2	13.9	179.2	-62.8	636.5	3.3	237.2
9	-32.5	747.2	12.1	137.2	-65.2	636.6	2.3	142.3
10	-25.8	748.5	10.8	89.9	-56.7	633.2	4.1	70.6
11	-23.2	746.5	2.0	89.2	-60.3	632.0	2.8	356.8
12	-22.5	752.4	6.9	85.8	-67.0	634.8	4.1	290.7
13	-25.8	745.8	18.0	133.2	-64.4	639.2	2.0	267.2
14	-29.5	746.9	14.2	136.2	-68.5	638.0	3.2	261.3
15	-33.7	749.9	8.2	162.2	-70.3	638.6	3.1	236.3
16	-39.4	748.8	9.5	192.5	-65.8	634.9	4.9	212.8
17	-30.8	754.6	13.0	140.9	-67.0	641.9	1.8	146.0
18	-24.3	764.9	17.2	135.1	-53.0	655.0	3.1	45.5
19	-19.2	764.2	21.1	103.2	-40.6	660.7	4.8	55.5
20	-18.6	756.4	15.9	133.0	-40.3	653.6	3.7	325.6
21	-28.3	756.3	11.5	174.0	-53.0	644.4	6.2	277.7
22	-30.9	764.6	8.7	181.9	-54.4	646.2	2.8	311.9
23	-21.9	760.8	2.9	308.1	-44.9	641.2	2.4	342.1
24	-24.2	758.3	5.5	194.8	-51.6	640.1	4.3	295.7
25	-36.1	743.8	14.4	192.0	-62.4	636.9	3.3	221.9
26	-43.6	739.0	21.1	183.5	-58.3	640.2	6.3	194.9
27	-34.1	754.6	16.7	170.9	-53.4	654.6	1.8	180.6
28	-35.2	765.0	13.1	178.0	-59.4	656.1	5.5	263.7
29	-40.7	758.7	19.7	181.9	-60.7	654.8	5.3	231.8
30	-40.5	757.1	20.0	180.0	-55.7	653.6	3.7	256.3
AVE	-28.6	756.2	9.0	160.3	-54.1	644.3	8.4	293.4

JUL 81	D-57				DOME C			
DATE	Temp.	Pres.	WSpd	WlDir	Temp.	Pres.	WSpd	WlDir
1	-41.3	754.4	16.3	177.7	-68.8	649.9	4.3	219.6
2	-44.8	752.6	19.2	180.1	-66.4	651.8	5.8	188.8
3	-40.1	745.8	19.1	176.6	-64.8	649.6	5.1	184.7
4	-40.5	741.4	15.4	171.2	-66.0	640.3	5.0	193.1
5	-41.7	739.6	12.8	166.7	-69.1	631.8	4.0	176.3
6	-42.5	747.9	7.5	150.2	-72.8	633.7	1.9	191.7
7	-46.3	754.8	11.5	173.2	-78.3	641.7	3.1	223.2
8	-38.2	758.2	14.7	156.8	-63.5	651.1	3.8	168.6
9	-31.8	756.3	12.8	141.7	-62.5	649.9	2.8	220.8
10	-40.5	748.9	13.8	170.5	-61.8	643.4	3.6	218.7
11	-34.6	750.7	11.2	156.8	-63.5	641.9	2.9	215.9
12	-27.6	751.7	10.9	151.6	-61.2	645.8	3.6	184.7
13	-31.4	748.9	16.1	143.3	-62.1	645.4	3.2	190.8
14	-32.9	754.7	12.8	147.5	-62.0	648.4	3.5	174.0
15	-28.8	742.8	21.5	138.6	-62.9	650.0	3.5	166.2
16	-24.8	753.7	14.3	134.3	-61.1	650.3	2.2	147.6
17	-27.8	753.7	15.3	138.6	-61.0	651.1	3.6	175.9
18	-31.0	745.5	13.8	140.8	-61.6	647.0	4.3	162.0
19	-37.8	742.2	9.3	159.8	-67.9	636.6	2.3	197.8
20	-42.2	744.2	9.7	165.8	-68.8	632.9	2.2	189.2
21	-43.6	749.4	10.8	168.4	-71.0	635.2	1.3	164.4
22	-37.9	753.3	11.2	151.6	-65.7	639.0	1.8	27.1
23	-25.2	757.9	10.1	122.5	-58.4	640.4	2.6	17.6
24	-15.1	768.6	8.1	75.8	-34.4	649.0	7.6	11.9
25	-14.0	767.7	13.4	89.7	-29.9	650.2	8.2	1.0
26	-17.5	755.6	7.2	99.8	-51.9	643.0	1.4	187.7
27	-28.2	753.0	8.2	148.7	-60.4	642.6	2.4	238.8
28	-22.4	764.6	10.0	118.0	-51.0	649.7	3.0	70.9
29	-19.8	774.3	11.0	121.3	-49.8	662.4	1.1	305.3
30	-20.3	767.3	12.3	109.6	-48.2	660.1	3.0	143.1
31	-23.0	758.6	11.0	134.2	-48.4	651.8	2.3	116.5
AVE	-32.1	753.6	11.4	147.3	-60.1	645.7	1.6	183.4

AUG 81	D-57				DOME C			
DATE	Temp.	Pres.	WSpd	WlDir	Temp.	Pres.	WSpd	WlDir
1	-20.7	763.1	8.2	131.3	-58.0	652.4	2.2	139.3
2	-22.4	771.7	15.7	134.9	-57.5	666.6	3.7	145.4
3	-28.4	766.5	16.3	143.9	-56.7	665.6	3.7	208.2
4	-31.2	753.3	15.6	153.0	-56.7	656.0	5.2	183.5
5	999.9	999.9	99.9	999.9	-60.0	651.4	3.7	216.9
6	999.9	999.9	99.9	999.9	-57.7	648.0	8.5	194.4
7	999.9	999.9	99.9	999.9	-50.7	645.2	8.0	162.2
8	999.9	999.9	99.9	999.9	-54.3	650.3	6.4	120.2
9	999.9	999.9	99.9	999.9	-51.8	657.4	3.6	66.2
10	-20.4	782.5	2.4	170.2	-41.1	662.7	5.4	334.1
11	-20.2	779.2	6.2	175.5	-39.7	664.0	4.4	292.3
12	-23.0	772.3	8.1	169.6	-46.0	663.3	3.7	258.0
13	-32.2	767.6	16.2	176.3	-51.7	666.7	5.0	229.0
14	-34.0	759.1	14.9	175.0	-56.6	664.2	4.8	195.3
15	-31.2	754.3	21.0	141.0	-53.1	665.7	6.4	162.0
16	-19.8	755.7	14.4	123.6	-40.9	670.6	7.7	144.8
17	-26.5	753.1	21.1	140.9	-55.9	661.1	6.1	180.8
18	-30.9	747.3	20.4	143.0	-59.5	650.8	5.8	179.1
19	-29.8	752.4	20.3	137.9	-61.1	651.8	4.8	170.5
20	-28.4	754.0	14.6	137.8	-60.4	653.6	2.8	163.0
21	-29.4	753.4	12.7	138.7	-62.4	647.6	3.6	176.3
22	-30.4	750.1	15.2	141.6	-62.9	645.5	2.9	175.8
23	-26.4	752.4	12.4	135.2	-61.1	644.9	2.7	177.9
24	-27.1	756.1	7.9	135.0	-54.8	643.1	0.8	153.1
25	-23.6	752.7	12.2	106.0	-48.7	642.0	5.2	92.2
26	-22.9	756.9	14.6	134.1	-49.6	651.8	4.8	89.3
27	999.9	999.9	99.9	999.9	-49.3	653.3	1.4	15.9
28	999.9	999.9	99.9	999.9	-54.0	650.3	1.4	229.9
29	999.9	999.9	99.9	999.9	-63.5	642.9	2.3	180.6
30	999.9	999.9	99.9	999.9	-64.2	640.0	2.1	218.5
31	999.9	999.9	99.9	999.9	-63.4	631.4	4.6	189.7
AVE	-26.5	760.7	12.6	143.5	-54.9	653.6	2.8	173.7

SEP 81	D-57				DOME C			
DATE	Temp.	Pres.	WSpd	WiDir	Temp.	Pres.	WSpd	WiDir
1	999.9	999.9	99.9	999.9	-61.6	631.5	4.6	145.3
2	-38.3	740.5	4.8	124.0	-58.9	636.6	5.0	188.5
3	-45.1	736.8	9.7	175.3	-58.7	635.5	8.7	173.8
4	-43.1	739.7	16.6	175.9	-62.5	639.1	5.7	181.0
5	-44.9	739.2	13.7	178.0	-62.3	653.3	5.4	198.0
6	-48.0	737.2	15.4	177.8	-67.2	629.4	5.4	198.8
7	-46.8	744.8	14.4	175.7	-66.9	632.5	3.0	247.5
8	-38.2	743.7	15.6	158.5	-65.5	636.8	2.9	218.6
9	999.9	999.9	99.9	999.9	-63.0	641.0	3.6	204.4
10	999.9	999.9	99.9	999.9	-57.3	637.0	0.8	258.2
11	-25.7	737.4	22.0	118.1	-58.6	637.2	2.7	142.5
12	999.9	999.9	99.9	999.9	-49.1	635.2	3.8	102.6
13	999.9	999.9	99.9	999.9	-47.4	633.0	3.4	101.8
14	-29.5	732.2	13.8	138.8	-58.7	630.0	3.2	138.7
15	-30.4	742.4	13.5	138.4	-59.1	633.0	1.8	65.9
16	-26.2	745.8	17.2	98.7	-51.8	637.8	3.2	73.5
17	-24.2	749.2	14.9	122.0	-51.1	640.6	1.7	24.3
18	-26.0	745.0	15.0	136.8	-56.9	639.7	2.1	125.6
19	-27.9	749.4	9.4	137.8	-56.3	636.5	1.6	54.5
20	-23.0	750.5	14.9	102.9	-54.3	640.8	1.6	62.7
21	999.9	999.9	99.9	999.9	-47.8	645.6	3.4	108.9
22	999.9	999.9	99.9	999.9	-49.3	658.8	2.3	328.8
23	-26.1	760.9	13.3	141.0	-38.9	658.9	4.0	315.4
24	-23.2	758.3	13.3	136.7	-48.8	652.6	1.8	191.0
25	-25.1	761.1	17.3	141.2	-54.6	659.3	1.9	194.8
26	-31.2	757.6	15.9	170.6	-51.8	658.7	2.5	238.4
27	-32.5	748.0	15.3	158.2	-49.7	653.8	5.0	192.0
28	-31.0	750.1	18.4	141.5	-49.0	654.1	4.6	186.6
29	-28.5	752.7	19.3	141.5	-50.1	654.5	3.2	210.6
30	-30.1	754.7	15.7	150.3	-51.2	651.9	3.5	227.9
AVE	-32.8	746.2	13.6	146.1	-55.2	642.3	1.9	175.6

OCT 81	D-57				DOME C			
DATE	Temp.	Pres.	WSpd	WiDir	Temp.	Pres.	WSpd	WiDir
1	-32.4	751.9	12.3	175.7	-54.2	650.6	3.0	199.7
2	-37.6	746.5	15.3	179.2	-53.5	648.8	5.0	188.4
3	-35.3	744.4	13.4	163.2	-55.3	645.2	4.2	191.9
4	-32.4	743.6	9.3	154.5	-54.3	642.0	3.3	209.4
5	-35.3	744.0	12.1	166.7	-56.2	641.7	3.3	191.5
6	999.9	999.9	99.9	999.9	-55.5	640.7	8.7	175.4
7	999.9	999.9	99.9	999.9	-50.9	639.5	8.0	149.3
8	999.9	999.9	99.9	999.9	-53.5	643.8	1.0	136.9
9	999.9	999.9	99.9	999.9	-55.2	643.8	2.5	209.9
10	999.9	999.9	99.9	999.9	-57.0	638.0	1.7	172.0
11	999.9	999.9	99.9	999.9	-55.3	637.3	1.5	114.9
12	-22.4	741.1	16.1	130.3	-49.3	637.7	1.4	64.0
13	-22.0	745.3	12.3	139.1	-49.1	640.8	1.4	117.7
14	-26.2	756.4	6.7	153.7	-46.0	645.5	1.1	285.9
15	-22.9	756.2	12.0	135.8	-37.4	648.2	2.5	46.9
16	-21.8	749.0	16.4	129.5	-36.3	639.3	4.3	44.3
17	999.9	999.9	99.9	999.9	-43.4	631.1	1.3	116.8
18	999.9	999.9	99.9	999.9	-47.1	624.6	2.5	166.6
19	999.9	999.9	99.9	999.9	-50.6	625.2	1.7	89.2
20	999.9	999.9	99.9	999.9	-47.2	628.1	3.3	67.4
21	999.9	999.9	99.9	999.9	-44.1	631.1	1.5	86.9
22	999.9	999.9	99.9	999.9	-44.2	630.8	0.9	119.0
23	999.9	999.9	99.9	999.9	-44.0	627.4	0.7	81.6
24	999.9	999.9	99.9	999.9	-51.6	623.7	1.1	178.0
25	999.9	999.9	99.9	999.9	-53.6	625.7	1.0	135.6
26	999.9	999.9	99.9	999.9	-52.5	634.0	1.1	357.9
27	-27.4	739.2	18.2	134.1	-49.6	637.3	1.5	173.7
28	999.9	999.9	99.9	999.9	-54.1	631.1	2.1	167.9
29	-24.7	734.2	16.9	132.8	-45.2	632.9	0.3	75.1
30	-25.7	739.5	12.9	139.9	-39.7	634.3	1.0	359.5
31	-22.7	737.6	10.1	124.3	-41.3	629.0	0.9	106.3
AVE	-28.0	745.1	11.9	147.4	-49.3	636.4	1.4	153.9

NOV 81	D-57				DOME C			
DATE	Temp.	Pres.	WSpd	WiDir	Temp.	Pres.	WSpd	WiDir
1	-25.4	737.1	6.8	136.0	-47.8	629.7	3.0	120.8
2	-29.4	734.3	8.1	148.0	-51.2	631.4	2.4	187.4
3	-28.3	734.0	12.4	139.9	-51.3	633.0	2.3	218.3
4	-29.8	738.3	11.5	141.6	-49.8	633.1	3.0	247.6
5	-31.6	739.7	8.6	155.0	-51.3	632.3	3.3	243.9
6	-33.1	736.7	7.7	153.5	-54.3	630.0	3.9	216.5
7	-35.3	731.2	10.7	173.5	-51.3	630.0	7.0	208.2
8	-32.5	731.3	13.5	167.2	-44.3	636.0	6.6	186.5
9	999.9	999.9	99.9	999.9	-42.0	644.3	3.8	204.0
10	999.9	999.9	99.9	999.9	-42.4	648.5	2.3	238.6
11	999.9	999.9	99.9	999.9	-43.2	646.0	3.9	203.0
12	999.9	999.9	99.9	999.9	-41.6	641.9	3.6	152.1
13	999.9	999.9	99.9	999.9	-41.3	639.8	2.3	151.1
14	999.9	999.9	99.9	999.9	-40.9	639.8	1.2	196.8
15	999.9	999.9	99.9	999.9	-42.6	638.1	2.0	261.8
16	999.9	999.9	99.9	999.9	-43.4	631.3	2.1	225.4
17	999.9	999.9	99.9	999.9	-45.4	632.7	2.7	157.9
18	999.9	999.9	99.9	999.9	-44.4	637.9	2.5	149.4
19	999.9	999.9	99.9	999.9	-42.0	637.6	1.2	233.3
20	999.9	999.9	99.9	999.9	-42.8	633.6	2.8	297.3
21	999.9	999.9	99.9	999.9	-40.9	638.9	0.9	182.7
22	999.9	999.9	99.9	999.9	-41.1	646.4	1.5	231.3
23	999.9	999.9	99.9	999.9	-39.1	650.1	4.9	252.0
24	999.9	999.9	99.9	999.9	-37.4	652.6	5.2	251.5
25	-25.3	761.6	13.2	183.3	-38.5	654.1	4.6	231.6
26	-22.4	758.6	10.7	180.4	-38.0	658.9	5.0	218.2
27	-20.2	763.2	8.4	171.6	-32.0	655.7	0.5	102.2
28	-16.2	756.4	3.3	153.5	-33.0	645.8	1.3	316.6
29	-15.9	755.0	7.1	136.2	-33.8	646.0	1.5	28.7
30	-16.5	754.5	4.9	122.2	-32.2	646.1	2.0	10.2
AVE	-26.0	744.2	8.5	155.1	-42.7	640.7	2.1	214.0

DEC 81	D-57				DOME C			
DATE	Temp.	Pres.	WSpd	WlDir	Temp.	Pres.	WSpd	WlDir
1	-27.4	749.3	12.6	181.2	-41.4	650.4	5.0	187.1
2	-24.5	751.2	11.4	177.9	-37.5	649.1	6.0	210.2
3	-23.9	754.1	8.6	176.6	-35.7	646.9	3.8	224.2
4	-18.6	752.1	6.5	163.3	-29.6	651.8	1.0	126.5
5	-13.6	759.9	6.4	130.9	-34.3	651.2	1.8	247.2
6	-16.5	752.4	12.2	140.3	-34.9	650.6	2.7	218.9
7	-19.3	753.2	13.2	141.6	-28.8	651.4	0.8	154.0
8	-19.3	756.8	11.6	141.7	-30.1	651.4	1.1	297.4
9	-18.8	750.7	9.5	141.8	-32.9	647.6	2.6	228.3
10	-19.6	746.5	7.6	144.3	-32.6	643.0	3.5	203.0
11	-20.3	746.3	4.3	162.8	-30.6	640.2	2.0	169.1
12	-22.0	740.9	5.9	151.6	-32.1	637.4	2.5	154.0
13	-22.7	740.3	6.2	151.6	-33.8	636.1	2.1	189.0
14	-22.4	749.2	9.5	177.2	-34.1	640.2	1.5	251.5
15	-18.1	748.4	11.8	157.6	-34.3	643.1	1.9	251.5
16	-19.7	749.4	7.2	104.3	-28.9	641.4	1.1	144.8
17	-17.5	752.8	8.6	122.4	-34.4	645.3	2.3	35.7
18	-19.2	758.4	6.3	149.1	-32.1	648.3	2.6	302.7
19	-20.3	752.0	4.5	160.7	-35.5	641.9	3.1	263.5
20	-19.5	745.5	2.6	173.2	-33.4	636.4	2.1	192.9
21	-19.9	748.7	2.6	185.5	-33.4	639.8	1.6	205.3
22	-17.3	750.8	7.0	118.5	-30.3	643.3	1.2	209.7
23	-16.8	752.5	8.8	116.8	-25.4	646.9	0.1	258.8
24	-18.1	746.7	10.8	140.9	-30.6	645.8	1.5	226.2
25	-17.1	742.2	8.6	139.7	-29.3	640.9	1.6	222.3
26	-13.2	752.7	1.8	74.6	-27.8	645.1	0.7	278.0
27	-16.0	752.8	2.2	141.5	-31.6	645.6	1.3	225.5
28	-20.5	751.6	4.9	185.0	-31.4	644.5	2.6	184.5
29	-21.0	752.0	4.4	162.0	-31.9	647.8	3.0	126.3
30	-17.7	750.7	8.4	134.2	-31.1	649.8	1.5	164.7
31	-19.0	754.2	7.2	140.1	-28.5	648.3	1.8	198.1
AVE	-19.1	750.9	7.0	147.3	-31.9	645.1	1.5	207.6

JAN 82	D-57				DOME C			
DATE	Temp.	Pres.	WSpd	WiDir	Temp.	Pres.	WSpd	WiDir
1	-17.2	759.1	9.5	121.9	-27.8	652.2	1.3	2.6
2	-16.5	766.7	10.0	116.0	-31.0	659.3	1.8	307.4
3	-18.0	765.3	9.7	157.7	-32.6	657.8	3.9	270.6
4	-17.9	760.6	8.4	158.1	-34.0	651.7	2.4	263.6
5	-19.0	760.8	4.2	150.8	-33.8	649.6	3.5	277.6
6	-16.3	763.4	4.5	129.1	-30.7	651.4	0.8	253.2
7	-16.5	763.6	13.1	120.2	-31.5	657.4	2.0	329.4
8	-17.1	762.8	14.0	140.6	-25.9	662.3	1.6	218.5
9	-18.7	756.1	14.2	140.6	-29.3	658.6	3.5	205.5
10	-19.5	753.6	10.6	141.5	-27.1	652.9	3.1	221.7
11	-19.1	754.6	6.5	139.3	-29.6	650.9	3.5	201.5
12	-17.3	754.0	3.1	126.5	-31.9	649.1	3.5	192.6
13	-19.6	753.8	2.9	126.5	-33.1	648.3	2.5	140.5
14	-21.2	757.0	4.3	164.3	-30.1	649.8	1.1	155.4
15	-22.1	760.1	7.0	178.6	-31.1	651.7	1.4	176.7
16	-21.5	757.9	6.0	152.3	-31.6	651.4	1.2	170.7
17	-21.0	759.3	4.1	153.5	-31.7	650.5	0.8	199.3
18	-21.5	761.4	8.1	154.6	-31.6	655.0	1.8	109.7
19	-17.3	759.6	14.1	122.8	-32.7	657.8	4.5	65.0
20	-16.1	759.3	15.7	136.0	-32.1	659.0	1.6	341.8
21	999.9	999.9	99.9	999.9	-34.5	654.5	4.6	226.2
22	999.9	999.9	99.9	999.9	-35.4	654.1	4.1	204.4
23	999.9	999.9	99.9	999.9	-34.6	654.4	4.6	212.8
24	999.9	999.9	99.9	999.9	-35.7	650.7	3.7	176.9
25	999.9	999.9	99.9	999.9	-34.2	649.4	2.1	155.5
26	-19.1	756.2	10.5	135.6	-35.1	650.7	1.8	85.8
27	-17.7	756.4	14.5	138.3	-33.2	655.0	0.7	284.7
28	-19.1	754.1	13.0	143.3	-35.3	653.2	2.5	247.8
29	-18.7	754.5	9.1	141.9	-34.6	653.1	1.8	143.4
30	-19.0	755.5	12.6	138.8	-36.4	656.8	2.7	133.3
31	-18.6	757.4	12.6	140.1	-35.4	657.2	1.8	139.8
AVE	-18.7	758.7	8.9	139.9	-32.3	653.8	1.2	205.1

FEB 82	D-10				D-57				DOME C			
DATE	Temp.	Pres.	WSpd	WlDir	Temp.	Pres.	WSpd	WlDir	Temp.	Pres.	WSpd	WlDir
1	999.9	999.9	99.9	999.9	-19.2	756.5	10.1	139.6	-36.4	652.6	1.4	189.7
2	999.9	999.9	99.9	999.9	-18.5	754.7	7.0	138.1	-34.7	648.8	0.9	239.1
3	999.9	999.9	99.9	999.9	-19.3	757.6	5.8	139.9	-34.1	650.4	0.4	139.3
4	999.9	999.9	99.9	999.9	-18.1	760.0	3.8	108.1	-37.1	650.9	1.3	59.1
5	999.9	999.9	99.9	999.9	-19:9	757.7	11.5	137.1	-38.6	650.8	1.8	49.6
6	999.9	999.9	99.9	999.9	-20.8	755.2	14.4	138.4	-35.1	652.3	0.8	311.9
7	999.9	999.9	99.9	999.9	-21.6	752.8	14.9	142.2	-37.0	652.6	2.5	261.4
8	999.9	999.9	99.9	999.9	-19.6	752.5	13.1	141.8	-37.5	650.9	1.4	235.6
9	999.9	999.9	99.9	999.9	-20.2	751.3	14.5	139.6	-37.8	652.1	1.7	178.8
10	999.9	999.9	99.9	999.9	-19.4	751.1	13.8	139.5	-40.0	654.4	3.6	161.5
11	999.9	999.9	99.9	999.9	-19.2	756.3	12.3	136.9	-37.0	657.4	2.9	164.2
12	999.9	999.9	99.9	999.9	-23.4	759.7	11.0	152.4	-38.4	658.7	3.5	223.0
13	999.9	999.9	99.9	999.9	-24.7	756.2	10.2	158.5	-39.0	656.0	5.1	204.4
14	999.9	999.9	99.9	999.9	-26.3	752.4	12.1	154.6	-37.7	652.0	3.3	221.2
15	999.9	999.9	99.9	999.9	-25.0	758.0	10.7	170.6	-36.3	653.0	1.6	185.0
16	999.9	999.9	99.9	999.9	-23.2	760.4	6.9	168.7	-34.5	651.7	1.0	97.4
17	999.9	999.9	99.9	999.9	-25.4	753.8	5.1	156.2	-39.2	645.3	1.4	145.1
18	999.9	999.9	99.9	999.9	-26.8	748.4	7.0	169.4	-44.3	640.7	2.7	176.8
19	999.9	999.9	99.9	999.9	-22.6	746.6	10.8	141.1	-42.9	642.5	3.5	129.8
20	999.9	999.9	99.9	999.9	-22.1	747.3	10.4	128.8	-40.2	645.4	3.4	107.8
21	999.9	999.9	99.9	999.9	-22.9	744.1	12.3	145.4	-44.3	644.8	1.7	165.1
22	999.9	999.9	99.9	999.9	-23.5	741.8	8.6	141.2	-48.4	638.5	2.3	180.6
23	-6.5	929.8	7.3	180.7	-19.5	747.9	6.0	134.7	-45.7	638.5	0.9	291.6
24	-5.1	931.6	7.7	174.9	-17.5	750.5	3.0	106.3	-51.4	640.0	2.0	248.7
25	-8.4	931.7	6.8	181.6	-22.8	748.6	4.3	148.9	-51.8	640.1	2.0	223.6
26	-8.1	932.2	8.8	163.8	-22.8	749.2	10.4	132.6	-48.3	640.1	0.8	153.4
27	-4.8	932.2	5.8	156.0	-21.4	750.8	10.7	135.0	-45.1	643.4	2.0	345.3
28	-5.7	937.8	7.2	175.5	-23.6	754.8	6.5	141.5	-44.7	644.9	3.2	295.8
AVE	-6.4	932.7	7.2	172.0	-21.8	752.6	9.3	143.4	-40.7	648.1	1.1	191.8

MAR 82	D-10				D-57				DONE C			
DATE	Temp.	Pres.	WSpd	WiDir	Temp.	Pres.	WSpd	WiDir	Temp.	Pres.	WSpd	WiDir
1	-6.7	983.5	12.6	152.1	-21.8	745.8	12.7	157.7	-44.4	640.7	1.7	335.1
2	-6.9	910.4	18.0	171.2	-21.5	737.1	17.0	141.8	-47.2	638.9	1.8	47.4
3	-7.8	929.6	7.8	177.7	-22.9	746.1	5.9	150.2	-43.1	637.5	2.6	18.1
4	-10.8	926.3	6.7	203.7	-26.9	742.3	6.5	194.7	-51.8	631.1	2.0	264.8
5	-12.6	921.2	9.9	178.3	-32.3	738.8	10.0	173.3	-56.2	629.7	2.6	266.5
6	-13.4	924.5	8.0	178.5	-30.7	740.4	7.9	147.7	-57.3	630.2	2.3	246.7
7	-11.6	932.4	6.3	146.9	-27.1	745.6	3.5	159.6	-52.8	632.6	1.7	283.5
8	-12.8	930.2	7.6	165.5	-28.5	744.4	6.3	153.9	-49.9	629.8	3.7	338.5
9	-12.3	933.5	9.8	174.4	-26.6	749.1	6.0	145.2	-51.0	629.0	2.8	333.5
10	-10.7	930.9	5.8	184.5	-24.6	747.1	2.4	145.4	-61.0	630.3	1.7	256.7
11	-10.8	934.1	3.7	180.8	-24.2	746.5	1.8	162.3	-61.2	630.5	0.6	149.4
12	-11.4	943.2	3.0	168.8	-26.3	753.7	0.6	181.9	-57.4	632.2	2.2	29.5
13	-10.0	928.5	10.4	138.5	-23.7	750.1	10.2	107.6	-38.6	629.8	5.5	31.8
14	-10.8	930.9	4.3	211.4	999.9	999.9	99.9	999.9	-47.1	622.2	5.3	334.7
15	-11.4	929.5	6.0	189.9	-31.4	745.2	11.1	206.0	-60.8	626.1	3.2	258.0
16	-15.7	941.1	8.7	182.2	-35.9	752.2	12.8	177.5	-61.8	634.3	0.9	146.9
17	-13.6	944.0	5.4	158.6	-31.3	755.9	6.1	169.6	-60.8	639.2	2.8	244.7
18	-13.7	937.9	8.2	167.7	-28.8	751.5	4.8	150.9	-62.2	638.7	3.8	241.1
19	-16.1	941.0	6.0	170.6	-32.4	750.0	5.1	169.6	-63.0	637.0	4.3	183.2
20	-17.3	939.7	6.5	168.1	-40.0	747.8	7.8	177.2	-63.5	636.9	2.2	195.9
21	-17.0	940.8	8.5	165.6	-37.7	750.2	10.6	167.8	-55.7	638.1	0.7	286.9
22	-14.0	936.0	15.1	155.9	-27.0	750.9	13.1	130.9	-55.6	640.6	1.1	43.3
23	-8.6	892.9	20.9	153.5	-24.9	726.4	20.9	139.0	-57.6	635.6	1.4	167.6
24	-9.2	911.1	7.0	176.6	-27.2	731.8	9.8	143.5	-56.8	631.0	2.9	136.1
25	-14.8	930.1	9.3	201.9	-34.3	744.2	7.8	177.6	-56.2	632.7	0.9	10.3
26	-16.6	922.5	11.0	188.9	-37.4	739.7	11.6	177.7	-61.1	628.5	4.2	263.4
27	-19.3	914.7	8.0	183.2	-39.7	735.6	13.8	182.0	-67.4	620.0	2.9	228.1
28	-22.5	918.4	6.3	193.1	999.9	999.9	99.9	999.9	-68.4	618.6	3.5	128.2
29	-19.5	929.7	5.1	216.9	999.9	999.9	99.9	999.9	-64.1	621.9	4.5	138.7
30	-14.0	924.7	7.2	138.2	999.9	999.9	99.9	999.9	-68.0	625.1	2.7	160.0
31	-14.0	918.9	14.6	147.4	999.9	999.9	99.9	999.9	-58.4	627.9	4.1	83.1
AVE	-13.1	928.2	8.2	170.4	-29.4	745.1	7.8	156.3	-56.8	631.5	0.4	260.3

APR 82	D-10				D-57				DOME C			
DATE	Temp.	Pres.	WSpd	WiDir	Temp.	Pres.	WSpd	WiDir	Temp.	Pres.	WSpd	WiDir
1	-16.0	937.5	8.6	143.5	999.9	999.9	99.9	999.9	-58.7	634.7	1.5	309.6
2	-15.4	929.6	11.5	148.7	999.9	999.9	99.9	999.9	-65.1	634.3	2.7	227.1
3	-14.7	920.0	17.6	159.2	-30.6	739.6	12.8	136.3	-66.2	633.8	1.8	196.4
4	-19.4	912.7	18.5	176.2	-38.6	732.8	12.9	164.3	-66.9	632.1	2.4	181.9
5	-17.2	913.6	11.0	178.4	-39.4	728.8	14.5	155.0	-68.1	627.7	3.8	149.6
6	-17.7	924.7	7.6	185.4	-42.3	743.5	3.9	173.4	-66.3	625.0	3.3	126.5
7	-12.1	936.5	7.7	145.4	-28.2	747.8	3.8	101.3	-69.7	625.2	1.3	274.8
8	-11.3	931.0	13.0	151.4	-26.1	748.0	9.3	140.1	-63.8	635.6	2.6	278.4
9	-14.7	917.6	18.1	168.2	-29.0	737.6	14.3	138.0	-59.4	629.1	2.4	336.1
10	-15.7	915.8	5.8	186.7	-30.9	731.4	4.6	158.7	-66.6	618.9	5.9	254.5
11	-24.2	910.5	13.2	185.3	-44.4	725.8	12.7	178.8	-63.0	622.0	6.1	197.8
12	-22.2	919.3	13.5	176.6	999.9	999.9	99.9	999.9	-63.0	626.7	5.2	178.6
13	-22.2	933.7	6.8	179.2	-43.1	742.2	7.8	167.1	-62.5	630.3	4.3	178.4
14	-21.2	939.8	5.2	191.7	-47.8	747.5	10.7	177.3	-66.5	633.2	2.4	175.9
15	-19.5	939.4	12.0	180.6	-43.8	750.3	11.6	179.6	-67.8	637.2	1.6	179.6
16	-19.2	939.1	12.3	164.7	-37.9	750.2	13.2	153.7	-67.3	642.9	2.1	168.7
17	-17.7	937.5	7.4	144.5	-33.9	747.8	12.9	139.6	-65.6	640.2	1.7	184.8
18	-17.5	924.3	14.5	169.5	-34.7	741.5	11.0	142.9	-66.2	635.8	1.5	148.1
19	-12.6	913.4	18.7	166.5	999.9	999.9	99.9	999.9	-59.4	638.1	2.2	144.9
20	-12.0	926.5	15.3	159.9	-26.8	743.7	12.9	127.9	-58.7	640.3	1.5	115.0
21	-12.0	931.6	10.6	159.8	-27.4	746.8	11.7	138.0	-57.9	641.8	1.8	100.3
22	-13.6	942.3	12.0	177.6	-30.8	756.5	8.8	146.5	-56.6	645.6	0.7	12.5
23	-13.3	943.2	17.3	176.8	-31.8	760.8	11.1	170.3	-58.6	649.7	3.9	271.1
24	-14.8	948.6	12.4	177.3	-36.5	758.7	16.4	186.8	-54.8	645.1	4.5	285.0
25	-11.9	942.1	3.8	178.8	999.9	999.9	99.9	999.9	-49.5	633.0	1.4	345.7
26	-17.5	928.4	7.0	200.4	999.9	999.9	99.9	999.9	-63.3	630.8	3.0	180.6
27	-26.1	922.5	10.3	177.7	-43.4	729.7	7.5	150.5	-70.5	626.8	2.8	171.9
28	-26.1	919.6	7.9	177.8	-43.6	727.0	3.0	104.1	-71.2	623.1	2.3	163.9
29	-24.6	921.6	12.0	174.8	-43.6	730.6	9.2	144.4	-71.3	621.9	1.8	165.0
30	-22.7	936.8	10.7	186.5	-46.3	744.5	11.8	172.3	-67.8	633.2	1.0	212.3
AVE	-17.5	928.6	11.1	170.6	-36.6	742.8	9.4	153.1	-63.8	633.1	1.5	196.7

MAY 82	D-10				D-67				DOME C			
DATE	Temp.	Pres.	WSpd	WlDir	Temp.	Pres.	WSpd	WlDir	Temp.	Pres.	WSpd	WlDir
1	-12.7	948.2	11.9	156.5	-29.7	755.0	11.1	147.3	-67.8	643.5	1.9	244.9
2	-9.9	948.5	11.0	140.6	-24.2	756.9	13.9	137.5	-57.9	653.3	2.3	129.4
3	-8.6	941.9	17.1	149.7	-27.3	761.5	13.8	138.9	-53.6	654.1	2.2	320.6
4	-6.7	927.1	17.1	159.7	-24.6	750.7	16.3	144.3	-56.6	647.7	4.0	264.5
5	-12.3	935.5	11.2	179.5	-35.0	752.7	11.2	177.3	-56.4	642.0	1.1	258.8
6	-11.6	942.2	4.1	137.8	-24.3	754.2	3.6	137.7	-47.6	638.8	2.5	6.8
7	-8.5	933.0	5.2	137.0	-20.6	748.1	4.6	183.5	-59.6	639.3	3.2	267.1
8	-12.9	927.5	7.7	186.9	-30.3	744.2	8.2	160.8	-63.5	637.4	1.9	175.6
9	-15.1	937.6	8.3	183.8	-39.6	752.0	9.3	181.0	-68.8	642.1	1.8	222.9
10	-16.5	939.9	6.4	181.2	-40.2	752.4	9.3	177.4	-61.6	645.0	1.6	198.8
11	-16.7	949.9	3.1	182.2	-36.9	759.5	6.3	168.6	-57.6	645.9	0.5	211.9
12	-15.1	946.7	4.3	170.5	-31.1	756.9	7.4	162.8	-62.0	646.7	1.8	224.2
13	-17.5	940.4	3.8	166.3	-39.7	752.5	11.6	178.0	-67.4	644.0	1.8	188.0
14	-24.8	943.2	2.5	202.8	-38.8	750.6	6.8	175.2	-69.5	639.0	0.9	192.3
15	-25.6	946.1	3.9	183.9	-40.1	750.8	6.9	174.5	-71.9	635.1	0.0	0.0
16	-25.4	944.4	2.0	165.6	-46.3	748.8	6.2	172.6	-77.3	630.5	0.0	0.0
17	-22.3	930.3	13.7	162.3	-43.4	746.7	1.9	112.1	-79.5	626.4	0.0	0.0
18	-18.0	925.7	16.0	159.6	-35.0	742.0	11.9	132.7	-73.3	628.8	0.8	51.2
19	-15.4	936.2	11.1	165.7	-32.1	748.7	11.5	136.2	-65.7	637.1	1.0	17.4
20	-16.5	939.4	18.1	182.8	-35.6	755.6	13.7	174.8	-67.2	649.9	0.7	237.4
21	-14.6	948.8	13.8	178.8	999.9	999.9	99.9	999.9	-54.1	647.6	2.5	327.1
22	-10.3	943.1	10.7	160.2	999.9	999.9	99.9	999.9	-57.2	649.2	0.9	114.0
23	-9.2	933.4	18.1	166.9	999.9	999.9	99.9	999.9	-51.3	644.2	3.2	52.0
24	-6.7	928.0	11.0	155.7	999.9	999.9	99.9	999.9	-53.9	643.8	1.7	56.0
25	-6.0	926.9	9.8	141.9	999.9	999.9	99.9	999.9	-54.6	643.2	1.2	71.6
26	-6.5	933.1	14.5	138.0	999.9	999.9	99.9	999.9	-57.2	646.8	2.0	55.4
27	-9.9	942.4	9.4	150.6	999.9	999.9	99.9	999.9	-56.7	643.5	1.3	347.4
28	-9.4	926.9	15.1	158.5	999.9	999.9	99.9	999.9	-55.8	643.8	0.1	299.3
29	-8.3	929.2	9.6	132.7	999.9	999.9	99.9	999.9	-51.6	643.4	5.2	95.1
30	-11.8	920.4	16.7	166.0	-30.7	736.1	11.8	97.7	-46.4	644.2	3.6	50.3
31	-15.2	924.4	18.7	162.2	-30.6	736.5	14.8	188.3	-49.9	637.0	2.3	304.0
AVE	-13.5	936.5	9.7	160.6	-33.5	752.1	8.9	157.2	-60.2	642.4	0.1	353.2

JUN 82	D-10				D-57				DOME C			
DATE	Temp.	Pres.	WSpd	WiDir	Temp.	Pres.	WSpd	WiDir	Temp.	Pres.	WSpd	WiDir
1	-12.6	930.5	11.1	180.5	-27.9	744.4	4.5	136.0	-61.1	631.6	0.6	219.0
2	-16.3	932.6	6.2	192.2	-35.1	743.0	4.8	170.0	-70.1	630.9	3.2	179.5
3	-22.3	937.2	14.4	182.9	-49.5	743.8	13.3	180.0	-70.6	637.5	1.7	186.7
4	-18.3	945.8	5.6	182.9	999.9	999.9	99.9	999.9	-69.8	637.3	0.3	212.5
5	-16.7	945.3	4.7	161.1	999.9	999.9	99.9	999.9	-67.2	639.1	0.5	233.7
6	-17.4	931.4	10.8	154.8	-37.5	742.5	13.8	167.2	-71.1	637.1	0.7	210.1
7	-24.6	944.6	5.2	187.5	-50.6	750.7	14.1	178.3	-70.6	636.0	0.3	279.6
8	-19.1	942.4	8.9	142.6	-37.8	750.6	9.8	145.8	-68.2	637.9	0.4	75.2
9	-15.9	944.7	5.5	138.5	-30.8	753.1	8.1	135.3	-70.7	640.6	0.5	163.9
10	-12.6	955.0	3.9	143.2	-26.5	763.9	6.3	152.0	-65.3	647.9	0.7	235.7
11	-10.6	960.6	6.4	127.1	-21.8	768.6	6.0	109.9	-43.4	652.0	3.3	17.3
12	-10.9	957.2	4.8	164.4	-28.6	768.0	7.7	162.8	-49.7	653.2	3.9	314.6
13	-9.9	946.3	4.7	126.8	-22.4	759.4	5.1	112.9	-43.4	642.2	2.6	357.5
14	-12.3	947.4	5.1	209.7	-27.3	760.2	4.2	159.8	-49.4	644.7	3.9	302.5
15	-10.5	956.2	4.6	134.8	-18.9	767.1	4.7	94.1	-35.0	646.5	5.3	359.6
16	-5.4	938.7	6.3	97.0	-13.5	753.3	9.2	32.8	-41.0	635.3	3.6	1.7
17	-7.1	931.2	1.8	298.7	-19.1	746.0	3.9	357.7	-59.0	627.7	1.1	310.1
18	-9.5	939.1	4.3	145.6	-19.7	752.0	4.2	40.9	-42.9	629.6	4.1	357.7
19	-5.9	925.1	6.0	122.9	-20.7	743.4	7.2	94.3	-50.8	626.6	3.7	354.9
20	-6.5	926.5	4.4	129.8	-26.1	743.8	6.2	140.0	-61.2	628.6	0.9	30.3
21	-14.1	928.5	4.4	188.4	-33.3	742.3	5.4	159.4	-64.9	627.5	2.7	288.4
22	-17.4	928.2	3.0	172.8	-33.0	740.5	5.2	152.0	-65.3	624.6	2.7	291.8
23	-15.7	932.4	3.7	125.1	-28.0	743.3	4.1	130.4	-58.8	624.3	1.4	353.2
24	-21.3	935.3	2.9	244.7	-36.5	741.8	7.4	231.8	-65.4	623.0	3.2	280.6
25	-18.1	943.6	10.5	204.3	-36.6	754.9	20.2	189.6	-61.9	646.5	4.7	263.2
26	-12.6	949.8	12.6	198.1	-31.6	763.3	13.7	180.7	-55.2	649.9	4.4	277.0
27	-11.4	939.4	6.4	144.2	-26.9	752.6	8.5	148.0	-62.9	640.0	3.9	265.9
28	-14.9	923.3	14.4	164.9	-25.1	747.2	10.7	136.7	-70.2	636.6	1.7	175.1
29	-17.4	932.1	8.7	171.0	999.9	999.9	99.9	999.9	-67.2	638.7	1.4	194.0
30	-18.3	935.5	10.9	170.1	999.9	999.9	99.9	999.9	-58.8	639.3	2.4	284.2
AVE	-14.2	939.6	5.8	165.3	-28.4	752.1	5.6	150.3	-59.7	637.1	1.3	305.8

JUL 82	D-10				D-57				DOME C			
DATE	Temp.	Pres.	WSpd	WiDir	Temp.	Pres.	WSpd	WiDir	Temp.	Pres.	WSpd	WiDir
1	20.4	939.9	4.8	183.5	999.9	999.9	99.9	999.9	-58.7	637.0	1.6	296.5
2	-18.6	952.6	7.2	198.4	999.9	999.9	99.9	999.9	-68.1	646.2	2.1	257.8
3	-14.8	976.0	6.6	197.1	999.9	999.9	99.9	999.9	-47.5	663.6	1.7	344.0
4	-10.3	975.3	5.1	204.7	999.9	999.9	99.9	999.9	-31.8	664.9	7.0	348.3
5	-7.2	962.0	5.5	216.9	999.9	999.9	99.9	999.9	-44.3	659.2	2.4	277.8
6	-6.8	958.3	4.7	112.3	999.9	999.9	99.9	999.9	-33.8	649.1	4.7	53.1
7	-12.4	948.7	3.8	200.3	999.9	999.9	99.9	999.9	-40.3	638.9	1.6	62.9
8	-16.1	941.4	7.6	216.8	999.9	999.9	99.9	999.9	-57.7	636.5	4.0	86.8
9	-17.9	941.7	3.1	177.8	999.9	999.9	99.9	999.9	-66.0	631.7	1.7	8.5
10	-23.1	938.7	3.8	216.6	999.9	999.9	99.9	999.9	-72.2	626.4	1.5	210.6
11	-21.1	937.2	7.4	174.5	999.9	999.9	99.9	999.9	-68.4	631.1	3.3	144.8
12	-20.2	945.8	5.9	191.1	999.9	999.9	99.9	999.9	-63.1	637.4	6.4	127.0
13	-25.4	949.1	8.6	190.8	-47.4	755.1	16.8	184.2	-65.3	651.3	4.3	185.0
14	-18.3	952.8	21.7	183.9	-37.8	770.4	16.0	179.2	-68.2	662.2	2.5	217.4
15	-19.0	959.6	21.7	182.0	-36.4	770.8	15.5	175.6	-59.2	667.9	2.9	232.5
16	-18.0	958.3	21.6	177.3	-36.5	767.6	18.3	179.5	-55.1	667.1	4.9	245.7
17	-11.5	956.2	11.8	181.3	999.9	999.9	99.9	999.9	-43.8	661.7	1.0	355.8
18	-13.0	944.8	5.0	173.3	999.9	999.9	99.9	999.9	-40.8	642.7	0.9	76.0
19	-17.1	944.3	3.5	148.0	999.9	999.9	99.9	999.9	-60.4	637.1	2.3	136.6
20	-16.8	934.9	5.8	156.7	999.9	999.9	99.9	999.9	-62.5	634.9	1.5	152.0
21	-22.4	936.0	5.9	195.5	-44.6	745.9	8.5	176.6	-69.8	626.6	3.9	265.8
22	-19.7	940.1	8.8	147.3	-35.9	747.3	11.6	154.2	-73.1	635.6	1.4	185.9
23	-18.3	943.0	6.8	128.8	-33.3	751.2	10.3	147.8	-67.9	642.3	1.9	207.2
24	-18.8	934.4	12.6	141.8	-34.6	746.9	13.1	141.9	-68.9	640.4	2.3	232.1
25	-22.8	927.6	11.0	163.4	-42.9	738.8	12.6	174.8	-69.2	633.3	2.9	222.8
26	-23.4	920.9	13.9	157.6	-38.7	732.6	14.0	143.9	-70.2	627.4	2.1	223.6
27	-19.6	916.3	11.3	174.7	-39.4	732.3	13.8	172.1	-67.4	625.2	2.5	282.9
28	-16.6	941.5	8.7	176.7	-41.1	750.0	14.4	183.8	-63.8	638.6	4.5	266.6
29	-14.7	958.8	7.0	187.1	-35.5	767.1	13.0	183.0	-57.5	655.4	3.0	269.0
30	-12.5	951.2	6.6	180.0	-33.4	764.1	13.2	178.5	-57.6	660.1	2.9	227.3
31	-14.6	935.6	11.1	165.5	-33.3	751.3	16.5	176.2	-54.7	652.5	4.8	226.3
AVE	-17.1	945.9	8.1	176.4	-37.2	750.9	13.0	168.8	-58.9	644.6	1.0	231.4

AUG 82	D-10				D-57				DOME C			
DATE	Temp.	Pres.	WSpd	WiDir	Temp.	Pres.	WSpd	WiDir	Temp.	Pres.	WSpd	WiDir
1	-21.4	925.1	6.1	173.3	-43.5	735.0	14.2	181.0	-59.8	635.9	5.9	217.3
2	-30.1	918.1	12.5	178.5	-49.5	725.8	14.3	175.9	-65.9	625.1	5.1	179.1
3	-26.7	920.1	15.8	170.4	-44.8	730.3	11.4	145.8	-71.8	623.5	3.6	170.8
4	-23.1	922.6	8.5	175.9	-40.5	732.0	9.7	168.6	-71.7	625.5	2.3	173.4
5	-24.5	923.3	5.5	170.7	-44.4	731.8	9.4	167.6	-66.5	625.5	3.5	170.2
6	-19.2	916.0	11.5	146.2	-34.5	729.2	13.0	138.4	-59.1	627.7	4.2	153.8
7	-25.2	923.7	3.8	159.4	-42.7	730.5	11.5	172.2	-68.2	627.8	2.9	175.5
8	-29.6	926.4	6.1	149.9	-41.4	730.2	12.6	160.3	-72.8	626.8	1.7	165.9
9	-28.5	932.0	10.6	153.7	-43.0	735.7	11.5	151.6	-63.4	629.5	0.9	91.0
10	-25.2	931.9	9.5	159.4	-41.5	738.3	9.2	152.9	-71.1	632.4	1.6	175.3
11	-25.1	923.5	6.6	169.3	-43.0	732.4	9.4	173.9	-67.0	631.2	3.6	164.7
12	-27.6	927.6	5.4	179.7	-45.2	733.1	8.4	175.0	-58.6	629.8	4.9	139.2
13	-26.0	934.3	4.7	165.2	-44.7	740.5	8.2	164.8	-65.6	630.2	2.2	125.7
14	-16.5	918.9	14.6	148.0	-30.5	735.8	15.1	136.5	-65.2	631.3	2.3	91.0
15	-17.3	914.9	7.6	155.6	-32.3	730.3	14.9	144.4	-58.7	629.4	2.2	108.8
16	-22.0	914.2	4.8	178.6	-41.2	728.7	13.8	179.7	-65.6	626.2	1.9	202.9
17	-28.1	929.9	6.6	176.5	-49.1	734.8	13.9	182.0	-69.9	629.0	2.1	188.1
18	-26.7	933.0	11.8	170.3	-41.7	739.2	10.4	164.7	-68.9	631.3	2.5	183.0
19	-25.2	938.1	9.5	156.6	999.9	999.9	99.9	999.9	-67.8	635.5	2.3	181.9
20	-20.3	927.2	9.2	146.9	999.9	999.9	99.9	999.9	-70.2	632.7	2.1	174.3
21	-21.8	931.8	3.3	122.7	999.9	999.9	99.9	999.9	-67.5	636.0	2.0	193.2
22	-26.6	937.0	2.6	131.9	999.9	999.9	99.9	999.9	-60.5	634.4	1.3	270.7
23	-25.9	927.3	4.0	162.6	999.9	999.9	99.9	999.9	-66.1	624.7	1.6	307.0
24	-30.1	926.1	3.3	188.9	999.9	999.9	99.9	999.9	-75.8	615.4	1.7	186.5
25	-30.3	920.6	2.5	181.0	999.9	999.9	99.9	999.9	-79.2	611.6	2.0	174.7
26	-25.8	919.6	4.5	186.0	999.9	999.9	99.9	999.9	-80.2	613.8	0.8	126.4
27	-21.4	926.4	5.1	190.9	999.9	999.9	99.9	999.9	-73.1	619.3	0.3	28.1
28	-22.1	931.5	10.1	183.9	999.9	999.9	99.9	999.9	-71.0	629.0	1.0	282.5
29	-24.5	927.7	9.0	178.5	-49.6	735.1	16.4	182.3	-70.0	630.3	1.7	252.8
30	-28.8	927.6	10.5	177.6	-50.2	734.0	14.8	177.6	-70.7	629.5	1.7	206.6
31	-22.8	920.1	9.4	178.9	-43.0	730.6	10.4	156.0	-71.9	627.4	2.0	174.7
AVE	-24.8	925.7	7.3	166.6	-42.5	732.9	11.5	163.6	-68.2	627.7	1.9	174.6

SEP 82	D-10				D-57				DOME C			
DATE	Temp.	Pres.	WSpd	WiDir	Temp.	Pres.	WSpd	WiDir	Temp.	Pres.	WSpd	WiDir
1	-19.6	930.0	5.7	156.4	-41.4	738.4	6.5	141.3	-72.5	624.1	1.6	154.8
2	-14.5	914.0	13.7	157.0	-31.4	732.7	13.5	139.4	-73.1	627.4	0.6	142.2
3	-16.1	912.3	1.6	176.3	-27.3	726.5	3.9	133.8	-57.0	622.8	8.6	117.7
4	-16.3	928.4	11.5	173.1	-29.8	742.4	7.2	121.4	-63.0	624.0	1.9	31.5
5	-13.2	928.9	8.1	171.6	-31.0	741.7	7.6	137.9	-58.4	627.0	2.3	78.9
6	-21.0	924.5	4.0	198.8	-41.0	732.5	3.5	172.1	-62.6	622.6	3.4	156.6
7	-15.7	918.1	17.5	149.9	-31.8	737.6	12.6	138.4	-69.9	629.1	1.1	179.1
8	-11.6	911.5	19.0	167.1	-27.9	737.1	16.2	141.7	-52.9	636.2	4.4	73.8
9	-11.3	906.4	14.0	178.0	-30.0	729.5	13.1	145.7	-54.9	632.4	2.6	69.7
10	-13.4	919.4	7.9	179.5	-32.4	735.6	8.4	142.9	-57.0	631.4	2.5	117.7
11	-16.7	929.9	5.6	191.1	-31.9	740.8	4.0	167.1	-62.5	625.7	1.3	94.5
12	-22.6	918.3	5.1	196.2	-42.3	729.0	9.4	178.8	-64.7	618.9	0.1	206.6
13	-23.3	923.7	7.2	168.0	-43.3	731.3	9.2	170.6	-61.1	617.4	0.1	309.0
14	-20.1	921.5	7.4	168.4	-34.5	731.5	5.1	147.8	-66.9	616.1	0.0	0.0
15	-25.2	930.4	5.4	212.6	-44.6	736.5	9.1	178.0	-71.8	621.1	0.0	0.0
16	-23.3	942.8	6.0	182.1	-46.2	748.5	13.2	177.0	-67.7	633.9	0.5	257.7
17	-19.3	931.0	13.6	174.2	-38.3	743.8	11.9	172.8	-68.8	633.4	1.7	262.1
18	-25.2	927.6	5.9	185.2	-48.5	735.3	11.4	176.9	-67.4	626.8	3.0	180.3
19	-22.8	921.8	7.0	182.9	-49.7	732.7	13.0	178.6	-58.2	628.9	4.7	154.1
20	-19.6	929.8	4.9	184.5	-42.3	740.2	10.7	175.4	-62.4	633.1	1.1	161.2
21	-16.7	936.2	5.7	181.5	-40.1	746.2	9.6	173.1	-59.9	636.2	1.8	227.9
22	-18.2	914.0	6.3	178.0	-39.2	729.9	11.3	171.3	-63.3	625.5	1.2	255.0
23	-23.9	922.0	7.0	175.2	-43.7	730.9	9.5	175.0	-68.2	620.3	0.0	0.0
24	-22.4	921.0	10.8	153.6	-38.5	729.9	9.8	140.5	-68.8	619.3	0.0	0.0
25	-23.6	924.0	9.5	172.1	-38.3	731.5	8.5	148.3	-68.7	622.5	0.0	0.0
26	-25.7	921.3	8.6	158.6	-39.8	728.2	8.6	149.9	-67.2	624.0	0.0	0.0
27	-25.7	916.1	8.9	172.6	-41.7	724.6	12.2	158.3	-67.0	621.8	0.0	0.0
28	-26.0	930.1	7.5	162.6	-46.1	735.8	10.3	175.8	-64.6	630.1	0.6	138.4
29	-23.0	918.4	10.6	161.6	-38.9	730.0	10.2	157.3	-59.4	629.0	3.6	192.7
30	-23.9	902.5	8.6	178.5	-40.6	716.5	12.4	174.5	-59.5	623.6	7.3	182.3
AVE	-20.0	922.5	8.3	171.5	-38.4	734.3	9.3	159.8	-63.9	626.2	1.2	144.7

OCT 82	D-10				D-57				DOME C			
DATE	Temp.	Pres.	WSpd	WiDir	Temp.	Pres.	WSpd	WiDir	Temp.	Pres.	WSpd	WiDir
1	-19.4	902.9	6.4	147.1	-54.8	719.2	13.7	143.7	-59.0	627.2	3.9	164.8
2	-16.6	922.9	8.4	174.7	-33.7	736.7	9.8	166.0	-53.6	652.8	1.1	236.5
3	-19.4	919.1	2.8	173.0	-37.7	733.3	12.3	176.5	-58.2	631.0	2.7	198.5
4	-20.7	925.4	1.8	197.7	-39.6	736.3	13.0	177.7	-60.3	629.4	1.7	224.5
5	-21.0	933.1	4.9	183.9	-37.5	741.5	8.3	174.5	-60.2	631.7	0.7	183.6
6	-19.6	937.7	3.2	207.3	-41.8	746.5	10.9	174.4	-61.1	636.3	0.4	219.7
7	-17.2	944.3	1.9	160.6	-39.4	752.8	11.9	178.6	-60.5	642.2	2.0	194.8
8	-16.4	936.3	8.9	150.8	-31.9	748.9	12.0	148.1	-61.3	641.7	2.2	181.5
9	-16.2	927.8	18.6	163.7	-32.3	744.1	17.0	142.6	-62.8	640.0	0.7	164.8
10	-15.8	932.9	10.4	171.7	-34.0	745.9	10.7	161.6	-60.3	635.7	0.8	228.6
11	-16.3	930.5	9.3	157.6	-34.5	742.4	10.5	148.2	-55.4	632.4	0.2	141.6
12	-16.0	929.6	13.1	171.5	-31.1	744.5	13.8	141.2	-55.5	635.6	1.2	42.4
13	-15.5	939.8	7.2	183.3	-32.1	749.9	8.1	151.1	-56.7	637.1	2.0	275.9
14	-15.9	938.9	4.9	179.6	-37.0	748.4	12.2	177.1	-60.4	637.9	3.0	258.9
15	-18.1	944.3	4.1	184.3	-39.8	750.2	11.5	176.6	-60.8	638.9	1.8	229.2
16	-20.3	948.5	6.5	174.4	-42.4	752.7	14.2	178.9	-62.4	640.4	2.3	246.2
17	-18.6	942.8	8.7	179.2	-40.6	751.5	12.8	178.6	-60.7	641.4	3.1	251.2
18	-18.1	938.9	7.9	176.4	-38.2	748.5	15.0	179.7	-57.7	644.7	2.6	224.4
19	999.9	999.9	99.9	999.9	-35.0	753.7	12.1	177.2	-52.2	647.0	2.8	240.8
20	999.9	999.9	99.9	999.9	-30.4	748.2	8.3	143.8	-51.9	642.4	2.4	229.2
21	999.9	999.9	99.9	999.9	-32.2	741.0	13.0	166.4	-52.0	638.6	2.1	258.2
22	999.9	999.9	99.9	999.9	-31.4	751.4	11.3	174.8	-52.9	638.6	2.0	297.5
23	999.9	999.9	99.9	999.9	-27.4	755.9	6.4	109.1	-41.4	638.4	2.8	334.2
24	999.9	999.9	99.9	999.9	-21.7	751.6	11.7	129.6	-39.8	642.8	2.7	337.0
25	999.9	999.9	99.9	999.9	-26.5	743.3	9.5	161.9	-38.9	638.0	2.7	71.3
26	999.9	999.9	99.9	999.9	-27.8	755.9	9.6	188.1	-44.9	636.6	6.4	311.8
27	999.9	999.9	99.9	999.9	-21.7	765.9	0.8	164.6	-35.9	645.2	4.1	347.6
28	999.9	999.9	99.9	999.9	-18.2	769.5	6.3	151.3	-33.3	655.7	6.1	321.0
29	999.9	999.9	99.9	999.9	-19.9	760.3	8.5	143.5	-37.7	653.9	0.7	224.3
30	999.9	999.9	99.9	999.9	-21.9	744.0	11.9	131.9	-44.5	645.5	4.4	151.7
31	999.9	999.9	99.9	999.9	-27.6	736.0	13.9	154.3	-45.9	638.3	4.7	191.3
AVE	-17.8	933.2	6.9	169.1	-32.3	747.5	10.4	161.3	-52.8	639.3	1.1	249.8

NOV 82	D-57				DOME C			
DATE	Temp.	Pres.	WSpd	WiDir	Temp.	Pres.	WSpd	WiDir
1	-32.1	733.9	10.5	176.4	-41.8	632.7	6.5	154.4
2	-24.5	746.0	5.4	115.7	-40.6	639.0	7.5	187.0
3	-25.5	748.1	10.0	131.4	-43.9	647.1	4.2	165.8
4	-25.5	746.9	14.0	153.6	-38.6	656.7	7.8	190.1
5	-22.7	746.3	15.7	178.4	-37.3	650.0	7.6	212.4
6	-31.3	742.0	15.7	146.4	-39.4	649.1	8.2	187.3
7	-31.3	743.4	13.2	147.3	-39.5	645.6	7.4	188.4
8	-31.4	742.8	9.5	148.2	-41.6	640.5	6.4	178.2
9	-31.3	739.1	9.1	152.9	-43.2	638.4	4.6	176.4
10	-29.0	738.3	9.8	145.9	-36.6	644.9	5.7	148.1
11	-20.9	751.6	8.0	137.7	-35.3	651.7	5.2	125.3
12	-20.5	758.9	10.5	136.0	-36.3	653.0	1.9	96.9
13	-22.7	756.4	12.3	143.4	-40.3	652.5	2.9	137.7
14	-24.1	752.8	12.2	142.1	-36.8	654.9	3.5	170.6
15	-23.0	751.4	10.8	140.3	-36.4	653.6	4.8	161.1
16	-23.3	750.1	7.6	154.2	-34.6	652.9	5.6	176.4
17	-20.2	749.3	11.2	148.0	-34.7	650.1	1.8	221.2
18	-23.1	746.0	10.9	166.9	-36.8	645.2	4.4	216.2
19	-29.1	742.3	12.9	172.1	-38.7	643.6	5.4	195.6
20	-26.9	741.9	14.3	167.7	-39.1	645.4	3.8	182.7
21	-21.9	743.6	15.9	147.0	-37.3	651.1	3.0	168.9
22	-18.0	749.2	13.9	134.4	-35.5	654.2	4.2	134.5
23	-20.0	756.4	12.4	140.8	-34.5	654.3	1.9	68.8
24	-20.1	753.8	12.1	150.6	-34.2	648.8	1.7	298.4
25	-20.1	751.3	11.6	143.7	-32.9	646.4	1.5	97.4
26	-19.8	754.3	11.2	142.3	-35.0	649.8	6.1	51.4
27	-18.0	759.9	9.5	141.0	-32.9	653.2	4.6	12.1
28	-18.6	761.8	7.4	140.2	-34.0	655.0	2.9	304.8
29	-19.4	756.8	11.1	136.4	-34.6	653.7	1.1	209.2
30	-19.8	755.9	12.1	138.7	-32.7	652.7	0.6	195.7
AVE	-25.7	749.2	10.9	147.6	-37.1	648.9	3.0	168.1

DEC 82	D-57				DOME C			
DATE	Temp.	Pres.	WSpd	WiDir	Temp.	Pres.	WSpd	WiDir
1	-18.8	759.6	10.8	140.0	-34.2	654.1	1.3	288.6
2	-16.9	745.7	13.7	125.6	-35.3	650.5	1.4	169.2
3	-15.1	761.4	4.8	62.4	-33.5	650.3	0.4	10.7
4	-16.8	766.1	3.7	160.4	-32.1	653.5	6.6	276.6
5	-15.3	760.3	4.6	137.5	-35.6	648.0	3.9	259.8
6	-13.7	764.4	5.5	131.2	-30.7	653.9	0.5	130.8
7	-15.1	767.5	9.9	118.6	-25.7	657.0	3.6	13.6
8	-15.1	759.2	10.5	130.0	-23.3	654.0	1.9	300.6
9	-16.5	757.9	8.1	156.2	-27.5	654.0	1.2	215.8
10	-19.5	761.5	10.0	173.6	-34.5	657.1	3.1	224.2
11	-18.6	768.5	8.7	163.5	-34.2	664.6	4.2	220.3
12	-18.9	766.3	12.2	173.3	-33.0	665.8	5.6	198.6
13	-18.2	759.2	14.0	142.5	-30.1	662.0	4.7	151.3
14	-17.0	759.3	12.9	142.7	-30.3	663.5	4.6	142.7
15	-16.5	753.9	10.9	126.8	-28.3	662.4	6.2	135.3
16	-13.7	759.2	8.6	116.8	-24.2	662.1	9.9	112.0
17	-12.7	762.1	12.0	140.5	-23.3	666.1	6.5	111.2
18	-11.4	761.1	12.4	138.8	-23.8	667.5	6.3	123.0
19	-12.5	766.4	12.0	141.0	-24.1	668.9	3.1	112.1
20	-15.7	763.7	13.2	145.1	-25.0	663.9	2.4	212.5
21	-17.8	761.6	10.2	141.0	-26.8	659.1	3.0	172.9
22	-18.5	761.8	7.5	145.7	-28.9	657.6	2.7	210.6
23	-19.1	762.3	4.9	157.0	-28.3	654.5	4.2	223.4
24	-18.6	764.9	5.6	173.6	-28.8	657.1	4.3	254.0
25	-17.6	767.7	6.9	169.0	-30.4	663.0	3.0	206.8
26	-19.4	764.0	9.9	156.1	-28.5	662.6	4.6	220.5
27	-17.5	760.3	10.7	136.1	-29.8	656.0	4.4	161.7
28	-15.6	765.2	10.9	136.2	-33.0	660.1	2.2	65.3
29	-14.5	766.6	13.8	121.5	-32.3	664.0	2.8	278.4
30	-14.6	763.0	17.2	127.4	-32.7	662.9	2.6	265.9
31	999.9	999.9	99.9	999.9	999.9	999.9	99.9	999.9
AVE	-16.4	762.0	9.4	140.7	-29.6	659.2	1.7	182.0

JAN 83

DATE	P 10 Temp	Pres	WSpd	WDir	P 47 Temp	Pres	WSpd	WDir	P 57 Temp	Pres	WSpd	WDir	P 80 Temp	Pres	WSpd	WDir	DONE C Temp	Pres	WSpd	WDir
1	0.8	957.4	10.1	132.7	999.9	999.9	99.9	999.9	14.4	761.1	13.9	139.6	999.9	999.9	99.9	999.9	31.1	660.2	4.8	267.9
2	1.4	956.6	5.8	135.7	999.9	999.9	99.9	999.9	14.1	757.6	9.7	136.2	999.9	999.9	99.9	999.9	29.9	654.1	8.2	175.3
3	3.6	961.5	4.6	145.1	999.9	999.9	99.9	999.9	15.9	760.6	5.6	136.7	999.9	999.9	99.9	999.9	24.4	654.1	1.6	194.5
4	4.0	957.3	6.6	130.4	999.9	999.9	99.9	999.9	16.1	757.6	8.9	140.3	999.9	999.9	99.9	999.9	28.2	652.7	4.6	210.8
5	3.6	957.3	5.6	149.7	999.9	999.9	99.9	999.9	16.8	757.6	7.6	133.2	999.9	999.9	99.9	999.9	27.0	651.5	3.7	199.5
6	3.8	954.2	9.8	151.7	999.9	999.9	99.9	999.9	17.5	754.5	8.7	150.8	999.9	999.9	99.9	999.9	24.5	653.5	0.4	25.4
7	3.0	954.6	7.4	136.6	999.9	999.9	99.9	999.9	16.4	756.9	9.8	138.4	999.9	999.9	99.9	999.9	28.6	652.1	2.7	275.0
8	1.9	954.6	8.6	154.9	999.9	999.9	99.9	999.9	17.6	756.1	11.1	138.5	999.9	999.9	99.9	999.9	26.6	645.0	4.7	280.6
9	2.4	954.6	11.0	161.4	999.9	999.9	99.9	999.9	17.6	756.0	11.0	137.6	999.9	999.9	99.9	999.9	26.1	644.8	3.2	255.4
10	3.2	958.7	10.1	155.7	999.9	999.9	99.9	999.9	18.6	761.5	11.6	141.4	999.9	999.9	99.9	999.9	25.8	645.7	3.7	183.1
11	1.0	956.1	5.2	136.8	999.9	999.9	99.9	999.9	16.1	759.2	8.4	137.8	999.9	999.9	99.9	999.9	25.0	645.3	3.6	161.6
12	1.7	952.8	5.7	136.1	999.9	999.9	99.9	999.9	14.4	762.0	5.7	118.9	999.9	999.9	99.9	999.9	25.5	642.6	5.1	223.7
13	2.7	956.8	4.7	147.3	999.9	999.9	99.9	999.9	16.1	758.7	6.9	144.0	999.9	999.9	99.9	999.9	31.6	636.3	2.9	215.9
14	2.2	953.7	3.3	138.1	999.9	999.9	99.9	999.9	17.3	761.8	5.7	137.7	25.8	721.3	1.8	178.8	28.2	641.0	2.1	243.7
15	2.5	959.6	6.4	124.3	999.9	999.9	99.9	999.9	16.7	759.2	8.6	136.8	24.0	719.6	4.4	142.1	25.3	641.9	1.3	212.4
16	3.0	954.1	10.2	131.9	999.9	999.9	99.9	999.9	16.6	756.0	12.5	127.6	21.0	717.8	9.7	103.7	27.4	642.4	1.9	82.8
17	2.8	958.6	7.9	116.2	999.9	999.9	99.9	999.9	14.8	759.6	11.8	129.8	19.9	720.8	8.4	100.6	28.4	644.7	4.1	58.4
18	2.7	963.4	2.8	125.8	999.9	999.9	99.9	999.9	13.8	762.5	6.4	117.1	19.7	722.8	4.9	113.6	23.8	646.0	1.8	340.4
19	1.8	962.1	3.8	148.4	999.9	999.9	99.9	999.9	15.3	762.4	6.3	137.1	18.9	722.7	5.0	130.2	23.8	642.4	1.8	241.0
20	1.9	961.7	6.7	141.7	999.9	999.9	99.9	999.9	18.1	764.1	10.3	142.7	23.3	724.9	6.4	146.2	24.7	651.6	0.8	289.5
21	0.1	967.4	3.5	152.2	999.9	999.9	99.9	999.9	14.9	767.2	8.8	137.6	19.8	727.8	6.6	183.1	23.8	647.7	1.4	89.6
22	1.8	965.1	3.8	150.8	999.9	999.9	99.9	999.9	13.5	764.6	9.3	139.8	19.8	728.2	7.0	122.7	22.5	651.0	0.9	109.0
23	2.8	964.6	2.1	95.8	999.9	999.9	99.9	999.9	16.3	762.0	7.8	136.1	22.9	723.3	6.1	146.8	24.7	653.2	1.7	181.5
24	3.3	960.6	4.2	148.0	16.6	814.4	6.4	151.2	18.4	758.6	6.0	137.8	25.5	719.0	6.6	151.5	25.4	648.5	2.0	195.1
25	5.4	959.3	4.3	137.0	16.6	813.2	6.0	164.7	19.7	756.7	8.8	141.1	27.1	716.9	4.6	159.9	27.1	649.1	2.1	108.5
26	4.8	958.8	10.8	136.0	18.3	808.6	13.1	137.5	20.7	753.6	10.9	138.1	27.8	716.1	7.6	148.5	29.9	657.4	2.8	179.8
27	5.6	944.8	18.1	148.0	18.2	804.7	17.6	138.4	17.7	751.8	14.0	134.1	28.6	715.2	9.8	158.8	999.9	659.0	3.1	148.1
28	1.1	950.4	14.3	140.0	9.6	810.4	16.1	137.4	13.8	757.0	12.8	136.4	21.2	720.1	8.5	129.0	999.9	659.0	2.2	111.6
29	0.2	955.0	14.1	139.3	9.6	813.6	17.4	137.3	13.4	761.0	14.4	133.2	21.3	725.1	10.6	135.8	29.3	646.5	1.5	125.0
30	0.3	958.6	16.9	143.8	11.2	817.8	15.6	141.7	15.4	764.3	10.2	138.9	24.8	727.4	9.8	146.0	26.1	652.1	1.2	178.0
31	2.3	957.7	12.9	141.0	13.3	816.3	14.1	145.4	17.6	762.0	11.5	141.0	27.0	725.0	7.8	159.2	28.3	647.4	2.0	214.1
AVE	2.8	959.7	7.5	141.1	13.2	812.5	13.4	141.0	16.2	760.8	9.3	136.8	25.1	721.8	6.6	134.1	26.9	647.8	1.5	203.5

FEB 83	D-10				D-47				D-57				D-80			
DATE	Temp.	Pres.	WSpd	WiDir	Temp.	Pres.	WSpd	WiDir	Temp.	Pres.	WSpd	WiDir	Temp.	Pres.	WSpd	WiDir
1	-0.7	954.2	8.9	137.1	-10.5	812.2	12.9	136.5	-14.5	758.0	10.5	133.3	-24.3	719.6	8.1	131.7
2	-1.4	957.2	12.5	139.7	-12.5	814.7	15.2	143.9	-15.9	760.9	12.0	138.0	-22.0	723.4	7.0	128.2
3	-4.4	957.0	12.5	156.1	-15.4	812.6	16.0	144.0	-19.3	758.1	14.2	143.5	-26.9	722.2	9.1	151.6
4	-3.2	960.0	7.9	160.1	-15.1	815.4	12.8	143.3	-18.4	760.4	11.5	138.6	-25.9	722.2	8.6	137.4
5	-0.5	965.6	4.4	149.9	-10.9	821.2	9.2	143.3	-14.7	766.0	9.3	136.5	-23.0	727.7	7.8	137.0
6	-1.7	965.9	2.6	113.4	-10.8	820.7	5.5	136.4	-13.5	764.8	5.0	133.2	-18.7	725.5	5.7	134.6
7	0.0	967.1	2.4	159.1	-11.2	822.4	8.0	142.0	-16.1	766.7	7.0	141.3	-26.4	726.9	5.1	168.8
8	-2.4	959.4	10.0	119.6	-10.3	815.6	15.8	130.0	-13.8	761.8	14.5	130.2	-26.4	725.2	10.1	136.2
9	-2.0	953.3	18.3	119.4	-9.9	811.5	19.2	112.1	-12.6	758.3	18.4	108.2	-19.2	722.6	13.3	109.7
10	-1.2	965.7	13.4	120.7	-9.5	822.3	15.6	109.6	-12.4	767.5	14.4	97.5	-13.5	729.6	8.6	81.0
11	-1.1	960.7	13.5	134.3	-8.9	818.4	16.6	135.7	-11.3	764.9	12.9	132.5	-15.4	727.9	7.4	124.7
12	-2.1	957.1	4.4	100.2	-9.6	813.3	6.5	111.9	-12.9	757.7	6.1	112.5	-18.7	718.3	6.3	129.3
13	-1.2	954.0	2.4	119.3	-11.8	810.7	7.8	136.6	-17.2	755.4	7.2	136.3	-26.8	716.0	5.4	137.6
14	-2.2	951.2	9.6	106.7	-10.9	808.6	12.7	109.4	-16.4	754.1	11.0	122.4	-27.8	716.4	8.6	132.7
15	-2.7	953.5	13.3	132.3	-13.5	811.2	15.0	135.1	-18.2	756.7	12.5	133.5	-27.8	718.8	7.9	134.0
16	-3.6	940.1	19.4	136.3	-13.7	800.7	19.7	132.9	-17.9	747.8	16.7	132.9	-27.6	712.8	11.1	132.9
17	-4.3	943.2	11.4	145.0	-15.2	801.4	14.1	140.1	-19.8	747.2	12.2	137.6	-30.3	710.3	8.8	145.7
18	-6.7	947.9	13.4	161.2	-17.3	805.4	13.6	145.4	-22.1	750.8	11.2	138.5	-32.8	713.0	7.1	146.1
19	-7.8	945.4	13.8	177.3	-19.7	803.5	12.2	170.4	-25.1	749.1	9.3	160.9	-35.4	711.0	5.2	173.2
20	-10.9	948.8	8.2	178.6	-23.5	802.6	11.5	175.4	-29.5	747.0	9.7	174.5	-38.9	708.3	5.8	172.7
21	-13.0	953.0	7.4	174.1	-25.9	804.2	11.5	173.5	-31.9	747.9	10.4	175.4	-40.3	709.1	6.0	170.0
22	-13.5	954.8	6.6	172.0	-26.2	805.5	10.7	175.2	-32.1	748.7	10.1	177.3	-40.8	709.1	5.1	177.4
23	-13.9	952.3	8.8	169.4	-26.0	804.1	10.7	167.6	-31.2	747.5	8.1	165.1	-41.1	707.3	3.8	180.3
24	-13.2	953.5	8.6	173.6	-26.4	805.5	10.7	162.2	-31.2	749.1	7.3	153.6	-43.5	709.2	4.8	161.4
25	-8.7	964.1	6.5	144.2	-20.2	816.3	7.8	154.4	-24.4	759.1	5.1	144.9	-40.6	717.3	2.7	159.6
26	-9.3	950.7	18.3	153.7	-18.0	808.3	14.8	143.9	-21.8	753.8	10.5	140.4	-34.5	714.6	4.0	154.3
27	-9.5	958.4	6.0	159.7	-20.4	810.8	9.2	161.1	-24.1	754.7	5.9	143.2	-36.8	713.9	3.4	158.7
28	-11.7	959.6	6.7	152.2	-24.1	810.7	11.6	172.7	-29.8	754.3	9.7	170.8	-42.1	714.2	3.3	183.6
29	-11.8	959.5	7.0	154.2	-24.3	810.7	11.6	173.4	-30.3	754.2	10.2	172.7	-41.8	714.0	3.1	185.4
30	999.9	999.9	99.9	999.9	999.9	999.9	99.9	999.9	999.9	999.9	99.9	999.9	999.9	999.9	99.9	999.9
31	999.9	999.9	99.9	999.9	999.9	999.9	99.9	999.9	999.9	999.9	99.9	999.9	999.9	999.9	99.9	999.9
AVE	-5.7	955.6	9.0	145.3	-16.3	811.0	11.6	143.8	-20.6	755.9	9.8	140.2	-30.0	717.5	6.2	141.4

MAR 83	D-10				D-47				D-57				D-80			
DATE	Temp.	Pres.	WSpd	WiDir	Temp.	Pres.	WSpd	WiDir	Temp.	Pres.	WSpd	WiDir	Temp.	Pres.	WSpd	WiDir
1	-12.9	956.9	5.8	185.5	-24.2	808.0	8.6	181.1	-30.2	750.8	7.8	180.0	-39.0	709.6	2.7	190.8
2	-13.2	954.2	11.1	172.4	-25.3	805.9	12.3	173.0	-32.7	749.1	10.7	171.5	-43.8	709.1	5.4	177.5
3	-12.1	958.4	11.0	176.4	-24.8	810.1	12.7	174.4	-29.7	753.8	11.1	170.3	-42.3	715.3	6.5	172.5
4	-9.9	957.4	9.8	170.0	-21.8	810.5	11.0	168.8	-26.1	754.9	12.1	159.5	-38.6	717.8	7.6	165.5
5	-9.3	963.1	11.5	170.2	-21.6	816.0	11.0	165.2	-27.4	759.8	9.4	160.3	-40.1	720.2	3.0	180.9
6	-12.4	961.2	4.8	174.6	-25.5	812.0	9.0	176.2	-32.5	755.1	8.7	175.5	-42.9	713.6	2.1	189.4
7	-16.0	953.1	7.0	171.0	-28.1	803.2	11.1	172.3	-34.1	746.3	9.0	160.9	-46.1	706.6	5.9	172.4
8	-17.1	951.0	9.0	154.6	-29.0	801.1	11.5	159.1	-33.1	744.3	9.5	142.1	-46.3	704.6	5.6	166.0
9	-13.0	943.7	16.3	169.5	-24.6	800.0	14.0	150.3	-30.0	745.0	10.8	139.2	-45.8	706.1	5.1	161.4
10	-10.3	951.8	10.9	175.6	-22.4	805.9	10.3	153.8	-27.9	749.8	7.6	141.2	-41.3	709.3	2.9	164.1
11	-11.8	955.1	4.0	170.9	-24.0	806.3	7.5	177.6	-32.2	749.1	7.5	177.2	-45.4	707.6	3.2	182.4
12	-13.2	952.6	10.1	168.0	-26.5	805.4	11.3	171.3	-35.0	749.3	8.7	173.8	-47.1	709.4	4.1	179.8
13	-15.6	947.9	11.1	174.3	-27.4	800.3	12.6	167.9	-33.3	744.8	9.4	166.9	-47.3	706.1	6.8	167.7
14	-17.7	948.3	8.2	170.7	-29.7	798.1	9.4	169.7	-35.1	741.3	8.1	165.0	-49.4	701.9	7.1	171.1
15	-17.4	942.5	11.9	150.5	-29.7	794.5	12.8	149.0	-34.9	738.3	10.3	151.4	-50.3	699.4	6.2	174.1
16	-15.1	944.2	11.8	173.3	-28.7	796.3	10.3	161.0	-35.1	739.7	8.0	152.9	-48.5	699.6	4.7	162.0
17	-17.4	945.3	10.3	174.9	-29.8	796.2	10.4	172.2	-38.9	738.9	8.9	168.7	-48.0	698.7	6.4	169.0
18	-15.4	937.7	8.7	159.0	-26.9	790.2	12.9	145.9	-34.4	734.7	11.6	140.6	-45.8	697.7	10.1	151.4
19	-15.0	942.4	18.9	175.6	-27.3	798.6	17.8	174.9	-35.4	745.2	15.9	176.7	-45.1	709.5	9.1	175.8
20	-13.1	945.0	8.7	166.9	-27.0	798.4	11.9	174.6	-34.7	742.8	10.4	171.8	-44.6	703.6	4.1	180.3
21	-16.5	938.7	5.5	171.3	-30.7	790.5	10.8	175.7	-39.5	734.7	9.6	175.9	-49.7	695.1	5.4	176.6
22	-17.8	943.7	6.1	170.3	-30.5	794.0	7.7	162.0	-36.5	736.8	5.9	144.2	-50.7	696.8	7.7	168.2
23	-13.9	945.5	9.1	179.5	-26.9	796.5	6.8	154.5	-34.6	739.4	5.4	141.0	-51.1	698.8	6.4	172.0
24	-8.0	928.7	5.0	143.1	-18.7	786.4	8.6	134.1	-24.6	731.9	9.2	131.9	-40.9	694.4	8.3	134.3
25	-9.5	938.1	14.2	151.7	-19.0	794.9	14.2	138.2	-24.2	741.1	14.2	131.4	-33.5	706.1	10.2	134.4
26	-13.3	953.5	19.4	177.0	-24.5	806.6	18.2	170.5	-30.9	754.3	16.1	170.0	-40.8	719.4	9.8	172.0
27	-12.2	962.6	19.2	178.9	-24.4	815.6	17.3	175.1	-31.6	756.8	16.2	176.4	-36.6	724.2	6.3	181.9
28	-9.5	959.8	3.4	179.1	999.9	999.9	99.9	999.9	999.9	999.9	99.9	999.9	-31.6	713.7	3.0	149.6
29	-12.3	952.3	8.0	156.2	999.9	999.9	99.9	999.9	999.9	999.9	99.9	999.9	-40.5	710.5	7.1	146.3
30	-10.3	953.8	13.4	137.0	-19.5	807.0	18.4	139.7	999.9	999.9	99.9	999.9	-39.5	715.7	9.5	140.3
31	-7.2	961.5	11.0	143.4	999.9	999.9	99.9	999.9	999.9	999.9	99.9	999.9	-27.3	719.3	2.5	119.9
AVE	-13.2	949.9	10.0	167.6	-25.9	801.1	10.9	163.7	-32.4	748.4	9.7	160.8	-43.3	707.7	5.7	164.1

APR 83	D-10				D-47				D-57				D-80			
DATE	Temp	Pres.	WSpd	WiDir	Temp.	Pres.	WSpd	WiDir	Temp.	Pres.	WSpd	WiDir	Temp.	Pres.	WSpd	WiDir
1	-7.2	961.4	4.9	132.2	999.9	999.9	99.9	999.9	999.9	999.9	99.9	999.9	-25.5	715.3	1.6	90.4
2	-11.4	955.4	6.4	171.0	999.9	999.9	99.9	999.9	999.9	999.9	99.9	999.9	-41.1	709.6	3.4	193.2
3	-13.3	947.1	12.4	164.7	-25.7	800.3	17.1	160.6	999.9	999.9	99.9	999.9	-45.6	708.5	8.1	174.2
4	-13.1	955.5	11.8	169.2	-25.3	808.5	14.9	166.1	-37.1	760.1	13.7	179.2	-46.1	717.2	9.4	177.3
5	-14.2	962.0	6.5	173.9	-26.6	811.9	10.0	175.2	-33.5	756.0	8.6	175.3	-41.8	714.7	2.9	182.7
6	-15.4	948.8	8.4	173.4	-26.2	800.1	11.7	174.9	-34.3	744.4	11.6	178.1	-44.6	707.6	7.4	179.7
7	-16.9	949.4	4.9	158.0	-31.4	798.8	14.9	174.9	-37.5	743.4	16.3	176.0	-47.7	705.9	7.3	178.5
8	-20.8	957.4	12.9	178.2	-34.5	804.4	16.9	178.6	-43.6	750.2	15.3	176.5	-51.0	709.8	7.7	178.8
9	-18.0	955.5	16.0	161.1	-29.0	804.4	17.9	141.4	-36.1	749.8	15.1	147.5	-54.0	711.2	8.2	171.3
10	-16.5	946.9	14.2	157.7	-27.4	798.9	15.7	147.6	-32.4	743.1	14.6	138.8	-50.0	705.9	8.5	165.9
11	-16.5	958.8	11.5	161.6	-27.3	808.3	11.5	143.8	-32.0	751.0	8.8	138.7	-50.7	710.6	5.3	168.9
12	-13.7	948.1	17.0	163.0	-24.5	802.6	14.5	152.7	-30.1	747.6	11.1	150.2	-49.8	709.3	6.3	177.5
13	-16.3	946.7	12.1	176.7	-29.2	799.3	15.4	180.2	-37.1	744.3	13.5	178.6	-46.3	707.4	8.3	179.8
14	-15.6	961.0	16.8	170.9	-28.0	807.2	18.6	171.6	-32.8	756.7	13.8	158.1	-47.2	719.1	7.3	173.3
15	-14.4	954.7	8.2	157.4	999.9	999.9	99.9	999.9	-31.9	749.3	10.0	156.2	-49.0	709.6	5.1	177.1
16	-19.1	953.8	6.4	183.4	999.9	999.9	99.9	999.9	-43.5	745.5	12.2	180.6	-55.6	704.4	4.5	185.0
17	-15.4	947.3	8.2	173.7	999.9	999.9	99.9	999.9	-40.7	743.3	10.8	173.8	-55.9	703.6	5.7	179.9
18	-16.2	957.4	4.8	190.0	999.9	999.9	99.9	999.9	-38.3	749.8	8.9	186.1	-54.0	707.3	1.9	200.4
19	-12.7	952.1	5.5	171.9	999.9	999.9	99.9	999.9	-35.6	748.4	10.7	175.5	-51.9	708.2	3.1	186.9
20	-17.7	951.5	4.6	188.7	999.9	999.9	99.9	999.9	-41.9	745.0	11.8	177.1	-51.4	705.8	7.0	180.6
21	-15.5	945.4	4.5	176.6	999.9	999.9	99.9	999.9	-38.6	741.3	8.3	176.1	-51.4	702.0	5.4	181.6
22	-21.0	943.3	11.0	170.1	-32.0	793.3	20.7	164.8	-38.8	740.9	8.2	174.1	-51.5	700.9	8.1	176.5
23	-19.6	945.5	14.8	172.7	-32.1	791.1	16.5	180.0	999.9	999.9	99.9	999.9	-52.4	703.4	7.0	176.4
24	-16.2	938.4	15.9	160.7	-29.8	791.7	16.6	160.1	999.9	999.9	99.9	999.9	-52.3	701.8	8.7	173.2
25	-17.8	956.8	11.2	179.8	999.9	999.9	99.9	999.9	999.9	999.9	99.9	999.9	-55.8	709.9	6.2	181.1
26	-19.4	953.6	5.7	181.4	999.9	999.9	99.9	999.9	999.9	999.9	99.9	999.9	-54.4	706.7	4.6	183.3
27	-14.6	945.2	13.1	138.7	-24.4	797.1	19.4	138.8	999.9	999.9	99.9	999.9	-50.2	707.4	7.1	160.6
28	-13.8	950.5	14.0	159.4	-26.1	804.2	15.7	158.0	999.9	999.9	99.9	999.9	-45.8	711.2	6.3	167.1
29	-15.7	954.6	5.3	176.5	-29.0	805.3	11.6	176.8	999.9	999.9	99.9	999.9	-49.3	710.5	5.5	181.5
30	-18.4	950.2	8.9	152.7	-30.3	799.7	14.8	174.5	999.9	999.9	99.9	999.9	-49.9	708.3	9.4	177.5
31	999.9	999.9	99.9	999.9	999.9	999.9	99.9	999.9	999.9	999.9	99.9	999.9	999.9	999.9	99.9	999.9
AVE	-15.9	951.8	9.7	165.0	-28.2	802.7	14.1	164.0	-36.4	747.6	10.8	165.8	-49.1	708.4	6.2	176.2

MAY 83	D-10				D-47				D-57				D-80			
DATE	Temp.	Pres.	WSpd	WiDir	Temp.	Pres.	WSpd	WiDir	Temp.	Pres.	WSpd	WiDir	Temp.	Pres.	WSpd	WiDir
1	-14.1	961.6	7.1	166.6	-28.0	812.1	13.4	174.6	999.9	999.9	99.9	999.9	-47.5	718.0	6.0	180.4
2	-12.1	955.2	5.4	187.7	-24.6	807.5	7.5	180.3	999.9	999.9	99.9	999.9	-43.3	708.7	2.2	188.9
3	-19.1	943.0	12.1	168.9	-32.4	794.7	13.4	172.6	999.9	999.9	99.9	999.9	-51.1	702.1	9.5	176.9
4	-16.2	964.5	15.2	174.8	-30.8	814.9	13.1	174.7	999.9	999.9	99.9	999.9	-50.3	719.3	8.2	178.7
5	-17.0	956.0	8.0	167.5	-31.1	805.8	17.1	176.5	999.9	999.9	99.9	999.9	-45.4	714.2	9.9	179.2
6	-19.6	963.5	10.4	167.8	-32.8	809.9	18.1	178.1	999.9	999.9	99.9	999.9	-46.2	717.3	7.2	183.0
7	-15.1	967.4	13.5	172.7	-29.7	817.8	15.9	177.6	999.9	999.9	99.9	999.9	-46.1	724.2	5.9	182.9
8	-11.3	964.0	9.5	170.2	-25.2	814.8	15.3	177.1	999.9	999.9	99.9	999.9	-40.4	720.1	5.9	178.8
9	-14.1	954.3	4.2	143.2	-26.2	804.1	10.1	163.9	999.9	999.9	99.9	999.9	-46.1	707.5	6.6	174.6
10	-17.6	947.7	9.7	133.9	-30.6	797.1	15.4	152.8	999.9	999.9	99.9	999.9	-55.4	703.3	9.4	173.0
11	-18.3	952.0	6.3	121.5	-28.6	800.8	13.1	147.7	999.9	999.9	99.9	999.9	-53.3	703.9	6.3	172.8
12	-15.2	942.4	15.3	153.1	-25.4	796.2	15.7	142.4	999.9	999.9	99.9	999.9	-44.2	702.8	4.0	176.6
13	-14.1	943.4	10.9	157.4	-25.9	796.6	11.6	153.1	999.9	999.9	99.9	999.9	-48.2	701.9	4.2	180.7
14	-16.9	945.1	10.8	161.4	-28.6	796.3	10.1	142.2	999.9	999.9	99.9	999.9	-52.9	699.6	4.8	179.4
15	-15.5	941.7	13.5	170.6	-27.9	795.5	12.2	156.5	999.9	999.9	99.9	999.9	-54.4	700.3	6.3	176.6
16	-20.5	948.2	12.4	178.5	-35.1	798.1	15.1	176.6	999.9	999.9	99.9	999.9	-58.9	704.1	7.1	179.4
17	-17.7	951.7	17.9	148.6	-27.5	802.2	19.0	141.0	999.9	999.9	99.9	999.9	-54.0	710.4	9.0	156.7
18	-18.5	958.2	16.3	159.0	-28.8	806.8	13.6	149.2	999.9	999.9	99.9	999.9	-46.8	714.0	7.9	168.5
19	-16.7	956.6	15.8	164.3	-29.7	790.2	17.6	162.4	999.9	999.9	99.9	999.9	-50.0	701.6	9.0	175.1
20	-17.9	937.1	13.7	156.0	-31.1	790.7	14.9	157.2	999.9	999.9	99.9	999.9	-48.7	698.3	7.9	174.0
21	-17.0	946.0	13.0	164.6	-28.9	797.4	14.3	161.8	999.9	999.9	99.9	999.9	-48.0	703.7	7.0	178.2
22	-19.9	952.6	9.6	150.8	-32.8	801.0	13.5	168.4	999.9	999.9	99.9	999.9	-48.5	705.5	7.4	179.1
23	-24.7	957.2	7.0	169.0	-39.0	802.1	11.0	171.9	999.9	999.9	99.9	999.9	-54.3	700.9	4.0	173.8
24	-20.5	952.8	12.9	171.4	-34.6	803.1	13.6	171.4	999.9	999.9	99.9	999.9	-56.8	707.1	5.2	182.4
25	-19.0	964.3	7.0	175.2	-31.7	812.1	14.0	175.1	999.9	999.9	99.9	999.9	-43.7	719.0	8.6	172.7
26	-13.0	976.4	16.7	177.4	-26.0	827.6	15.7	173.3	999.9	999.9	99.9	999.9	-40.9	735.5	9.2	177.8
27	-9.8	982.1	13.3	170.8	-24.4	833.8	16.9	176.1	999.9	999.9	99.9	999.9	-39.8	741.4	9.3	179.4
28	-8.4	972.9	13.3	171.0	-22.9	826.1	19.4	175.4	999.9	999.9	99.9	999.9	-36.5	736.4	8.9	178.9
29	-5.1	970.9	13.9	170.8	-17.6	826.4	17.1	172.2	999.9	999.9	99.9	999.9	-39.8	736.5	6.3	182.1
30	-5.6	971.8	8.0	181.4	-20.0	827.6	12.1	174.3	999.9	999.9	99.9	999.9	-46.7	732.6	3.3	186.8
31	-11.9	957.6	6.5	214.4	-25.1	813.1	7.6	183.9	999.9	999.9	99.9	999.9	-37.2	714.6	0.4	251.2
AVE	-15.5	956.2	11.0	165.5	-28.4	807.5	13.7	166.9	999.9	999.9	*****	84.3	-47.6	713.1	6.6	176.8

JUN 83	D-10				D-47				D-80			
DATE	Temp.	Pres.	WSpd	WiDir	Temp.	Pres.	WSpd	WiDir	Temp.	Pres.	WSpd	WiDir
1	-12.8	938.3	8.6	144.1	-23.5	792.4	9.8	149.9	-48.6	696.5	5.1	157.6
2	-18.1	946.8	6.6	183.1	-30.7	796.8	9.3	174.0	-52.2	698.4	3.3	177.4
3	-15.0	963.3	2.2	157.2	-26.7	812.1	4.3	196.6	-45.9	708.2	2.3	318.9
4	-16.0	958.9	1.7	180.7	-26.3	808.9	5.6	188.9	-36.4	706.1	4.2	303.3
5	-17.8	952.1	5.3	160.1	-29.5	801.5	8.2	175.5	-54.9	702.0	6.0	178.4
6	-24.9	949.8	7.6	173.1	-39.1	796.2	12.2	177.9	-54.5	699.6	8.3	179.6
7	-24.6	956.7	3.8	165.5	-35.1	803.3	11.1	172.9	-55.2	705.4	5.1	181.0
8	-16.9	960.2	5.3	132.9	-24.8	809.5	11.0	142.4	-51.3	712.1	5.0	175.2
9	-11.8	962.1	12.6	137.4	-22.8	813.4	15.1	134.3	-37.4	716.7	6.1	128.0
10	-11.9	952.5	10.3	172.8	-23.0	806.1	11.0	147.5	-37.3	709.6	4.6	142.3
11	-12.7	942.2	11.4	168.3	-25.5	797.6	11.9	160.3	-40.2	703.2	5.5	144.4
12	-10.0	932.5	8.9	161.5	-22.4	789.4	10.9	143.3	-40.6	695.1	4.7	147.6
13	-13.9	929.4	9.9	175.5	-26.2	785.5	11.4	168.5	-48.7	692.3	4.8	177.8
14	-12.4	939.9	4.1	118.9	-23.0	792.2	5.0	122.6	-45.4	693.9	2.7	163.9
15	-19.6	943.6	6.8	174.6	-34.9	793.2	8.2	171.4	-53.2	696.8	8.0	181.0
16	-17.9	960.4	8.9	183.4	-31.0	810.5	16.9	182.0	-44.3	716.1	7.7	193.1
17	-13.4	967.4	5.0	171.0	-26.0	817.8	12.5	177.9	-44.4	721.3	4.3	184.1
18	-11.5	971.5	6.3	165.7	-25.8	821.4	13.6	177.0	-45.1	725.7	5.5	187.5
19	-8.5	977.0	3.4	130.0	-16.8	828.2	10.2	149.0	-35.9	732.2	5.3	177.9
20	-11.0	971.4	5.9	132.4	-17.1	823.3	12.9	140.5	-35.7	729.4	6.7	152.6
21	-14.3	963.8	3.2	156.7	-20.8	812.9	15.7	139.7	-35.0	723.2	10.1	149.4
22	-18.7	969.7	15.9	137.6	-27.8	815.7	18.3	140.4	-42.0	723.2	9.4	156.8
23	-16.9	968.2	15.0	139.0	999.9	999.9	99.9	999.9	999.9	999.9	99.9	999.9
24	-18.2	974.3	7.0	160.6	999.9	999.9	99.9	999.9	-39.5	722.3	7.1	141.7
25	-14.2	985.3	7.7	162.8	999.9	999.9	99.9	999.9	-34.0	738.1	7.6	162.3
26	-8.3	985.8	14.1	179.0	-20.9	829.4	17.9	173.6	-39.7	744.0	6.4	180.9
27	-6.9	969.2	8.6	181.9	-18.5	823.8	11.7	179.9	-35.7	727.0	2.5	233.1
28	-18.8	943.0	9.9	179.0	-30.6	793.4	13.6	184.2	-43.4	698.4	9.6	183.7
29	-25.1	955.7	10.3	166.4	-38.3	800.4	13.1	168.6	-54.9	702.1	6.3	173.9
30	-23.6	955.0	14.8	152.5	-35.6	802.5	14.9	155.4	-55.7	704.9	7.6	164.6
AVE	-15.4	958.1	7.6	161.6	-26.7	806.1	10.9	161.6	-44.2	718.1	5.2	169.2

JUL 83	D-10				D-47				D-80			
DATE	Temp.	Pres.	WSpd	WiDir	Temp.	Pres.	WSpd	WiDir	Temp.	Pres.	WSpd	WiDir
1	-23.5	966.1	8.1	136.4	-35.6	808.9	12.8	164.1	-58.6	710.1	5.2	174.8
2	-21.5	949.3	15.1	146.8	-32.7	798.0	16.8	148.6	-51.0	702.8	7.4	155.8
3	-23.7	951.5	5.7	172.5	-35.3	797.1	13.2	170.1	-57.2	700.9	7.4	178.8
4	-27.1	957.3	5.1	162.9	-38.2	800.2	13.0	173.0	-57.2	703.7	8.1	177.5
5	-25.3	962.2	2.7	172.5	-37.7	806.3	13.0	176.5	-56.5	708.9	7.3	182.2
6	-24.9	967.1	3.8	179.0	-38.8	810.9	14.2	179.4	-54.9	713.0	6.7	186.4
7	-21.0	953.0	10.2	179.4	-36.3	802.0	15.0	178.6	-53.5	705.5	6.9	187.8
8	-25.8	946.5	4.3	164.7	-37.4	792.3	16.3	177.0	-52.8	698.4	8.0	181.5
9	-27.0	946.8	4.3	121.4	-37.4	790.9	11.2	169.8	-54.9	693.8	8.2	176.4
10	-23.1	942.3	8.6	133.2	-33.1	790.7	11.8	147.2	-58.0	694.3	8.3	171.8
11	-16.7	947.9	14.1	141.8	-28.6	798.3	14.8	138.2	-51.2	703.8	8.2	149.5
12	-6.9	949.1	12.2	107.3	999.9	999.9	99.9	999.9	-33.8	709.7	4.9	105.4
13	-8.7	957.7	5.8	137.0	999.9	999.9	99.9	999.9	-34.4	713.0	2.5	139.2
14	-15.2	949.8	9.8	173.2	999.9	999.9	99.9	999.9	-47.9	708.9	6.4	177.5
15	-17.7	948.3	7.8	174.2	999.9	999.9	99.9	999.9	-54.1	704.5	6.3	177.8
16	-19.0	948.6	7.7	170.0	999.9	999.9	99.9	999.9	-59.2	702.6	3.2	181.4
17	-18.9	945.6	6.9	166.2	999.9	999.9	99.9	999.9	-60.2	699.8	2.9	183.3
18	-24.5	945.3	7.7	177.1	999.9	999.9	99.9	999.9	-60.4	692.7	3.7	176.6
19	-28.2	954.1	7.9	185.7	999.9	999.9	99.9	999.9	-65.9	695.8	2.2	185.0
20	-17.1	944.4	11.8	131.8	999.9	999.9	99.9	999.9	-50.4	699.0	3.8	102.0
21	-21.2	943.4	12.6	194.2	999.9	999.9	99.9	999.9	-54.0	698.9	7.9	178.2
22	-22.5	951.8	13.6	180.2	999.9	999.9	99.9	999.9	-54.2	705.5	6.8	181.9
23	-22.8	946.1	5.7	180.6	999.9	999.9	99.9	999.9	-57.5	695.5	3.7	177.2
24	-31.0	939.9	9.3	178.8	999.9	999.9	99.9	999.9	-59.7	684.7	5.1	91.6
25	-26.0	936.1	11.4	137.7	999.9	999.9	99.9	999.9	-54.3	686.2	9.9	139.7
26	-27.8	953.1	6.3	170.1	999.9	999.9	99.9	999.9	-56.3	681.0	5.9	154.4
27	-31.0	934.2	7.0	181.0	999.9	999.9	99.9	999.9	-60.0	682.2	7.9	176.5
28	-32.6	935.5	8.7	185.7	999.9	999.9	99.9	999.9	-64.7	683.6	8.2	177.8
29	-31.9	946.7	6.8	180.1	-45.3	797.3	14.6	180.0	-64.9	694.1	7.1	179.1
30	-21.2	948.7	10.4	142.0	-34.1	797.2	13.8	149.1	-60.3	700.4	6.0	173.0
31	-19.5	935.4	17.7	144.8	-29.4	788.8	17.6	140.3	-49.9	696.6	7.0	148.9
AVE	-22.6	947.8	8.0	159.7	-35.1	798.7	13.6	162.0	-55.1	699.0	5.8	167.9

AUG 83	D-10				D-47				D-80			
DATE	Temp.	Pres.	WSpd	WiDir	Temp.	Pres.	WSpd	WiDir	Temp.	Pres.	WSpd	WiDir
1	-18.2	929.4	11.7	157.6	-29.8	782.2	16.0	142.3	-45.1	692.0	10.8	147.3
2	-21.2	944.9	6.4	169.1	-33.1	793.0	8.1	158.1	-50.2	695.4	5.4	161.5
3	-24.7	941.7	5.8	166.8	-36.7	788.1	11.4	176.3	-55.1	693.6	7.5	177.2
4	-26.8	950.2	4.3	166.3	-40.0	794.6	15.8	178.7	-55.2	700.8	10.1	179.6
5	-21.9	952.8	7.5	155.1	-34.4	800.1	15.6	174.1	-52.5	707.0	8.7	179.5
6	999.9	999.9	99.9	999.9	999.9	999.9	99.9	999.9	999.9	999.9	99.9	999.9
7	-24.9	927.2	7.2	143.1	-39.0	776.6	12.9	173.5	-57.2	682.8	9.0	171.4
8	-24.8	939.7	11.5	144.9	-37.1	787.4	12.9	163.3	-56.4	690.6	7.0	172.5
9	-18.5	939.6	14.7	152.3	-29.8	791.7	14.4	141.1	-55.2	697.7	6.0	173.7
10	-14.9	932.9	10.2	146.0	-27.1	786.1	15.1	140.8	-44.7	693.9	5.8	155.5
11	-16.0	946.7	7.5	184.7	-28.9	798.0	9.0	174.6	-54.6	700.8	3.9	183.7
12	-16.5	962.4	6.6	180.2	-30.7	811.9	11.6	181.9	-54.7	713.4	2.4	204.9
13	-11.9	953.8	9.5	136.8	-22.9	805.7	11.2	140.6	-44.5	709.1	5.6	157.0
14	-15.2	955.1	7.1	128.8	-25.1	804.1	9.4	134.1	-37.9	705.1	3.6	120.8
15	-17.7	957.3	3.0	168.8	-27.6	803.5	5.0	185.0	999.9	999.9	99.9	999.9
16	-24.3	942.7	5.4	155.2	-36.0	789.6	13.5	173.6	-55.5	695.5	9.3	177.2
17	-30.9	949.3	14.7	148.5	-41.4	788.8	16.7	163.9	-50.7	699.1	14.4	170.2
18	-27.6	953.8	6.3	137.6	-37.1	797.0	14.4	172.3	-47.7	703.9	10.8	174.9
19	-28.5	957.0	6.4	136.3	-38.1	798.1	15.1	177.4	-52.0	704.5	11.9	174.9
20	-28.1	958.8	3.8	139.8	-35.2	802.9	14.6	175.3	-55.3	707.6	7.7	179.7
21	-26.4	957.4	5.1	194.8	-38.1	803.4	12.2	179.6	-56.3	705.4	5.5	182.4
22	-20.4	962.4	6.7	143.2	-32.6	809.9	13.5	161.2	-54.8	713.0	6.1	177.3
23	-17.3	975.9	4.0	129.5	-25.7	822.2	9.9	155.5	-44.1	722.4	3.8	172.1
24	-12.0	955.3	13.2	137.2	-21.9	807.0	16.2	134.5	-35.4	713.2	10.4	136.7
25	-16.4	954.7	9.7	160.8	-27.4	804.6	11.4	159.1	-45.0	710.9	10.1	166.1
26	-18.1	971.9	8.4	157.7	-29.5	817.4	11.7	156.8	-49.8	719.7	6.0	176.8
27	-14.1	964.7	6.6	147.2	-24.6	815.2	10.8	166.6	-47.3	719.2	6.0	179.3
28	-14.6	960.2	9.8	170.8	-28.9	811.1	13.7	178.0	-47.1	716.3	6.5	184.1
29	-16.6	965.3	10.1	177.1	-31.9	814.6	14.4	177.6	-47.4	719.2	7.1	182.1
30	-21.0	956.3	12.4	171.9	-33.9	804.7	15.1	165.7	-47.2	712.3	9.3	177.5
AVE	-20.6	953.0	7.9	154.8	-31.7	801.1	12.4	163.5	-49.9	705.7	7.4	170.9

SEP 83	D-10				D-47				D-80			
DATE	Temp.	Pres.	WSpd	WiDir	Temp.	Pres.	WSpd	WiDir	Temp.	Pres.	WSpd	WiDir
1	-19.9	962.7	16.6	140.8	-31.9	809.7	14.2	136.0	-53.3	710.6	4.9	158.0
2	-15.2	958.9	18.5	139.8	-26.5	811.0	19.0	134.1	-38.4	718.5	9.3	120.1
3	-9.0	946.0	18.7	136.1	-21.5	802.1	21.1	129.3	-32.6	711.6	12.8	110.2
4	-10.4	958.2	3.0	92.5	999.9	999.9	99.9	999.9	999.9	999.9	99.9	999.9
5	-15.7	959.9	12.5	183.5	-27.6	811.7	14.7	186.2	999.9	999.9	99.9	999.9
6	-7.1	970.4	11.7	212.5	-19.2	825.0	12.1	188.5	999.9	999.9	99.9	999.9
7	-7.9	969.6	8.4	185.4	-20.7	823.9	9.9	182.1	999.9	999.9	99.9	999.9
8	-8.5	965.8	4.2	147.4	-19.7	818.3	8.6	168.2	999.9	999.9	99.9	999.9
9	-12.1	945.0	8.2	158.0	-24.6	799.1	13.3	175.0	999.9	999.9	99.9	999.9
10	-21.5	940.3	12.3	146.2	-30.7	788.4	15.8	172.6	999.9	999.9	99.9	999.9
11	-20.2	943.1	6.1	157.6	999.9	999.9	99.9	999.9	999.9	999.9	99.9	999.9
12	-20.6	951.0	10.0	149.9	-30.0	799.7	13.3	148.2	999.9	999.9	99.9	999.9
13	-19.4	949.3	19.0	178.3	-31.5	798.7	20.4	180.1	-44.7	713.0	18.8	178.9
14	-17.5	958.1	15.3	150.0	-29.1	808.6	15.9	146.9	-41.1	715.8	11.4	157.9
15	-16.5	973.0	7.4	144.3	-28.8	820.2	11.2	144.6	-39.6	723.3	6.9	137.1
16	-10.3	973.0	9.7	110.0	-18.7	822.1	12.8	126.0	-28.3	726.5	6.5	125.0
17	-11.8	953.3	4.0	129.0	-20.3	804.7	9.1	136.3	-28.7	710.6	8.5	129.2
18	-15.4	941.0	9.6	169.9	-27.1	794.4	10.3	157.1	-41.5	699.7	6.5	159.3
19	-14.9	937.8	14.1	156.9	-25.5	794.1	15.3	153.2	-46.0	702.7	7.8	174.3
20	-17.2	937.0	10.2	168.6	-29.4	790.6	14.5	171.1	-47.7	698.9	6.7	179.3
21	-23.4	935.0	13.1	165.5	-34.6	784.7	15.9	173.7	-52.1	693.1	8.9	177.0
22	-23.8	941.7	9.6	173.8	999.9	999.9	99.9	999.9	-54.8	694.1	6.2	176.9
23	-19.0	941.5	7.8	176.3	999.9	999.9	99.9	999.9	-54.3	696.8	5.8	178.4
24	-13.7	940.0	15.0	146.6	-25.1	793.3	15.9	122.1	-43.8	701.1	7.1	144.7
25	-13.6	945.5	8.7	159.5	999.9	999.9	99.9	999.9	-38.6	702.0	3.7	154.3
26	-16.7	946.2	5.9	185.2	999.9	999.9	99.9	999.9	-47.2	700.0	3.9	184.9
27	-14.5	951.1	5.6	146.9	999.9	999.9	99.9	999.9	-44.5	702.9	3.6	169.2
28	-18.8	934.4	21.0	141.8	-22.6	791.0	17.6	151.7	-36.4	702.5	6.1	135.7
29	-15.0	933.9	11.8	154.8	-25.7	786.7	14.6	142.4	-43.9	696.3	8.2	165.2
30	-20.7	930.7	13.0	159.5	-30.6	783.0	13.6	146.5	-51.1	689.7	7.0	175.3
31	-21.0	930.2	13.1	160.5	999.9	999.9	99.9	999.9	-51.3	689.2	6.8	176.2
AVE	-15.7	949.0	10.4	155.7	-25.7	804.1	12.9	154.0	-43.9	703.8	6.4	156.8

OCT 83	D-10				D-47				D-80			
DATE	Temp.	Pres.	WSpd	WiDir	Temp.	Pres.	WSpd	WiDir	Temp.	Pres.	WSpd	WiDir
1	-23.8	918.3	6.6	176.6	999.9	999.9	99.9	999.9	-54.0	675.5	6.7	177.5
2	-25.7	923.7	8.0	166.7	999.9	999.9	99.9	999.9	-57.4	677.4	9.7	168.6
3	-24.9	942.3	8.4	170.4	999.9	999.9	99.9	999.9	-59.6	688.8	3.4	171.2
4	-19.1	933.1	11.7	151.3	-31.1	782.4	11.1	143.9	-48.3	688.5	3.9	161.2
5	-19.7	942.6	4.1	177.5	-31.1	791.4	6.8	172.6	-48.2	691.3	1.3	185.7
6	-22.4	934.1	6.8	189.2	-33.0	785.2	5.6	194.5	-51.4	685.8	3.2	185.9
7	-23.3	927.1	11.3	179.7	-36.9	778.2	12.5	173.5	-53.3	683.7	5.8	180.8
8	-25.0	934.4	6.4	175.8	-37.5	782.1	10.8	173.2	-56.0	685.9	6.3	178.2
9	-23.1	934.6	8.5	171.5	-36.9	784.1	12.2	177.7	-52.3	689.1	7.1	181.5
10	-22.9	937.5	8.3	171.1	-35.9	787.1	14.1	176.1	-51.3	691.6	8.3	179.0
11	-21.8	943.8	9.0	181.4	-35.8	793.1	11.6	176.0	-50.2	695.9	6.0	178.5
12	-15.7	938.9	12.4	152.8	-26.4	791.6	13.5	142.6	-48.1	699.2	8.0	158.2
13	-16.2	955.2	8.7	178.9	999.9	999.9	99.9	999.9	-46.6	710.6	7.8	178.2
14	-16.8	958.9	14.1	176.9	-30.1	807.7	10.6	172.0	-41.6	715.5	7.5	178.1
15	-15.7	956.9	12.1	142.4	999.9	999.9	99.9	999.9	-41.1	713.7	8.2	166.1
16	-16.1	961.5	11.9	155.8	-28.2	813.5	13.4	162.2	-44.9	716.2	8.6	168.7
17	-16.4	970.8	6.3	141.3	-27.9	817.1	13.4	168.7	-46.5	721.9	8.0	171.0
18	-16.0	965.0	8.0	144.2	-27.9	813.6	13.7	164.8	-47.0	718.8	6.5	177.5
19	-18.1	949.7	11.0	161.8	-31.0	799.5	14.4	171.7	-43.3	706.3	8.1	173.5
20	-20.0	940.8	7.8	137.4	-31.9	788.9	11.1	143.4	-42.0	694.4	12.9	143.8
21	-15.8	940.7	10.0	140.3	-28.3	791.5	9.0	122.7	999.9	999.9	99.9	999.9
22	-14.6	946.0	7.8	140.9	-26.4	796.4	7.3	136.7	999.9	999.9	99.9	999.9
23	-16.4	934.2	12.3	159.8	-27.4	787.2	11.7	138.8	999.9	999.9	99.9	999.9
24	-18.0	939.4	8.6	168.2	-30.1	790.0	8.3	153.2	999.9	999.9	99.9	999.9
25	-14.1	941.7	5.0	164.5	-27.8	792.8	7.0	145.6	999.9	999.9	99.9	999.9
26	-13.9	945.5	5.3	169.3	-26.5	796.9	7.5	157.3	999.9	999.9	99.9	999.9
27	-14.2	929.8	12.3	156.5	-24.2	786.7	13.8	150.7	999.9	999.9	99.9	999.9
28	-14.4	926.7	8.9	136.8	-25.5	783.1	12.1	139.2	-41.9	693.9	13.1	147.7
29	-14.0	940.6	6.7	143.3	-25.6	792.0	7.2	126.4	999.9	999.9	99.9	999.9
30	-15.0	939.7	11.3	156.9	-26.3	792.4	10.3	154.8	999.9	999.9	99.9	999.9
31	-16.3	937.3	6.6	174.8	-26.9	789.2	9.4	174.9	999.9	999.9	99.9	999.9
AVE	-18.3	941.7	8.6	160.8	-30.0	792.6	10.1	159.3	-49.2	697.4	6.8	170.8

NOV 83	D-10				D-47			
DATE	Temp.	Pres.	WSpd	WiDir	Temp.	Pres.	WSpd	WiDir
1	-17.5	938.7	6.0	181.0	-30.3	789.2	9.1	176.6
2	-15.8	942.8	10.1	152.8	-29.0	794.4	9.6	154.7
3	-16.5	946.4	5.7	176.8	-28.5	796.3	8.5	171.1
4	-13.6	943.6	7.9	144.9	-25.3	795.5	9.3	154.5
5	-10.8	947.4	8.1	153.7	-22.9	800.2	9.1	156.5
6	-11.2	953.4	3.7	195.7	-21.6	805.7	7.3	179.8
7	-8.5	964.0	3.7	189.2	-19.1	815.3	6.1	177.8
8	-7.1	971.0	5.6	126.8	-15.9	822.0	7.5	125.7
9	-5.6	963.2	9.7	128.3	-15.7	816.0	16.8	136.7
10	-5.4	952.5	13.5	138.1	-15.8	807.7	17.6	139.6
11	-4.3	948.6	8.3	135.0	-14.5	805.3	13.7	143.2
12	-6.7	952.2	9.8	147.8	-18.4	807.2	13.2	148.4
13	-8.4	953.3	5.4	127.0	-18.7	805.7	10.8	141.4
14	-11.8	950.1	7.0	130.8	-22.0	801.5	12.8	150.4
15	-13.6	951.3	7.8	137.5	-23.8	801.7	11.7	146.5
16	-13.0	945.9	7.7	153.1	-24.2	797.4	10.9	156.2
17	-12.4	942.3	5.3	163.0	-22.9	794.8	9.7	161.4
18	-11.9	951.1	5.6	164.4	-23.4	802.5	7.9	146.6
19	-10.5	947.4	8.4	172.7	-22.0	800.6	7.2	161.0
20	-10.3	953.4	5.7	166.4	-22.4	805.4	7.8	158.8
21	-8.2	952.8	7.8	118.2	-17.6	805.3	8.6	125.2
22	-5.8	941.9	4.6	102.0	-15.4	797.4	10.3	118.1
23	-6.5	955.6	5.2	284.3	-17.1	807.0	6.6	291.6
24	-6.9	950.5	2.7	206.3	-21.1	803.6	3.7	216.3
25	-11.7	941.5	5.4	199.5	-22.8	794.9	5.1	170.1
26	-11.2	943.1	5.4	187.5	-22.9	796.3	7.3	172.6
27	-9.5	939.2	9.3	140.2	-20.1	794.2	10.0	137.6
28	-7.6	948.4	3.7	164.8	-18.9	801.6	4.4	163.4
29	-10.4	946.9	5.3	209.0	-21.9	799.8	4.8	187.0
30	-8.7	945.4	6.2	149.2	-20.9	798.7	6.3	143.4
31	-8.9	945.3	6.8	148.0	-20.9	798.7	6.7	141.9
AVE	-10.0	949.3	5.9	153.5	-21.2	802.0	8.3	152.5

DEC 83	D-10				D-47			
DATE	Temp.	Pres.	WSpd	WiDir	Temp.	Pres.	WSpd	WiDir
1	-9.6	943.6	15.6	151.8	-20.6	800.2	14.3	139.9
2	-7.2	943.4	9.0	152.8	-18.1	799.4	11.0	139.4
3	-5.5	939.1	7.1	158.3	-16.5	796.1	10.1	143.5
4	-6.2	942.2	6.1	165.8	-18.2	798.2	9.3	158.4
5	-2.5	948.8	5.7	140.4	-12.1	805.5	8.8	125.8
6	-3.9	941.4	15.2	143.8	-13.6	800.5	18.9	140.1
7	-4.7	944.8	9.5	145.3	-16.7	801.6	13.1	142.3
8	-5.3	950.6	7.9	166.4	-16.8	806.3	10.0	141.4
9	-4.0	956.4	5.7	117.4	-12.5	810.9	5.4	108.8
10	-6.4	962.4	6.6	173.4	-16.6	815.8	6.3	166.9
11	-6.9	959.1	5.8	164.5	-18.4	812.6	8.3	158.2
12	-4.7	956.8	8.1	141.6	-16.0	811.6	10.2	141.6
13	-4.8	951.2	12.0	132.2	999.9	999.9	99.9	999.9
14	-3.4	952.6	6.3	102.1	999.9	999.9	99.9	999.9
15	-2.8	954.5	1.2	214.5	999.9	999.9	99.9	999.9
16	-0.6	955.5	1.2	187.3	999.9	999.9	99.9	999.9
17	999.9	999.9	99.9	999.9	999.9	999.9	99.9	999.9
18	-2.5	953.9	6.0	128.4	999.9	999.9	99.9	999.9
19	999.9	999.9	99.9	999.9	999.9	999.9	99.9	999.9
20	999.9	999.9	99.9	999.9	-10.7	795.1	21.9	134.8
21	999.9	999.9	99.9	999.9	-10.0	786.0	20.4	133.4
22	999.9	999.9	99.9	999.9	999.9	999.9	99.9	999.9
23	999.9	999.9	99.9	999.9	999.9	999.9	99.9	999.9
24	999.9	999.9	99.9	999.9	999.9	999.9	99.9	999.9
25	999.9	999.9	99.9	999.9	999.9	999.9	99.9	999.9
26	999.9	999.9	99.9	999.9	-9.8	821.3	3.7	174.9
27	999.9	999.9	99.9	999.9	999.9	999.9	99.9	999.9
28	999.9	999.9	99.9	999.9	999.9	999.9	99.9	999.9
29	999.9	999.9	99.9	999.9	999.9	999.9	99.9	999.9
30	999.9	999.9	99.9	999.9	999.9	999.9	99.9	999.9
31	999.9	999.9	99.9	999.9	999.9	999.9	99.9	999.9
AVE	-4.8	950.2	7.2	147.2	-15.6	805.6	10.1	142.4

JAN 84	D-10				D-47				D-57				DOME C			
DATE	Temp.	Pres.	WSpd	WiDir	Temp.	Pres.	WSpd	WiDir	Temp.	Pres.	WSpd	WiDir	Temp.	Pres.	WSpd	WiDir
1	999.9	999.9	99.9	999.9	999.9	999.9	99.9	999.9	-16.4	759.9	6.9	122.2	999.9	999.9	99.9	999.9
2	999.9	999.9	99.9	999.9	999.9	999.9	99.9	999.9	-16.3	759.8	3.1	108.7	999.9	999.9	99.9	999.9
3	999.9	999.9	99.9	999.9	999.9	999.9	99.9	999.9	-15.8	755.3	9.1	132.9	999.9	999.9	99.9	999.9
4	999.9	999.9	99.9	999.9	999.9	999.9	99.9	999.9	-13.5	745.6	4.8	133.8	999.9	999.9	99.9	999.9
5	999.9	999.9	99.9	999.9	999.9	999.9	99.9	999.9	-15.6	758.4	1.3	63.1	999.9	999.9	99.9	999.9
6	999.9	999.9	99.9	999.9	999.9	999.9	99.9	999.9	-15.2	756.3	13.7	113.5	999.9	999.9	99.9	999.9
7	999.9	999.9	99.9	999.9	999.9	999.9	99.9	999.9	-13.5	757.2	10.0	79.2	999.9	999.9	99.9	999.9
8	999.9	999.9	99.9	999.9	999.9	999.9	99.9	999.9	-12.5	763.4	5.0	116.0	999.9	999.9	99.9	999.9
9	999.9	999.9	99.9	999.9	999.9	999.9	99.9	999.9	-11.9	764.7	6.4	119.3	999.9	999.9	99.9	999.9
10	999.9	999.9	99.9	999.9	999.9	999.9	99.9	999.9	-11.5	760.2	11.2	94.0	999.9	999.9	99.9	999.9
11	999.9	999.9	99.9	999.9	-9.5	818.8	7.2	117.3	-13.3	763.6	7.3	113.9	999.9	999.9	99.9	999.9
12	999.9	999.9	99.9	999.9	-11.9	818.1	6.9	143.1	-16.0	763.0	6.3	139.7	999.9	999.9	99.9	999.9
13	999.9	999.9	99.9	999.9	-14.8	813.2	6.6	142.7	-19.1	757.7	6.7	139.4	999.9	999.9	99.9	999.9
14	-4.0	957.9	9.6	136.8	-15.0	813.9	10.0	126.7	-19.6	758.6	8.6	127.2	999.9	999.9	99.9	999.9
15	-3.8	962.3	8.7	144.6	-14.9	817.1	8.8	122.9	-18.0	761.2	7.9	118.8	999.9	999.9	99.9	999.9
16	-2.5	965.1	4.4	152.2	-13.8	819.8	8.3	136.7	-18.1	764.4	6.4	131.6	999.9	999.9	99.9	999.9
17	-2.1	965.7	6.0	143.0	-13.7	821.2	9.2	139.3	-18.1	766.3	7.9	131.8	999.9	999.9	99.9	999.9
18	-0.1	958.1	8.6	133.5	-9.4	816.7	14.6	120.2	-13.3	763.6	12.3	118.8	999.9	999.9	99.9	999.9
19	-0.1	968.2	2.2	94.8	-8.6	823.0	5.4	87.4	-12.1	767.3	6.4	85.8	999.9	999.9	99.9	999.9
20	2.5	969.6	4.4	200.0	-9.5	826.4	5.7	180.0	-13.4	771.1	6.0	180.9	999.9	999.9	99.9	999.9
21	1.1	965.5	7.7	164.5	-11.9	822.6	10.1	156.6	-16.8	768.5	9.5	162.3	999.9	999.9	99.9	999.9
22	1.7	964.6	5.2	138.4	-10.8	821.1	9.7	136.3	-15.3	766.2	9.1	136.0	999.9	999.9	99.9	999.9
23	0.8	967.0	3.6	164.0	-11.4	822.8	7.6	144.1	-14.9	767.7	7.7	141.5	999.9	999.9	99.9	999.9
24	0.1	962.4	2.9	151.9	-12.3	817.8	7.1	137.1	-15.8	762.8	7.2	134.5	-30.7	661.1	3.7	178.7
25	-1.6	959.3	2.6	130.4	-12.0	814.3	6.6	123.8	-15.9	758.9	6.4	125.9	-30.0	658.5	4.3	167.9
26	-2.2	959.1	4.1	143.0	-13.0	814.4	7.8	125.6	-16.7	758.9	6.5	120.7	-30.6	655.7	1.9	146.0
27	-1.8	961.6	8.4	143.8	-14.0	817.3	9.0	133.1	-18.6	761.9	8.6	132.4	-28.5	656.3	0.1	346.7
28	-1.5	961.9	12.4	143.7	-14.1	819.0	11.9	136.0	-20.1	764.1	9.8	132.9	-32.6	659.0	1.2	54.3
29	-1.9	969.4	11.2	146.0	-14.0	824.8	11.7	134.6	-18.7	769.4	9.4	132.3	-32.9	662.3	1.7	29.5
30	-2.9	976.9	5.9	146.1	-15.9	829.7	10.2	149.6	-20.2	773.7	8.9	141.9	-33.7	666.2	2.1	273.4
31	-2.4	976.5	4.9	135.5	-14.0	829.5	8.9	133.1	-18.8	773.4	8.1	129.9	-32.6	663.6	1.9	279.7
AVE	-1.1	965.2	6.0	145.4	-12.6	820.1	8.5	134.4	-16.0	762.7	7.3	125.6	-31.6	660.5	0.8	181.6

FEB 84	D-10				D-47				D-57				DOME C			
DATE	Temp.	Pres.	WSpd	WiDir	Temp.	Pres.	WSpd	WiDir	Temp.	Pres.	WSpd	WiDir	Temp.	Pres.	WSpd	WiDir
1	-2.3	972.3	5.8	137.0	-13.2	826.6	8.7	131.5	-16.8	770.8	7.8	128.1	-34.6	662.1	2.4	273.6
2	-2.9	970.3	6.1	130.4	-13.4	823.8	8.9	135.7	-16.5	768.1	8.4	137.8	-34.4	662.8	2.9	258.8
3	-5.2	968.7	5.1	132.7	-16.7	821.0	9.9	145.2	-20.3	765.4	8.3	145.5	-35.2	661.2	2.7	230.2
4	-5.3	961.3	9.3	137.3	-18.0	815.3	11.5	140.3	-22.8	760.2	11.1	137.8	-35.7	658.5	1.5	204.6
5	-4.4	965.2	6.2	134.5	-16.7	818.7	9.6	140.0	-21.4	763.3	9.2	135.8	-35.0	661.9	2.9	137.6
6	-3.1	955.9	13.4	135.0	-14.3	813.9	14.7	128.8	-18.9	760.4	13.0	128.4	-35.1	662.8	1.5	148.1
7	-2.4	948.5	15.9	138.0	-13.9	807.5	15.6	122.9	-18.3	754.4	13.4	126.5	-34.7	658.1	2.1	142.4
8	-1.0	953.0	16.6	142.2	-12.8	813.0	14.0	132.0	-16.9	760.0	11.5	131.1	-34.9	657.7	1.0	97.1
9	-4.8	959.0	10.1	162.7	-17.5	814.5	10.1	149.5	-21.6	759.6	9.0	151.1	-35.5	653.6	0.5	210.6
10	-6.2	950.7	9.6	147.2	-19.5	806.0	10.7	133.1	-24.7	750.5	9.9	130.3	-39.4	646.3	0.5	188.0
11	-6.5	949.9	9.6	170.6	-20.3	805.7	9.8	142.4	-25.4	750.2	9.6	138.1	-41.2	645.0	0.7	119.9
12	-5.2	952.5	7.2	172.5	-19.3	808.1	8.5	150.1	-24.9	752.6	6.2	144.8	-41.2	644.6	1.1	78.5
13	-5.7	953.5	4.5	167.8	-19.2	808.3	5.8	145.9	-23.0	752.1	4.1	129.5	-39.8	643.3	0.6	328.1
14	-7.1	957.9	6.6	177.7	-20.7	811.4	6.4	173.3	-26.2	754.6	6.1	172.6	-43.2	643.8	0.9	244.4
15	-6.7	960.0	7.5	137.2	-16.9	814.0	10.7	129.7	-21.8	758.4	7.9	133.4	-46.5	647.3	2.1	282.1
16	-7.3	954.2	10.0	145.2	-18.4	808.7	12.9	133.1	-22.1	754.0	10.9	128.2	-45.3	647.2	2.4	274.1
17	-6.5	954.1	6.2	140.6	-19.5	808.5	10.4	148.4	-24.0	753.4	8.2	145.1	-44.4	647.1	1.7	235.7
18	-8.7	946.0	12.7	164.0	-21.5	802.7	13.8	151.0	-26.3	748.9	10.9	147.9	-40.8	644.0	1.1	302.9
19	-7.5	959.0	6.1	158.1	-20.5	811.8	7.2	145.1	-26.3	755.4	5.8	143.8	-42.9	641.9	1.3	327.7
20	-8.1	956.3	6.5	145.8	-20.5	809.5	7.5	128.5	-23.5	752.9	6.4	109.5	-42.3	642.3	0.3	80.2
21	-7.5	957.0	8.1	171.6	-20.1	811.4	9.5	166.0	-24.3	756.0	8.1	173.9	-44.0	643.8	1.4	330.8
22	-10.2	953.1	7.8	147.2	-23.1	806.5	13.2	153.5	-28.4	751.8	10.6	167.1	-49.7	643.7	3.2	267.5
23	-13.8	948.6	13.7	162.1	-26.4	803.4	15.6	153.8	-32.2	748.8	12.3	162.3	-51.8	643.1	3.1	226.3
24	-5.8	933.2	16.6	142.2	-18.2	794.3	16.9	124.9	-23.8	741.6	15.0	125.3	-52.6	643.8	3.9	157.2
25	-4.0	939.0	16.3	137.6	-15.2	798.2	18.9	119.0	-19.9	745.7	15.8	121.0	-43.2	646.7	5.7	104.9
26	-7.0	954.3	9.9	154.9	-18.2	808.9	10.8	135.7	-22.3	753.7	10.1	131.7	-42.9	646.9	2.4	47.5
27	-7.0	950.1	12.2	155.2	-19.1	806.5	12.0	136.9	-21.9	751.3	11.2	126.2	-47.1	647.2	0.8	178.1
28	-8.2	951.5	8.2	172.6	-20.7	806.0	11.8	149.4	-25.0	751.3	11.0	143.5	-50.5	646.1	1.4	171.9
29	-9.5	950.7	10.4	159.4	-21.4	805.0	10.6	133.7	-25.8	749.6	10.0	126.5	-46.3	641.5	1.5	63.7
30	999.9	999.9	99.9	999.9	999.9	999.9	99.9	999.9	999.9	999.9	99.9	999.9	-46.1	641.3	1.5	60.1
AVE	-6.2	954.7	9.3	150.5	-18.4	809.9	11.0	139.1	-22.9	755.0	9.4	137.6	-42.0	649.1	0.5	197.5

REFERENCES

Allison, A., 1985: Diurnal variability of the surface wind and air temperature at an inland antarctic site: 2 years of AWS data. In Australian Glaci. Res.: 1982-1983, Jacka, T. H., ed., ANARE Research Note, in press.

Ball, F. K., 1956: The theory of strong katabatic winds. Australian J. of Physics, 9(3), 373-386.

Ball, F. K., 1957: The katabatic winds of Adelie Land and King George V Land. Tellus, 9(2), 201-208.

Ball, F. K., 1960: Winds on the ice slopes of Antarctica, Proc. Symp. Antarctic Meteorol., Melborne, 9-16.

Berson, F. A. and U. Radok, 1960: Antarctic surges and the zonal circulation. Proc. Symp. Antarctic Meteorol., Melborne, 193-216.

Bonner, W. D., and J. Paegle, 1970: Diurnal variations in boundary layer winds over the south-central United States in summer. Mon. Wea. Rev., 98(10), 735-744.

Budd, W. F., W. R. J. Dingle, and U. Radok, 1966: The Byrd snow drift project: Outline and basic results.

(In Rubin, M. J., ed., Studies in Antarctic Meteorol.), Antarctic Res. Ser., 9, Amer. Geoph. Union, 71-134.

Budd, W. F., D. Jenssen and U. Radok, 1971: Derived physical characteristics of the Antarctic ice sheet, Meteorol. Dept. Publ. no. 18, Univ. of Melborne, 178pp.

Chapman, S., and R. S. Lindzen, 1970: Atmospheric tides, thermal and gravitational. D. Reidel Publi. Co., Dordrecht, Holland, 200pp.

Caughey, S. J., J. C. Wyngaard, and J. C. Kaimal, 1979: Turbulence in the envolving stable boundary layer. J. Atmos. Sci., 36, 1041-1052.

Dabberdt, W. D., 1970: A selective climatology of Plateau Station, Antarctica. J. Appl. Met., 9, 311-315.

Dalrymple, P. C., H. H. Lettau and S. H. Wollaston, 1966: South pole micrometeorology program: data analysis. (In Rubin, M. J., ed., Studies in Antarctic Meteorol.), Antarctic Res. Ser., 9, Amer. Geoph. Union, 13-58.

Defant, F., 1949: Zur Theorie der Hangwinde, nebst Bemerkungen zur Theorie der Berg- and Talwinde. Arch. Meteor. Geophys. Bioklim., A1, 421-450.

Defant, F., 1951: Local winds. Compendium of Meteorology, T. F. Melone, Ed., Amer. Meteorol. Soc., 665-672.

Dyunin, A. K., 1967: Fundamental of the mechanics of snow storms. (in Oura H, ed. Physics of Snow and Ice), Vol.I, Part 2, Institute of Low Temperature Science, Sapporo, Japan, 1065-1073.

Fairbridge, R. W., 1967: The encyclopedia of atmospheric sciences and astrogeology, encyclopedia of earth sciences series. 2, Reinhold Publishing Corporation, 1200pp.

Fleagle, R. G., 1950: A theory of air drainage. J. Meteorol. 7, 227-232.

Gosink, J., 1981: A review of some models of katabatic flow, Univ. of Alask, Tech. Rept., UAG-R-282, 1-34.

Gosink, J., 1982: Measurements of katabatic winds between Dome C and Dumont d'Urville, Pure and Applied Geophysics, 120, 503-526.

Gutman, L. N., 1953: On "slope winds" over a surface of small slope. Bull. Acad. Sci. USSR, Ser. GEogr., 4, 377-379.

Kane, H. S., 1970: A study of 10m firn temperatures in central East Antarctica, I.A.S.H., Publ. no. 86, 165-176.

Kobayashi, D., 1972: Studies of snow transport in low-level drifting snow. Contributions from the Institute of Low Temperature Science, Series A, 24:1-58.

Lettau, H., H., 1966: A case study of katabatic flow on the south polar plateau. (In Rubin, M. J., ed., Studies in Antarctic Meteorol.), Antarctic Res. Ser., 9, Amer. Geoph. Union, 1-11.

Lettau H. H., A. J. Riordan, and M. Kuhn, 1977: Air temperature and two-dimensional wind profiles in the lowest 32 meters as a function of bulk stability. Meteorol. Studies at Plateau Station, Antarctica, Paper 6, Antarctic Res. Ser., 25, Amer. Geoph. Union, 77-91.

Lettau, H. H., and W. Schwerdtfeger, 1967: Dynamics of the surface wind regime over the interior of Antarctica. Antarctic J. U. S., 2(5), 155-158.

Loewe, F., 1953: Glaciological work in Terre Adelie in 1951, preliminary report. J. Glaci., 12, 248-249.

Loewe, F., 1969: On the coreless winter of the polar regions. Gerlands Beitrage zur Geophysik, 78(6), 453-476.

Loewe, F., 1970: Screen temperature and 10m temperature, J. Glaci., 9(56), 263-268.

Loewe, F., 1974: Die taegliche Windschwankung ueber dem Innern von Inlandeisen im Sommer. Arch. Met. Geoph. Biokl., Ser. B, 22,219-232.

Loewe, F., 1974: Considerations concerning the winds of Adelie Land. Zeitschrift fur Gletscherkunde und Glazialgeologie, 10, 189-197.

Lykosov, V. N., and Gutman, L. N., 1972: Turbulent boundary layer above a sloping underlying surface. Izv. Atmos. Oceanic Phys., 462-467.

Mahrt L. J., and W. Schwerdtfeger, 1970: Ekman spirals for exponential thermal wind. Boundary Layer Meteorol., 1, 137-145.

Mahrt, L.,1981: Modeling the depth of the stable boundary-layer. Boundary Layer Meteorol., 21, 3-19.

Mahrt, L., and S. Larsen, 1982: Small scale drainage front, Tellus, 34, 579-587.

Mannins, P. C., and B. L. Sawford, 1979: Katabatic winds: A field study. Quart. J. R. Met. Soc., 105, 1011-1025.

Mather, K. B., and G. S. Miller, 1967: Notes on topographic features affecting the surface winds in Antarctica with special reference to katabatic winds; and bibliography, Univ. of Alaska. Tech. Rept. UAG-R-189, 125pp.

Mawson, D., 1915: The home of blizzard, being the story of the Australian Antarctic Expedition 1911-1914, Heinemann, London, 1:349pp, 2:338pp.

Miller, S. A., 1974: An analysis of heat and moisture budget in the inversion layer over the Antarctic Plateau, for steady state conditions. Res. Rept., Dept. of Meteorol., Univ. of Wisconsin, Madison, 54pp.

Parish, T. R., 1980: Surface winds in East Antarctica, modified version of Ph.D. thesis, Dept. of Meteorol., Univ. of Wisconsin, Madison, 121pp.

Parish, T. R., 1981: The katabatic winds of Cape Denison and Port Martin. Polar Record, 20, 129, 535-522.

Parish, T. R., 1982: Surface airflow over East Antarctica, Mon. Wea. Rev., 110(2), 84-90.

Petkovsek, A. and A. Hocevar, 1971: Night drainage winds. Arch. Met. Geoph. Biokl., Ser.A, 20, 353-360.

Phillpot, H. R., and J. W. Zillman, 1970: The surface temperature inversion over the Antarctic continent, J. Geophys. Res., 75, 4161-5169.

Pinty, B., and Isaka, H., 1982: Analysis of the diurnal oscillation of surface geostrophic wind over Western Europe. Tellus, 34, 545-554.

Radok,U., 1974: On the energetics of surface winds over the Antarctic ice cap. WMO Tech. Note No. 179, Energy fluxes over polar surfaces. Proc. of the IAMAP, IAPSO/SCAR/WMO Symp., Moscow, 2-5 August, 1971.

Renard, R. J., and M. G. Salinas, 1977: The history, operation and performance of an experimental automatic weather station in Antarctica, Naval Postgraduate School, Monterey, CA, NPS-63Rd7710, 57pp.

Riordan, A. J., 1977: Variations of atmosphere and air motion in 0 to 32 meter layer at Plateau Station, Antarctica. Meteorol. Studies at Plateau Station, Antarctica, Paper 8, Antarctic Res. Ser., 25, Amer. Geoph. Union, 113-127.

Schmidt, R. A., 1982: Vertical profiles of wind speed, snow concentration, and humidity in blowing snow. Boundary Layer Meteorol., 23, 223-246.

Schwerdtfeger, W., 1970: The climate of the Antarctic. (In Chap. IV, Vol. XIV, Orvig, S. ed. World Survey of Climatology (Landsberg. H. E., ed.), Elsevier, Amsterdam), 253-355.

Schwerdtfeger, W., 1975: The steady state structure of the boundary-layer wind field over the Antarctic

Plateau, Dept. of Meteorol., Univ. of Wisconsin, Madison, Wisconsin, Unpublished manuscript.

Schwerdtfeger, W., 1984: Weather and Climate of the Antarctic. Developments in Atmospheric Scence, 15, Elsevier Science Publ. Co., New York, 261pp.

Sinclair, M. R., 1981: Record high temperatures in the Antarctic - a synoptic case study. Mon. Wea. Rev., 109(10), 2234-2242.

Simpson, G. C., 1919: British Antarctic Expedition 1910-1913. Meteorol., Vol. 1, Discussion, Tacker, Spink and Co., Calcutta, 326pp.

Sorbjan. Z., 1983: Rossby number similarity in the atmospheric boundary layer over slightly inclined terrain. J. Atmos. Sci., 40, 718-728.

Sorbjan, Z., 1984: A model study of the stably stratified steady-state atmospheric boundary layer over a slightly inclined terrain. J. Atmos. Sci., 41, 1863-1874.

Sorbjan, Z., Y. Kodama, and G. Wendler, 1985: Observational Study of the atmospheric boundary layer over Antarctica. Submitted to J. Climat. Appl. Met..

Stearns, C., and M. Savage, 1983: Automatic weather stations, 1980-1981. Antarctic J. U. S., 1981 Review,16(5), 190-192.

Streten, N. A., 1963: Some observations of Antarctic katabatic winds, Australian Meteorol. Magazine, 24, 1-23.

Streten, C. M., N. Ishikawa, and G. Wendler, 1974: Some observations of the local wind regime on a Alaskan Arctic glacier. Arch. Met. Geophys. Biokl., Ser. B, 22, 337-350.

Sumner C. J., 1965: A long period recorder of Antarctic katabatic winds. Quart. J. R. Met. Soc., 91(389), 364-375.

Sumner, C. J., 1966: A sunshine sensing device for long period recording. Quart. J. R. Met. Soc., 91(389), 567-574.

Sutton, O. G., 1953: Micrometeorology. McGraw-Hill, 331pp.

Turner, J. S., 1973: Buoyancy effects in fluids. Cambridge Univ. Press, 367pp.

Takahashi, S., 1985: Characteristics of drifting snow at Mizuho Station, Antarctica. In press, Annals of Glaci..

Thompson, D. C., 1969: The coreless winter at Scott Base, Antarctica. Quart. J. R. Met. Soc., 95, 404-407.

van Loon, H., 1967: The half-yearly oscillations in middle and high southern latitudes and the coreless winter. J. Atmos. Sci., 24, 472-486.

Weller, G. E., 1969: Meridional surface wind speed profile in MacRobertson Land, Antarctica, Pure and Applied Geophys., 77, 193-200.

Wendler, G. and P. Nicpon, 1975: Low-level temperature inversion in Fairbanks, Central Alaska. Mon. Wea. Rev., 103(1), 34.

Wendler G, and A. Poggi, 1980: Measurement of the katabatic wind in Antarctica. Antarctic J. U. S., 1980 Review, 15(5), 193-195.

Wendler, G., and Y. Kodama, 1982: Climate of Dome C. Antarctic J. U. S., 1982 Review, 17(5), 201-203.

Wendler, G., Y. Kodama, and A. Poggi, 1983: Katabatic wind in Adelie Land. Antarctic J. U. S., 1983 Review, 18(5), 201-203.

Wendler, G., and Y. Kodama, 1984: On the climate of Dome C, Antarctica in relation to its geographical setting. J. of Climatol., 4, 495-508.

Wexler, H., The "kernlose" winter in Antarctica, Geophysika, 6, 577-595, 1958.

Wippermann, F., 1973: The planetary boundary layer of the atmosphere. Deutscher Wetterdienst, Offenbach, 346pp.

Wyngaard, J. C., 1981: Wind shear in the baroclinic convective PBL. Proc. Symp. on Turbulence, Diffusion and Air Pollution, March 9-13, 1981, Atlanta, Georgia, 54pp.

Yamamoto, S., O. Yokoyama, and M. Gamo, 1979: Observational study on the turbulent structure of the atmospheric boundary layer and stable conditions. J. Met. Soc. Japan, 57, 423-341.

Yamanouchi, T, and S. Kawaguchi, 1985: Effects of drifting snow on the surface radiation budget in the katabatic wind zone, Antarctica. In press, Annals of Glaciology.